AD NUMBER

AD469041

LIMITATION CHANGES

TO:

Approved for public release; distribution is unlimited.

FROM:

**Distribution authorized to U.S. Gov't. agencies and their contractors;
Administrative/Operational Use; AUG 1965. Other requests shall be referred to Arnold Engineering Development Center, Arnold AFB, TN.**

AUTHORITY

AEDC ltr, 7 Mar 1966

AEDC-TR-65-151

W. B. Stephenson

UNCLASSIFIED

EXPANSION OF A JET INTO NEAR VACUUM

R. A. Cassanova and W. B. Stephenson
ARO, Inc.

August 1965

AEROSPACE ENVIRONMENTAL FACILITY
ARNOLD ENGINEERING DEVELOPMENT CENTER
AIR FORCE SYSTEMS COMMAND
ARNOLD AIR FORCE STATION, TENNESSEE

UNCLASSIFIED

NOTICES

When U. S. Government drawings specifications, or other data are used for any purpose other than a definitely related Government procurement operation, the Government thereby incurs no responsibility nor any obligation whatsoever, and the fact that the Government may have formulated, furnished, or in any way supplied the said drawings, specifications, or other data, is not to be regarded by implication or otherwise, or in any manner licensing the holder or any other person or corporation, or conveying any rights or permission to manufacture, use, or sell any patented invention that may in any way be related thereto.

Qualified users may obtain copies of this report from the Defense Documentation Center.

References to named commercial products in this report are not to be considered in any sense as an endorsement of the product by the United States Air Force or the Government.

EXPANSION OF A JET INTO NEAR VACUUM

R. A. Cassanova and W. B. Stephenson
ARO, Inc.

AF - AEDC
Arnold AFS Tenn

FOREWORD

The authors wish to express appreciation to General Electric for the use of the cantilevered flat plate system and to Lockheed Space Systems Division and NASA for their assistance in preparing computer programs. Messrs. M. R. Reed, W. C. Armstrong (Scientific Computing Branch, AEDC), and G. C. Westjohn (AEDC) deserve particular recognition and sincere thanks for their assistance in computations and data reduction. Acknowledgements are also extended to F. G. Moore for Test Operations and to F. L. Heltsley for equipment design.

The research presented in this report was conducted in Aerospace Research Chamber (8V) from November 9 to December 1, 1964, by ARO, Inc. (a subsidiary of Sverdrup and Parcel, Inc.), contract operator of the Arnold Engineering Development Center (AEDC), Air Force System Command (AFSC), Arnold Air Force Station, Tennessee, under Contract AF 40(600)-1000, Program Element 65402234, ARO Project No. SA0418. The report was submitted by the authors on June 16, 1965.

This technical report has been reviewed and is approved.

William D. Clement
Major, USAF
AF Representative, AEF
DCS/Test

Jean A. Jack
Colonel, USAF
DCS/Test

ABSTRACT

The flow field of nozzles exhausting into a vacuum was investigated both analytically and experimentally. The applicability of the method of characteristics for jet expansions into a free molecular environment is discussed. Fifteen-degree, half-angle, conical nozzles with area ratios of 1.0 to 207 were tested with argon and nitrogen at total pressures of 100, 50, and 35 psia. Ambient pressures of 10^{-4} to 10^{-6} torr yielded total pressure to ambient pressure ratios of 10^{7} to 10^{9}. Properties of the flow field were determined by the use of flat plates and flow direction vanes.

CONTENTS

ILLUSTRATIONS

Figure

Figure | Page

Figure | Page

NOMENCLATURE

A	Area
A^*	Nozzle throat area
C_D	Drag coefficient
F	Normal force on the flat plate
Kn	Knudsen number based on flat plate dimension
Kn^*	Knudsen number based on throat radius
M	Mach number
$\dot{M}$	Mass flow rate
P	Pressure
R	Gas constant
r	Radial distance from axis
r^*	Throat radius
T	Temperature
V	Velocity
X	Axial distance from nozzle exit
γ	Ratio of specific heats
δ	Boundary layer thickness
δ^*	Boundary layer displacement thickness
θ_N	Nozzle half angle
λ	Mean free path
ν	Prandtl-Meyer angle
ρ	Density

SUBSCRIPTS

c	Nozzle chamber conditions
e	Nozzle exit conditions
Max	Maximum conditions
o	Standard temperature pressure and density (300°K, 1 atm, 1 amagat)
∞	Background conditions

SECTION I
INTRODUCTION

When the exhaust from a nozzle discharges into a low ambient pressure, it expands to a much larger extent than at sea level pressure. It is desirable to study this plume for several reasons. The effects of the jet plume on a vehicle system, such as impingement on vehicle surfaces and radio wave attenuation, require knowledge of the plume properties. The use of exhaust scavenging systems in space environmental chambers requires detailed information of the jet properties. Also the free expanding jet may be used as a research tool for studying the rarefied gas flow regime if its properties can be determined.

Most of the past measurements (Ref. 1, 2, and others) have been made to determine the shape of the boundary of the jet by observing the boundary shock wave by optical methods. However, at the pressures characteristic of the space environment, the mean free path is much too great for a shock wave to be defined. Thus, it becomes necessary to survey the jet flow field to determine the spatial distribution of its properties, i.e., velocity, density, etc.

The present study is an extension of a development test for the Nimbus attitude control jet reported in Ref. 3. In that work, the jet from a specific nozzle was surveyed by determining the normal force on a small flat plate. The tests reported herein are primarily concerned with determining the applicability of the method of characteristics for predicting the flow field and developing techniques for rarefied flow investigations.

SECTION II
CALCULATION OF THE FLOW FIELD DOWNSTREAM FROM A NOZZLE EXHAUSTING INTO A LOW PRESSURE ENVIRONMENT

2.1 METHOD OF CHARACTERISTICS

The method of characteristics is a computational procedure by which the properties of a flow field of a compressible fluid can be determined. The state of the ideal exhaust gas and its local velocity vector can be mapped over a field defined by the boundary conditions. In essence, a point in the field has a zone of influence over a region downstream within a wave which makes an angle $\sin^{-1}$ (acoustic speed/stream speed) with the velocity vector. Through the isentropic flow relationships, the effects on flow velocity and gas state within the zone

of influence can be evaluated (Ref. 4 and 5). The boundaries of the zones of influence are termed characteristic lines. The behavior of the flow properties along these lines is governed by differential equations which are put in finite difference form for computation. The program used in the present calculations was developed for the IBM 7090 computer by Lockheed Missile and Space Company (Ref. 6). The computation starts with uniform flow properties on a spherical surface at the nozzle exit. The other initial condition is defined by a Prandtl-Meyer expansion of the flow at the nozzle lip to the ambient pressure, P_∞.

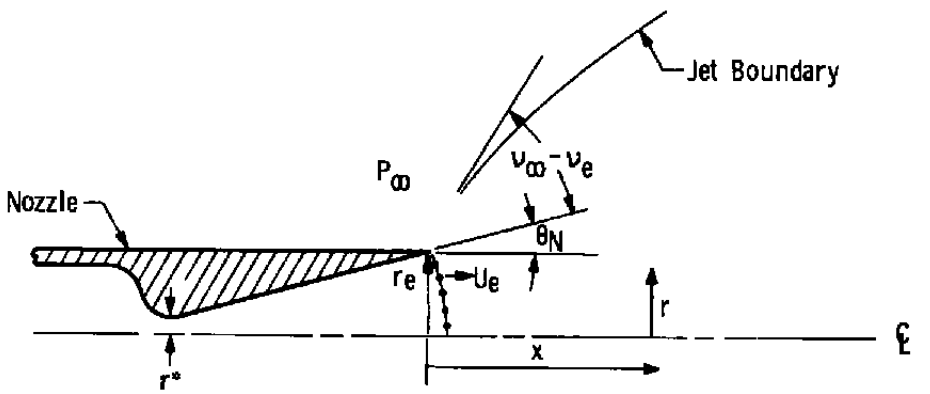

θ_N = Nozzle Half-Angle

ν_∞ = Prandtl-Meyer Angle Corresponding to Background to Stagnation Pressure Ratio

ν_e = Prandtl-Meyer Angle Corresponding to Nozzle Exit Mach Number

r^* = Throat Radius

U_e = Velocity at Exit

From a number of points at the exit, a network of characteristics lines is built up step-by-step to yield the flow properties at the intersection points. The results of the computation are coordinates of the intersection points, Mach number, and flow inclination to the axis. Since the flow is isentropic, the Mach number uniquely relates the density, pressure, temperature, and velocity to the state in the reservoir. A subprogram devised by the Scientific Computing Branch of AEDC interpolated the data to provide contours of constant Mach number and constant mass flow stream tube boundaries. Figure 1 shows a typical example of the form of the computed results. The spread of the computed points about the faired contour results from a finite mesh size. The numerical difficulties in the vicinity of the axis are mentioned by Ferri (Ref. 5) and require judgment in the fairing of the contours.

The variables of the problem are: ratio of ambient pressure to nozzle chamber pressure (P_∞ / P_c), gas specific heats ratio (γ), nozzle area ratio, and nozzle exit half-angle (θ_N). For the present calculation, the nozzle half-angle was constant at 15°, and the area ratio varied from 3.73 to 207 to conform to the experiments. Two specific heat ratios, γ = 1.4 and 1.67, which apply to diatomic and monatomic gases were used. No significant difference between the computed flow properties within the $\dot{m}/\dot{m}^* = .9$ contour for the two pressure ratios ($P_\infty/P_c = 2 \times 10^{-6}$ and 2×10^{-7}) was observed, and it can be concluded that the flow field comprising at least 90 percent of the mass flux would be the same if the ambient pressure were reduced to zero.

The Mach number loses its physical significance in a rapidly expanding flow. The constant Mach number contours are replaced in Figs. 2 through 11 with constant density ratio curves that can be interpreted as mass or number density. These figures give a description of the momentum flux field, which determines the forces and heat transfer to surfaces in the flow. It is important to observe that beyond 200-300 throat radii from the exit the streamlines become practically straight and the density variation is inverse with the square of distance (source flow). The source-like flow is established in about 100 throat radii for γ = 1.67 and by 400 for γ = 1.4. If the flow behaves ideally to a density ratio of $\rho/\rho_c = 1 \times 10^{-5}$, then subsequent deviations (such as non-continuum or internal mode freezing effects) will not influence the flow field shown. The field can therefore be extended to infinity for the zero ambient pressure situation.

In the present experiments ($P_\infty \sim 10^{-4}$ to 10^{-3} torr), the mean free path in the ambient region is about the length of the flow field shown in the figures and about the same as along the $\rho/\rho_c < 10^{-7}$ contour. A boundary shock, characteristic of higher ambient pressures, could not form and the interference between the nozzle flow and background gas is simply a linear addition in density with no significant momentum exchange.

Figures 12 and 13 show the effect of nozzle area ratio on the expansion of the flow field for diatomic and monatomic gases. As more expansion occurs within the nozzle - i.e., higher area ratios - the closer the flux will be to the axis. The effect of γ reflects the distribution of energy in the internal modes of the gas molecular motion. At the nozzle exit, the density ratio is about the same for the diatomic and monatomic gas. However, the temperature of the monatomic gas is only 60 percent of the other; thus it is much nearer to full expansion (static temperature $\longrightarrow$ 0) at the nozzle exit, and the jet lies closer to the axis. A limitation of the numerical solution by the method of characteristics is the convergence of the characteristics lines at high expansions. The angle

between the characteristics and the streamlines is the Mach angle $\left(\sin^{-1}\frac{1}{M} = \sin^{-1}\frac{a}{u}\right)$. At large Mach number, the intersections of the characteristic net become far apart and poorly defined. The numerical difficulty combined with the fact that the ideal representation of the gas is no longer physically realistic, dictates terminating the solution at a Mach number of 40 in the program. This is the reason that the monatomic flow fields are reproduced to a larger scale than are the diatomic ($\gamma = 1.4$) fields.

In summary the method of characteristics is based on the following simplifications:

(a) The gas has an ideal isentropic behavior, i.e., it can be represented as having a constant ratio of specific heats beyond the nozzle exit.

(b) The gas is inviscid or the effects of viscosity are negligible.

(c) The gas is a continuous medium.

The departure of the real physical situation from these conditions is discussed in the following sections:

2.1.1 Condensation

Condensation may occur within the nozzle or beyond the exit plane. Within the nozzle it can take the form of a condensation shock resulting from the release of the heat of condensation. The Mach number behind the shock will be reduced to a subsonic or a lower supersonic value (Ref. 7) with the result that the nozzle exit Mach number is less, and jet expansion outside the nozzle will be larger than predicted by the isentropic calculation. The experimental results for argon strongly suggest that condensation caused the large expansion.

The condensation of nitrogen is discussed in detail in Appendix I. It is concluded that condensation of nitrogen in the nozzle will not occur in the present geometry when the area ratio is less than 70. For the two larger area ratios ($A_e/A^* = 70$ and 200), the data on which the estimates were made leave uncertainty as to the probability of condensation. There are insufficient data for argon to make a similar prediction.

Beyond the nozzle exit, the collision frequency decreases rapidly and condensation is less probable than in the nozzle. However, the total number of collisions is proportional to size of the nozzle and supply stagnation density. If condensation occurs in the intermediate field between the exit and the source-like outer part, a two phase separation of

flux would be expected with the gaseous component expanding further than for no condensation. The solid part of the mass flux would be more concentrated near the axis.

If condensation appears in the field where the streamlines are already linear, it would be impossible to detect it by momentum flux measuring techniques such as are presently employed. The energy in modes other than directed velocity is so small that condensation would be a minor perturbation.

2.1.2 Viscosity

Viscous effects on the flow field will have an influence where velocity gradients or large rates of change of density are present. These conditions exist at the nozzle wall and at the exit lip where the corner of the Prandtl-Meyer expansion starts. The most obvious effect of the nozzle boundary layer is to reduce the effective area ratio below the geometrical area ratio. The subsonic portion of the boundary layer will expand into the background gas to help establish the ambient pressure. The flow outside the boundary layer will turn through the Prandtl-Meyer angle determined by exit Mach number and ambient pressure. The supersonic region of the boundary layer will turn through an angle determined by the local Mach number. The lip of the nozzle will be effectively rounded by the boundary-layer (see figure below).

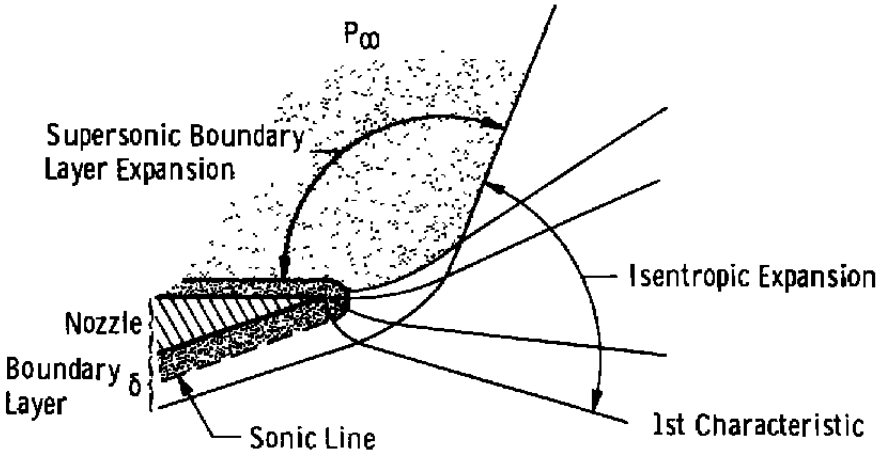

The primary effect of the nozzle boundary layer is to move the limit expansion line downstream from the lip leaving a gap through which the boundary layer gas expands into the ambient background. The change

from the inviscid flow field to that with a boundary layer is indicated in the figure below.

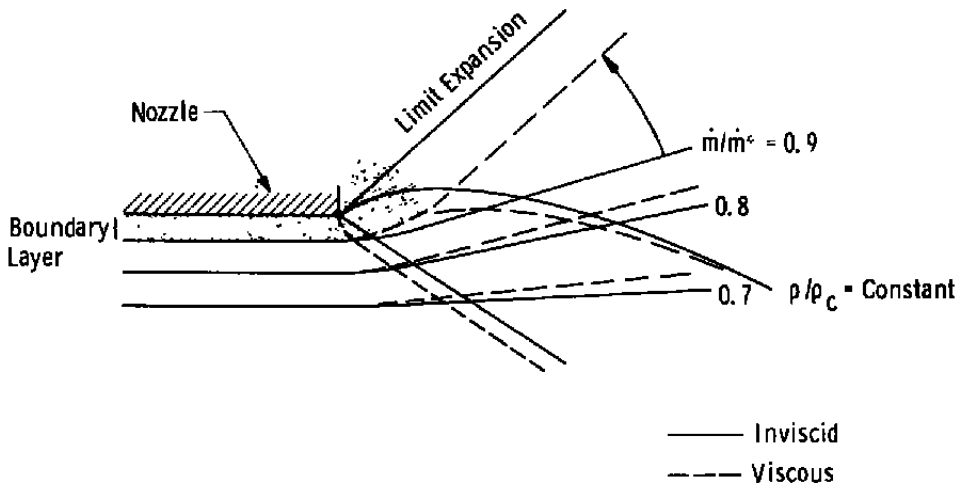

If, for example, the boundary layer is 10 percent of the total flow, the 90 percent mass flux streamline takes the slope of the limit expansion line, and there is a slight displacement of the other mass flux lines. The constant density lines are shifted toward the axis for $\dot{m}/\dot{m}^* > 0.8$ since the total flux between 80 percent and 90 percent remains the same. The effect of the nozzle boundary layer will be to reduce the momentum flux near the outer edge of the inviscid jet. The effective area ratio of the nozzle will be reduced from the geometrical area ratio by the boundary layer displacement thickness. The nozzle boundary layer has been computed by the Cohen-Reshotko method (Ref. 8) for the range of pressures used in the experiments. Figures 14a and 14b show the results in terms of the effect on nozzle Mach number and the boundary layer thickness. At the same supply pressure, boundary layer will be thicker for argon than for nitrogen.

The estimated effect of the boundary layer on exit Mach number is small (< 4%) for nitrogen and would not produce an appreciable influence on the flow field. However, when the viscous layer reaches 10 percent of the nozzle radius, 20 percent of the mass flow will be entrained. Therefore, the flow field outside the streamtube for 0.8 mass flux will be modified by the effects of viscosity. This is the situation when nitrogen is the gas at a pressure of 2.4 atm in the area ratio 70 nozzle and about 5 atm for the largest area ratio (207).

2.1.3 Continuum Limitations

One of the interesting aspects of the expansion of a jet into a vacuum is that the gas traverses smoothly through a series of gas dynamic

regimes that are usually represented by different analytical models: (a) the continuum, (b) a transition, and (c) free-molecule. These are distinguished by the magnitude of the Knudsen number: the ratio of the mean free path to some significant body or boundary surface dimension. If the distance between molecular collisions is small relative to the size of the surface, a continuum model-- such as the method of characteristics--is applicable. In free-molecule flow, the intermolecular collisions have no influence on the flow about the body in the stream. The streamlines are linear while the paths of the individual molecules are the resultant of the mean stream velocity and the random velocity corresponding to the translational temperature.

In the transition regime, there is an interaction of one region of the flow field on another. This region has been attacked from the free-molecule limit for deriving pressures on bodies immersed in the flow. The free-molecule flow is modified in the "first collision" theory by impacts of surface emitted molecules with those approaching the surface. However, in the case of a free expansion field, it is difficult to designate a significant dimension to define a Knudsen number. The radius of curvature of a streamline might be considered, but the functional relationship between such an arbitrary dimension and the mean free path is not obvious.

There is a close analogy between the disturbance wave of the continuum theory and the particle velocity in the actual gas that suggests that the transition regime is not sharply distinguishable for an expansion. For the continuum, the zone of influence is a cone whose half-angle is $\sin^{-1} \frac{u}{a}$; for the kinetic model gas, the mean zone of influence is also a cone about the velocity vector $\sin^{-1} \frac{\bar{u}}{u}$. "a" is the acoustic speed, $\sqrt{\gamma \frac{RT}{M}}$; and $\bar{u}$ is the mean molecular speed, $\sqrt{\frac{8}{\pi} \frac{RT}{M}}$, while u is the flow speed. The similarity of these quantities and the fact that macroscopic properties of the gas can be predicted from the kinetic molecular model lead to the expectation that the transition from a continuum flow model at the nozzle exit to a free molecule state downstream will be nearly the same as the characteristics method results.

A conservative criterion for applicability of the continuum analysis can be specified as follows: $Kn = .1$, for a 100 r^*-long segment, s, of the contour, $\frac{\rho}{\rho_c} = 10^{-5}$. Then $Kn = \frac{\lambda}{s} = \frac{10^5 \lambda_c}{10^2 r^*} = 10^3 Kn^*$ or $Kn^* \left(Kn^* = \frac{\lambda}{r^*}\right)$ is 10^{-4}. For the test nozzle with a 0.5 mm throat, the reservoir density must be unity or greater (the product $\frac{\rho_c}{\rho_s} r^* \geq 0.5$ amagat - mm.

2.1.4 Freezing of Internal Energy Modes

The internal energy of a gas is distributed among several modes: ionization, chemical (commonly dissociation for poly-atomic molecules), vibration, rotation, and translation of the molecules. In equilibrium these modes become inactive at progressively lower temperatures and influence the form of the state equation. When a gas undergoes a rapid expansion, the time to deactivate the various modes is important, and it is reasonable to associate this time with the number of particle collisions. There is approximately one collision for translation and 10 for rotation, etc. It is usual to consider the expanding gas an ideal (const. γ) medium until "freezing" of a mode occurs. At this point a new γ describes the expansion process until the next mode freezes.

Vibrational equilibrium in nozzles is considered in Ref. 9. The nozzle supply temperature was near 300°K for the present experiments so that only rotation and translation energies are important for the diatomic gas (N_2). As the expansion progresses, the collision rate drops (cf Appendix I), and equilibration of the rotational mode ceases to be important. The gas then acts like a monatomic medium with $\gamma = 1.67$ rather than 1.4. Further expansion results in translational freezing which is equivalent to free-molecule flow. Reference 10 derives a dimensionless parameter to predict the rotational freezing Mach number in an isentropic expansion from a sonic orifice:

$$f(\dot{M}) \frac{dM}{d(x/d^*)} = \frac{d^*}{\tau_{r_c} a_c}$$

d^* is the throat diameter, a_c is stagnation acoustic speed, and τ_{r_c} is the rotational relaxation time. Figure 15 shows the freezing parameter, $d^*/\tau_{r_c} a_c$, as a function of Mach number for the sonic orifice flow from Ref. 10 and for two nozzles along streamlines bounding 0, 50 percent, and 90 percent of the mass flux. The rotational freezing parameter can be put in a convenient form for a rigid sphere molecule:

$$d^*/\tau_{r_c} a_c = \frac{d^*}{\tau_{r_c} a_c} \frac{P_c}{P_o} \frac{T_o}{T_c} = 3.9 \times 10^4 \left(\frac{300}{T_c}\right) \frac{P_c}{P_o} d^* = 3.9 \times 10^4 \left(\frac{\rho_c}{\rho_o}\right) d^*$$

for N_2: $\frac{P_c}{P_o}$ is the supply pressure in atm and d^* is in cm. In Figs. 2 and 6 the contours of rotational freezing points are superimposed for a throat diameter of 1.0 mm. For the nozzles used in these experiments, rotational freezing effects on the flow field may be anticipated at supply pressures less than about 2 atm.

The freezing of the translational mode is downstream of the rotational freezing point and will not influence the flow field in terms of velocity and

density. Of course the pressure and temperature are entirely different when translational freezing occurs since the temperature approaches a constant instead of zero. This phenomenon has been widely investigated in the literature of molecular beam velocity distributions (for instance, Ref. 11 is a good example).

2.1.5 Summary of Limitations of Applicability of Characteristics Calculations

1. Condensation: At supply pressures from 1 - 7 atm and temperature of 300°K, condensation may occur for nozzle area ratio > 70 for nitrogen. For argon, there are insufficient data to predict condensation, cf Appendix I.
2. Viscosity: The nozzle boundary layer reduces the exit Mach number and the density in the outer edge of the jet. The effect of viscosity is expected to be negligible outside the boundary layer because the velocity is practically uniform.
3. Continuum Effects: At supply conditions where the product of reservoir density and throat radius, $\frac{\rho_c}{\rho_o} r^* \geq 0.5$ amagat-mm, the flow field will be unchanged by the transition from a continuous medium.
4. Rotational Freezing: Rotational freezing will not affect the flow field appreciably if $\frac{\rho_c}{\rho_o} r^* \geq 1$ amagat-mm.

SECTION III
APPARATUS

3.1 GENERAL TEST DESCRIPTION

The tests were performed in the Aerospace Research Chamber ARC (8V). The nozzle flow was pumped with 20°K cryosurfaces and a diffusion pump-mechanical pump system. The jet exhaust flow field was investigated with flat plates nearly normal to the flow direction pitot probes, and streamline vanes.

3.2 AEROSPACE RESEARCH CHAMBER

The Aerospace Research Chamber (8V) is a nickel-plated steel chamber, 8 ft in diameter by 16 ft long; a removable ellipsoidal dished head on one end provides access to the chamber. A 6-in. diffusion pump in series with a mechanical pump is installed on the chamber. A liquid-nitrogen-cooled liner shrouds the sides and downstream end and provides

a radiative heat sink (Fig. 16). A 1-kw gaseous helium refrigerator is available for cooling 240 ft^2 of 20°K cryosurfaces. The pumping system is able to maintain 10^{-4} to 10^{-6} torr at test nozzle mass flow rates of up to 1.0 gm/sec with argon and nitrogen. Reference 12 gives further information on the chamber design. A schematic of the nozzle installation is shown in Fig. 16.

3.3 NOZZLE ASSEMBLY

The test articles were a 15° half-angle conical segmented nozzle and a sonic orifice (Fig. 17). The throat diameter for all nozzles and the orifice was 0.044 inch. Detachable segments provided area ratios of 3.73:1, 12.8:1, 36.9:1, 69.6:1, and 207:1.

A stainless steel stagnation chamber supported the nozzle and the propellant supply line. The stagnation chamber and nozzle assembly were rotated in the vertical plane through 50 degrees of pitch from the horizontal position by a 10:1 worm gear driven by a shaft extending through the door. This shaft also provided nozzle assembly axial movement of 20 inches by a push-pull motion of the handle. The combination of pitch and axial movement was used to map the plumes using stationary instrumentation. Nozzle angle was measured by a potentiometer attached to the rotation shaft; axial position was measured externally on the driving shaft by a tape measure.

3.4 PROPELLANT SUPPLY SYSTEMS

A schematic of the nozzle propellant supply system is shown in Fig. 18. Stagnation pressure was controlled by line regulators and monitored by a Kollsman gage.

3.5 CANTILEVERED FLAT PLATE

The jet properties were defined by measuring the forces on 1 in. x 1 in. and 1/4 in. x 1/4 in. square flat plates nearly normal to the flow direction. The plates were maintained stationary while the nozzle was positioned as described in Section 3.3. The flat plate was mounted on a 36-in. aluminum beam. The lower end of the beam was clamped to a support mount in the chamber floor. The beam was shielded from the flow by 3-in. diameter tubing and aluminum sheet (Fig. 19). Four 120-ohm thin-film strain gages were cemented to the base of the aluminum beam. These gages yielded an output proportional to the horizontal force on the flat plate. Eddy-current damping was employed to diminish the effect of vibration on strain-gage output.

The flat plate was calibrated after installation as illustrated in Fig. 20. The method provided a horizontal resultant from a vertical force by the use of a 45-deg inclined thread. Horizontal force and plate displacement were calibrated with strain gage output. The calibration curve is shown in Fig. 21.

3.6 PITOT PROBES

Pitot pressure was determined by two pitot probes (1/16 in. OD, 1/32 in. ID) attached to 5 and 15-psi full-scale transducers, respectively. A swing arm supported the pitot probe transducer units and allowed the probes to be swung away from the nozzle during flat plate and streamline vane runs. Pitot pressure was investigated in the region 0 to 1-in. from the nozzle exit. Minimum resolution for the transducers was approximately 0.05 psi.

3.7 STREAMLINE VANE ASSEMBLY

The streamline vanes were constructed of 0.0015-in. thick steel shim stock. The vanes were mounted on steel pins protruding from the top and bottom of the assembly which permitted the vanes to rotate with a minimum of force to align with the flow direction (Fig. 23). Photographs of the vanes were made through a port in the top of the chamber. Two 500-watt flood lamps were installed above the vane assembly to illuminate the vanes.

3.8 PRESSURE AND TEMPERATURE INSTRUMENTATION

Ambient pressure was monitored by an ionization gage mounted on the nozzle assembly and pointed toward the chamber wall. Copper-constantan thermocouples, referenced to liquid nitrogen, were used to monitor temperatures of the insulated heater box, flat plate strain gages, and nozzle surface. A thermocouple probe was inserted into the nozzle stagnation chamber to monitor propellant total temperature.

3.9 DATA RECORDING SYSTEM

Cantilevered plate forces, nozzle pitch angles, pressures, and temperatures were recorded on a recording digital voltmeter. Streamline direction vane photographs were taken with a 70-mm camera using Tri-X film.

SECTION IV
PROCEDURE

4.1 FORCE AND PRESSURE RUNS

During cooldown of the ARC (8V) cryosurfaces to operating temperature, the beam temperature near the strain gages was monitored to assure that no zero shift occurred. Propellant flow was then started and continued until equilibrium pressure had been reached. The nozzle assembly was then moved to the most remote position from the flat plate and was rotated upward to the 50-deg position.

The nozzle was then rotated from 50 to -50 deg and returned while recording the force on the plate. This was done at a series of different axial positions. For the 1-in. plate, sweeps were made at 2-in. axial intervals at distances between 8 and 29 inches from the nozzle exit and for the 1/4-in. plate at 1-in. axial intervals at distances between 1 and 10 inches from the nozzle exit. Pitot pressure sweeps were made at 1/4-in. axial intervals at distances 0 to 1 inch from the nozzle exit, although probe contact with the nozzle prevented full ±50-degree sweeps. Each run took approximately 10 minutes.

4.2 STREAMLINE VANE RUNS

The startup procedures were similar to those described for the force runs. When flow was stabilized, the flood lamps were energized and the nozzle moved to the 26-in. axial position and set at zero degrees. Photographs were then made of the vane angular positions at 2-in. axial intervals from 26 inches to 6 inches.

4.3 RANGE OF VARIABLES

Nozzles with stagnation pressures of 35, 50 and 100 psia and a stagnation temperature of 300°K were investigated. Argon and nitrogen were used as nozzle fluids. Nozzle area ratios of 1.0, 3.73, 12.8, 36.9, 69.6 and 207 were tested.

4.4 DATA REDUCTION

Nondimensionalized flat plate force and position data were reduced by a computer program. Plots of nondimensionalized force versus angular position for various radial positions from the nozzle exit were obtained from the cantilevered flat plate runs (typical, Fig. 23). A fifth-order, least-squares curve was fitted to the experimental data,

and the constant-force contours were crossplotted from the fitted curves. Data point scatter bands were determined from the nondimensionalized force versus angular position plots and is indicated on the corresponding constant-force maps.

SECTION V
RESULTS

Computed Mach number distribution and boundary layer displacement thickness (Cohen and Reshotko solution) in the nozzles for $\gamma = 1.4$ and $\gamma = 1.67$ are shown (Figs. 14a and 14b). The centerline exit plane Mach number obtained from pitot probe results for $A_e/A^* = 207$ are compared with inviscid and viscous Mach number solutions. Experimental Mach numbers were computed for isentropic flow using the Rayleigh formula for pitot pressure.

Experimental constant force contours and centerline force plots are compared with the characteristics method calculations for $A_e/A^* = 1.0$ through 207 with nitrogen at $P_c = 100$ psia and for $A_e/A^* = 1.0$ and 3.73 with argon at $P_c = 100$ psia (Figs. 24 through 33). The force plots for $A_e/A^* = 1.0$ with argon and nitrogen are compared with the predictions of Sherman (Ref. 13) since the present characteristics program could not be used for $M_e = 1$ (sonic orifice) at the exit. Sherman calculated by the method of characteristics the centerline Mach number of the sonic orifice exhaust flow field by assuming an exit Mach number slightly greater than unity. Density and Mach number values were obtained from the characteristics method calculations; normal flat plate force was determined by the method outlined in Appendix II and the solution compared with experimental results. Knudsen number, based on the flat plate dimension (1/4 in. and 1 in.), is shown in Fig. 33.

The random error in data, indicated by the maximum deviations from the least squares curve fit, is shown on the constant force data points. The systematic error is summarized in Table I. The tare drag on the 1/4 in. x 1/4 in. flat plate support beyond the windshield caused the 1/4-in. flat plate force readings to be approximately 12 percent high. The flat plate calibration (Fig. 21) indicates a possible zero shift or nonlinearity of the balance of approximately $\pm 0.5 \times 10^{-4}$ lb. The nozzle chamber pressure deviation is negligible (±0.5 percent). The possible systematic errors in the data are shown on the constant force contours and centerline plots.

Streamline vane photos for $A_e/A^* = 1.0$ through 207 with nitrogen and for $A_e/A^* = 1.0$ and 3.73 with argon are compared with characteristics predictions (Figs. 37 through 44).

SECTION VI
DISCUSSION OF RESULTS

6.1 EXIT MACH NUMBER

Theoretical calculations and experimental test results both indicate that boundary layer effects on the exit Mach number for nitrogen at P_c = 100 psia are negligible. The actual Mach number distribution across the exit plane could not be determined because of the small size of the nozzle. The trend in the pitot results for argon is inconclusive because of possible condensation in all nozzles. Exit Mach numbers for argon could not be determined because static pressure was not monitored and cannot be inferred from P_{pitot}/P_c since isentropic theory is not applicable if condensation shocks occur in the nozzle.

6.2 EXHAUST FLOW FIELD – NITROGEN

Constant force contours for N_2 suggest that noncondensed flow existed for all area ratio nozzles since all forces fell inside the theoretical maximum expansion angle. The flat plate results cover the plume expansion up to a mean free path of approximately 5 cm (K_n = 2 for 1-in. flat plate) based on the assumption $\rho\lambda$ = constant.

The 1-in. flat plate results show agreement with the predictions except near the axis where the measured density is lower than predicted. Computation difficulties with the method of characteristics along the centerline may account for part of this deviation. Characteristics predictions in this region were approximated by fairing from the outer portions of each curve. In Fig. 29a, the $(F/A)P_c = 2.5 \times 10^{-5}$ contour for P_c = 35 psia shows the trend of the force field with decreasing nozzle chamber pressure. The outward shift of the 2.5×10^{-5} contour is predicted by the outward shift of the theoretical contour with increasing Knudsen number. The experimental contours (P_c = 100, 35) show the same trend as the corresponding theoretical contours.

The 1/4-in. flat plate results show higher density than predicted near the axis and a lower density than predicted in the outer portions of the plume. The disagreement in the outer portion could have been caused by the boundary layer effects and/or by the force gradient on the flat plate. The flow impingement on the supporting beam would result in forces that are approximately 12 percent high (see Table I).

Axial distribution of the flat plate force shows the effects of varying stagnation pressure, thereby changing the Knudsen number and drag

coefficient. The effect is in the expected direction with the lower stagnation pressure yielding a higher $(F/A)P_c$. The effect of plate size on the Knudsen number (and C_D) is in the anticipated direction, although the difference in the results cannot entirely be accounted for by the effects of plate size alone. Even if tare effects are taken into account, the 1/4-in. flat plate results ($A_e/A^* = 3.73 \longrightarrow 207$) indicate a higher density while the 1-in. flat plate indicates a lower density than predicted. This discrepancy could be due to a systematic error, i.e., a zero shift or a nonlinearity which is larger than the magnitude assumed. The indicated density by both flat plates for the sonic orifice is higher than predicted by Sherman (Ref. 13).

The streamline directions indicated by the vanes align with the predicted directions. The streamlines become linear, as in source flow, a short distance from the nozzle exit. The apparent source position varies with area ratio. The streamline vane misalignment in the outer portions of the flow field is large because of low momentum flow and static moments on the vanes.

The agreement of the constant force contours with the predictions in the outer, near free molecule, portion of the plume indicates that the method of characteristics is useful for free expansions from initial continuum conditions into a rarefied environment. Flow velocity and direction are established in the continuum (near the exit) flow regime. For $\gamma = 1.4$, 99 percent V_{max} is reached by $M = 16$ which occurs in the continuum region of the plumes investigated.

Even though Mach number and temperature are frozen at some point in the field, density can still be predicted from velocity and mass flow. The normal flat plate, which measures momentum, is then a density indicator since velocity is essentially constant. The similarity of the continuum and free molecular flow relations is discussed in Section 2.1.

6.3 EXHAUST FLOW FIELD – ARGON

The results for argon are presented, even though no direct comparison with characteristics predictions of the present program is possible. The sonic orifice axial distribution of flat plate force is compared with the predictions of Sherman (Ref. 13).

The constant force maps for $A_e/A^* = 12.8$ to 207 show expansion angles greater than the maximum expansion which suggests condensation; however, $A_e/A^* = 1.0$ and 3.73 did not. Decreasing the stagnation pressure in the $A_e/A^* = 12.8$ nozzle did not cause a significant decrease in the

expansion; this indicates that the condensation shock was not positioned near the exit. Decreasing the stagnation pressure would increase the supersaturation of the flow, thereby positioning the condensation shock farther downstream in the nozzle. The similarity of the $A_e/A^* = 3.73$ constant force maps for nitrogen and argon should be noted. The similarity was not anticipated because of the different expansion properties of the two gases.

The axial distribution of flat plate force for $A_e/A^* = 1.0$ indicates a higher density for both plates than calculated by Sherman (Ref. 13). A slight Knudsen number effect is indicated with the changing plate size and stagnation pressure, whereas theoretical calculations indicated no effect on the Knudsen number.

The streamlines indicated by the vanes align well with the estimated streamlines, which are linear extensions of the calculated streamlines.

Even though Mach number is not a physically significant quantity in free expansion analyses, the method of characteristics relations involving Mach number still yield meaningful density predictions. The flow fields tested essentially become source-like early in the expansion; i.e., the density varies inversely with the square of the distance.

SECTION VII
CONCLUSIONS

The analysis of a flow field expanding to low background pressures and the experimental results have demonstrated that:

1. The method of characteristics yields accurate density predictions for expansions from continuum to the rarefied flow regimes if (a) the transition to free molecular flow takes place in the source-like flow region and (b) condensation does not occur in the continuum or transition region.
2. Condensation in the nozzle apparently causes expansion greater than predicted for argon.
3. The normal flat plate technique is a useful tool for rarefied flow investigations and is limited primarily by force balance sensitivity.
4. The light streamline vane is useful for determining flow direction in the continuum and transition regimes.

REFERENCES

1. Vick, A. R., Andrews, E. H., Jr., Dennard, J. S., and Craidon, C. B. "Comparisons of Experimental Free-Jet Boundaries with Theoretical Results Obtained with the Method of Characteristics." NASA TN D-2327, June 1964.
2. Latvala, E. K. "Spreading of Rocket Exhaust Jets at High Altitudes." AEDC-TR-59-11 (AD215866), June 1959.
3. Cheeseman, C. E. "Testing of a Nimbus Attitude Control Nozzle at Simulated Altitudes of 400, 000 to 500, 000 Feet." AEDC-TDR-64-210(AD449864), October 1964.
4. Courant, R. and Friedrichs, K. O. Supersonic Flow and Shock Waves. Interscience Publishers, New York, 1948.
5. Ferri, A. Elements of Aerodynamics of Supersonic Flows. MacMillan, New York, 1949.
6. Prozan, R. J. "PMS Jet Wake Study Program." Lockheed Aircraft Corporation, Report No. LMSC 919901, October 1961.
7. Shapiro, A. H. The Dynamics and Thermodynamics of Compressible Fluid Flow. Ronald Press, New York, 1953.
8. Cohen, C. B. and Reshotko, E. "The Compressible Laminar Boundary Layer with Heat Transfer and Arbitrary Pressure Gradient." NACA Tech. Report No. 1294. 1956.
9. Phinney, R. "Nondimensional Solutions of Flows with Vibrational Relaxation." AIAA Journal, Vol. 2, No. 2, February 1964, pp. 240-244.
10. Knuth, E. L. "Rotational and Translation Relaxational Effects in Low Density Hypersonic Free Jets." UCLA Report No. 64-53, November 1964.
11. Anderson, J. B. and Fenn, J. B. "Velocity Distributions in Molecular Beams from Nozzle Sources." Princeton University, August 5, 1964.
12. Test Facilities Handbook (5th Edition). "Aerospace Environmental Facility, Vol. 5." Arnold Engineering Development Center July 1963.
13. Sherman, F. S. "Self-Similar Development of Inviscid Hypersonic Free-Jet Flows." Fluid Mechanics Report 6-90-63-61, Sunnyvale, California, Lockheed Missile and Space Company, May 23, 1963.

TABLE I
SYSTEMATIC ERROR OF FORCE BALANCE

P_c (psia)	ΔF (lb)	ΔP_c	$\Delta [(F/A)/P_c]$ 1/4" Flat Plate	$\Delta [(F/A)/P_c]$ 1" Flat Plate
100	$\pm.5 \times 10^{-4}$	±.5%	$\pm .8 \times 10^{-5}$	$\pm .5 \times 10^{-6}$
50	$\pm.5 \times 10^{-4}$	±.5%	$\pm.16 \times 10^{-5}$	$\pm1.0 \times 10^{-6}$
35	$\pm.5 \times 10^{-4}$	±.5%	$\pm2.4 \times 10^{-5}$	$\pm1.5 \times 10^{-6}$

NOTE: Additional frontal area exposed to the flow for the 1/4" x 1/4" flat plate by the supporting beam is 0.0078 sq. in. Therefore, the 1/4" x 1/4" flat plate readings are estimated to be 12% high. (See Fig. 17)

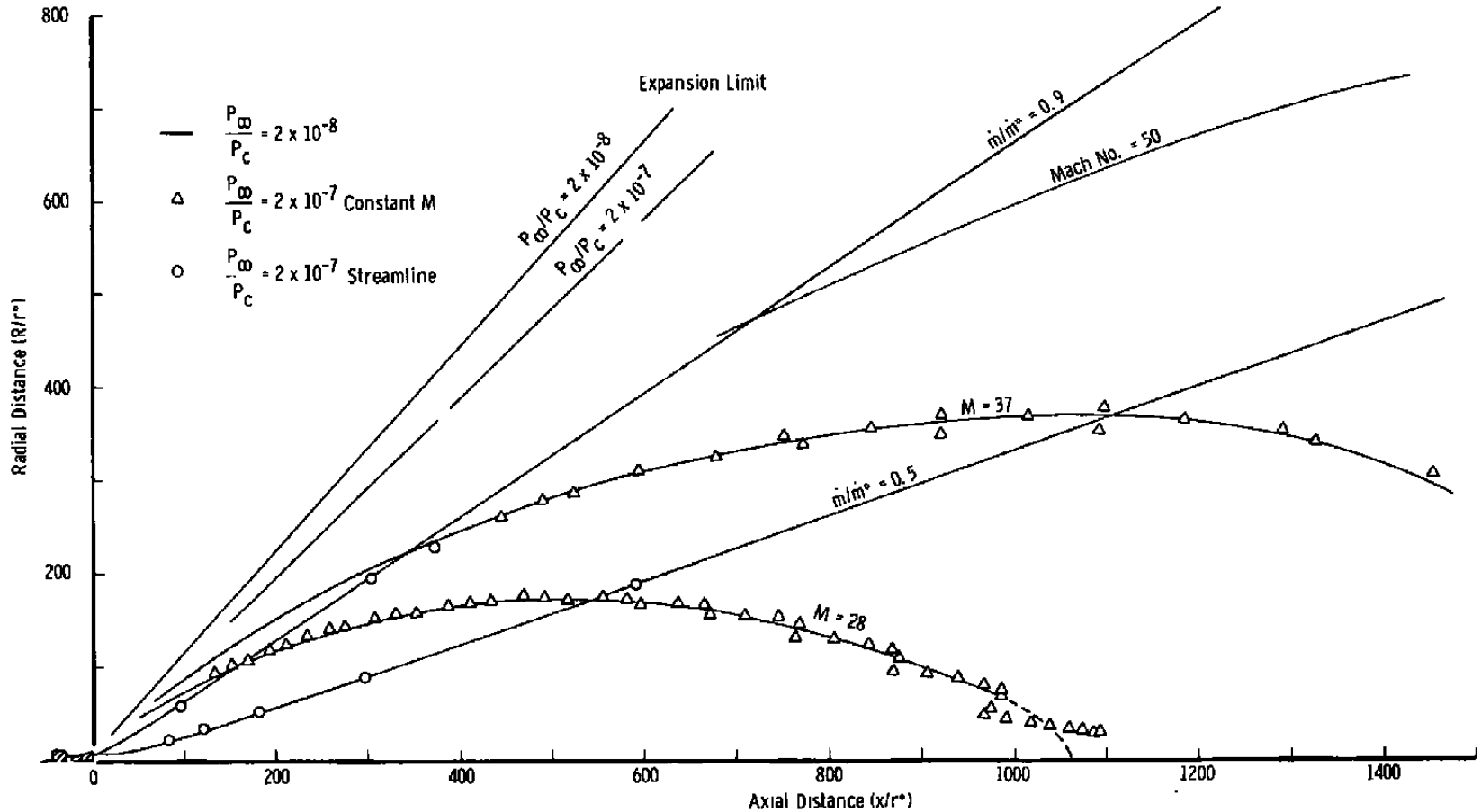

Fig. 1 Effect of Ambient Pressure on Mach No. and Streamlines from Characteristics Computation; $A_e/A^* = 69.6$, $\gamma = 1.4$, $M_e = 6.39$

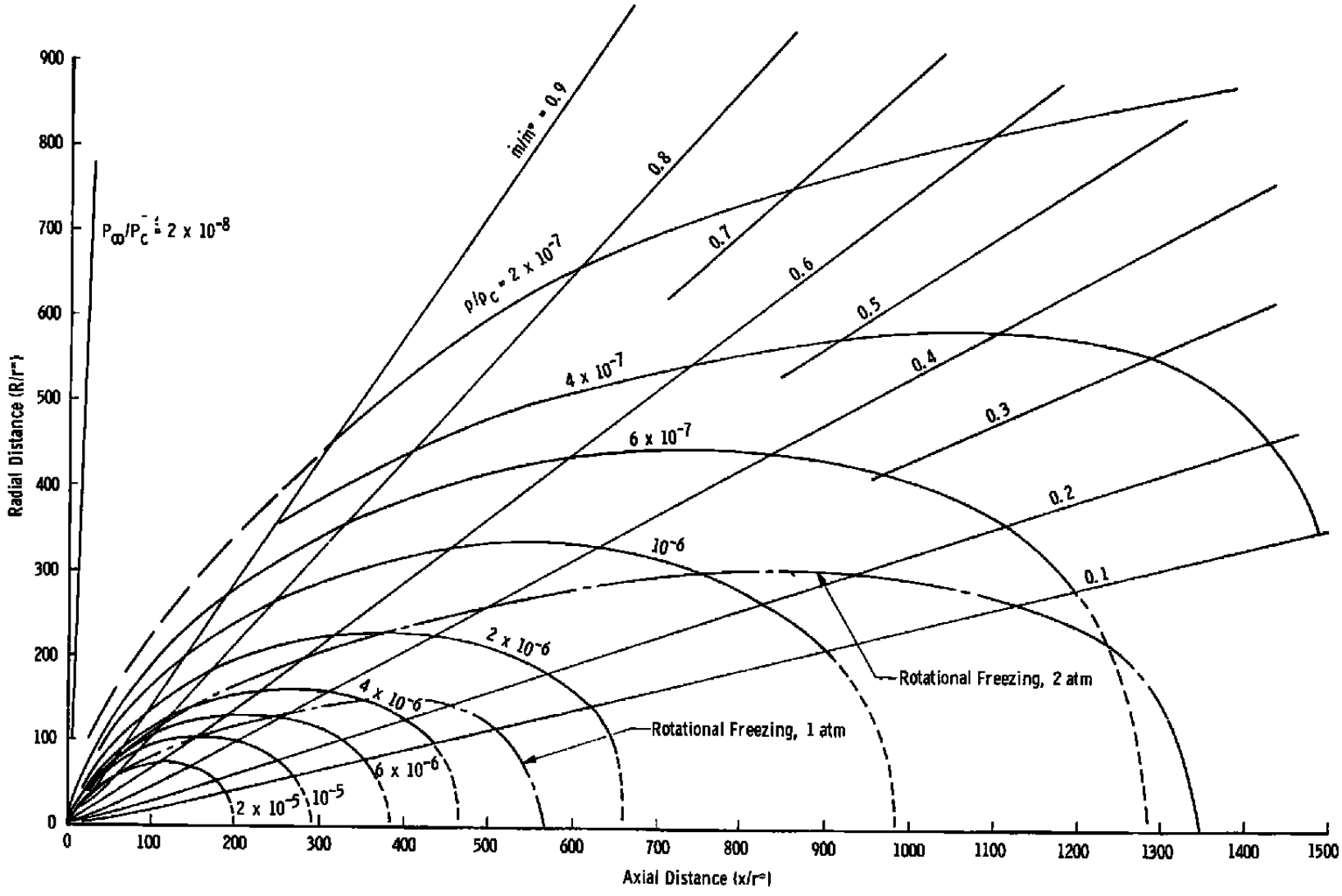

Fig. 2 Method of Characteristics Flow Field Solution; $A_o/A^* = 3.73$, $\gamma = 1.4$, $M_o = 2.88$

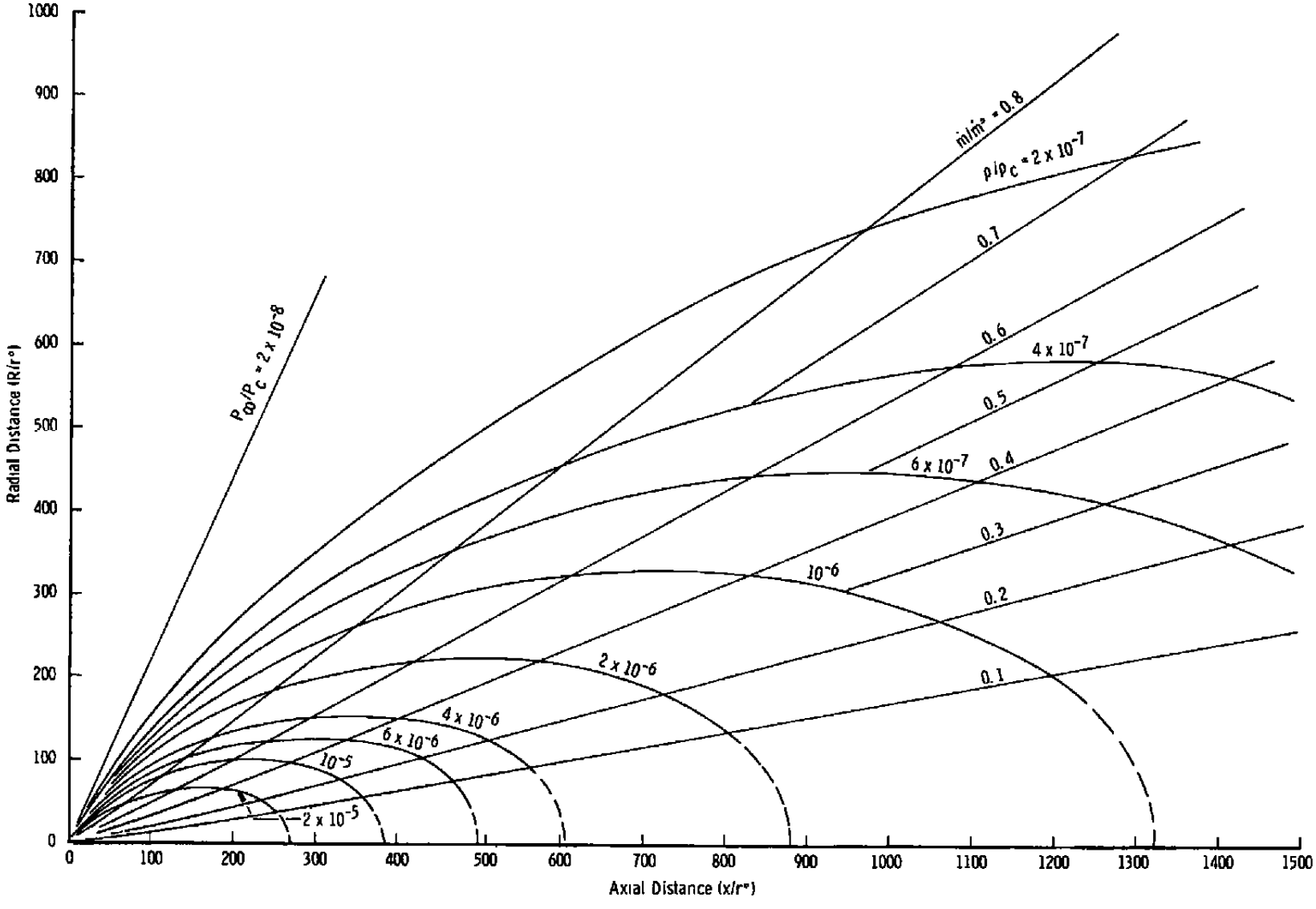

Fig. 3 Method of Characteristics Flow Field Solution; $A_e/A^* = 12.8$, $\gamma = 1.4$, $M_e = 4.20$

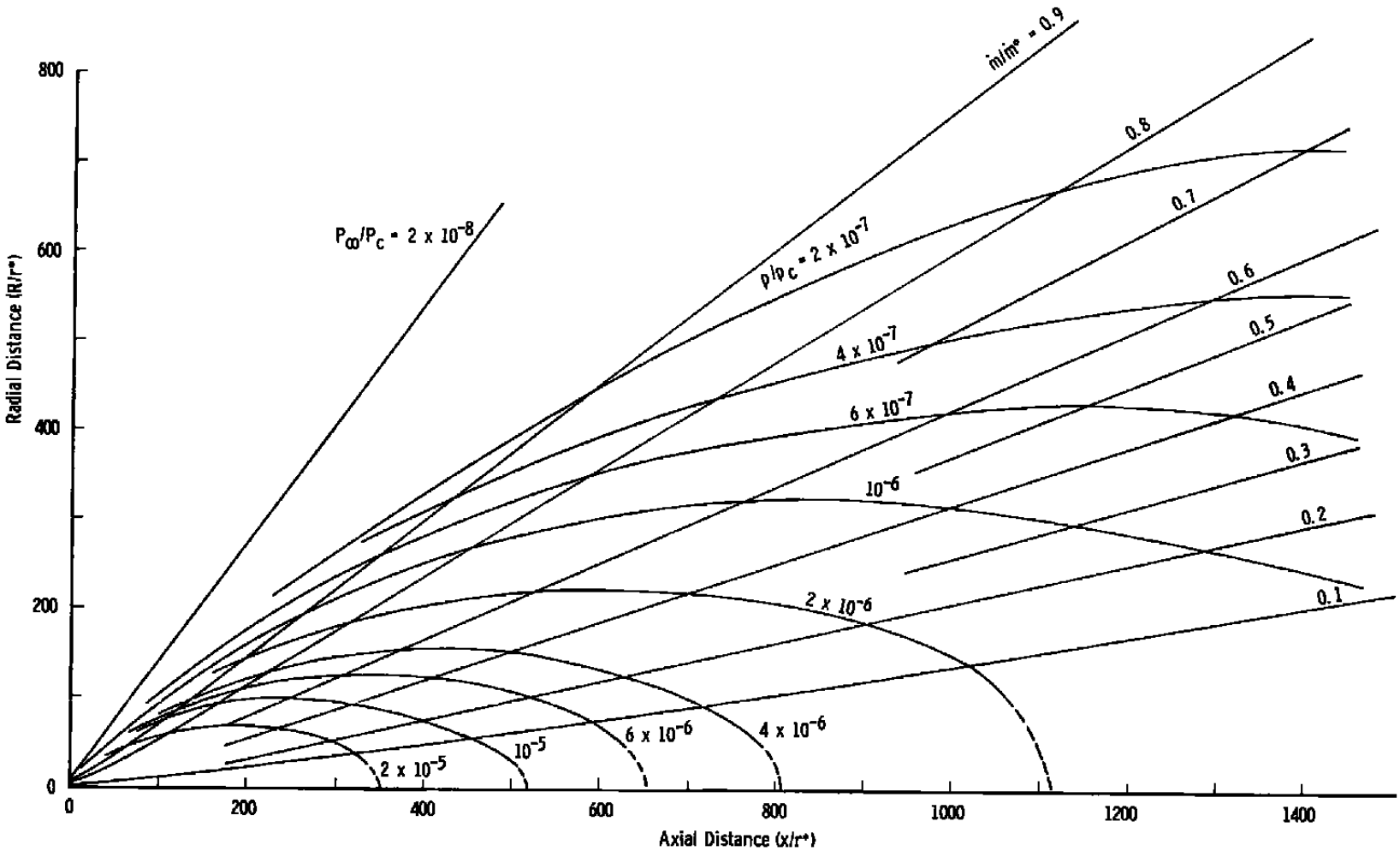

Fig. 4 Method of Characteristics Flow Field Solution; $A_e/A^* = 36.3$, $\gamma = 1.4$, $M_e = 5.48$

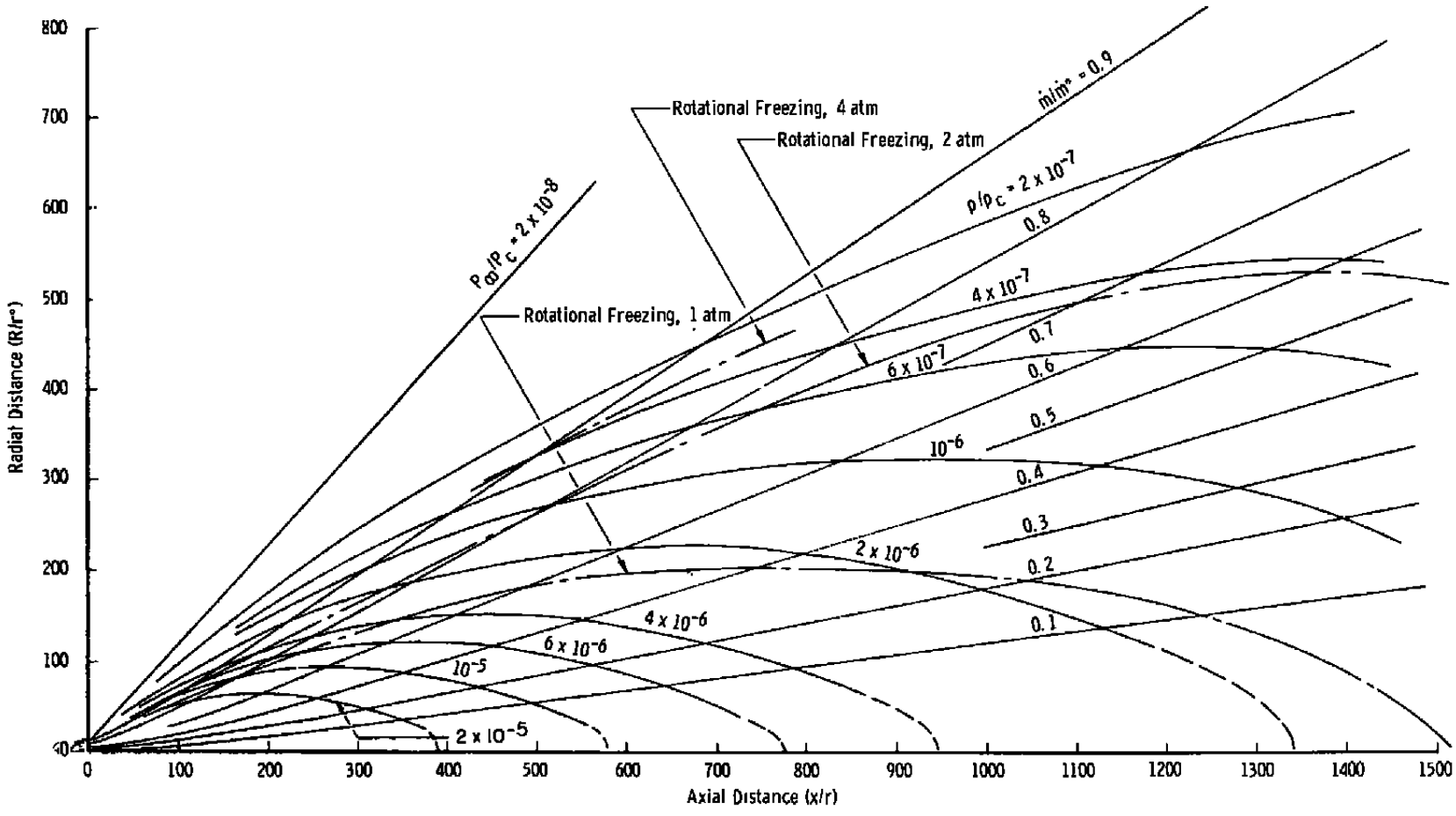

Fig. 5 Method of Characteristics Flow Field Solution; $A_e/A^* = 69.6$, $\gamma = 1.4$, $M_e = 6.39$

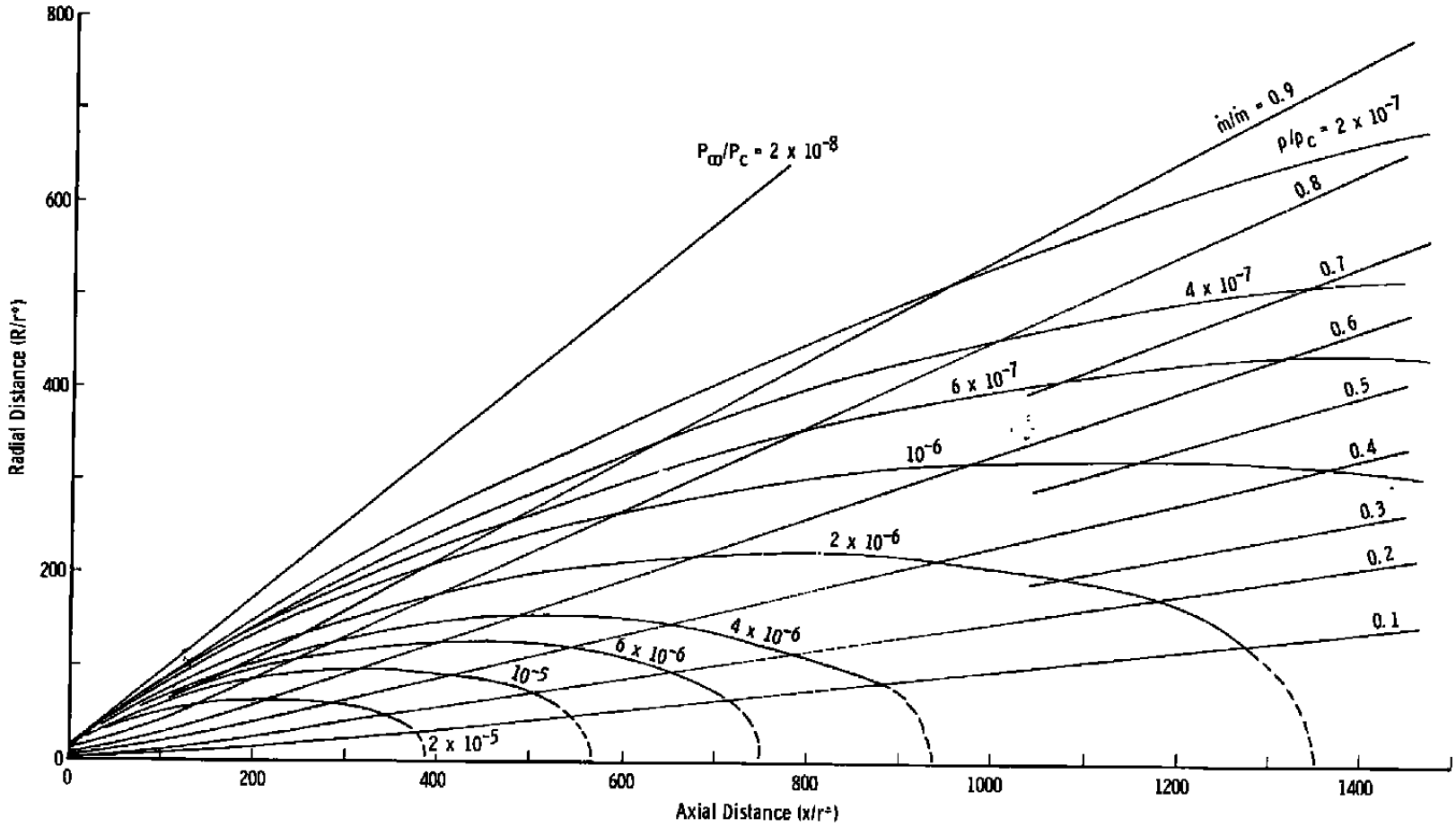

Fig. 6 Method of Characteristics Flow Field Solution; $A_e/A^* = 207$, $\gamma = 1.4$, $M_e = 8.15$

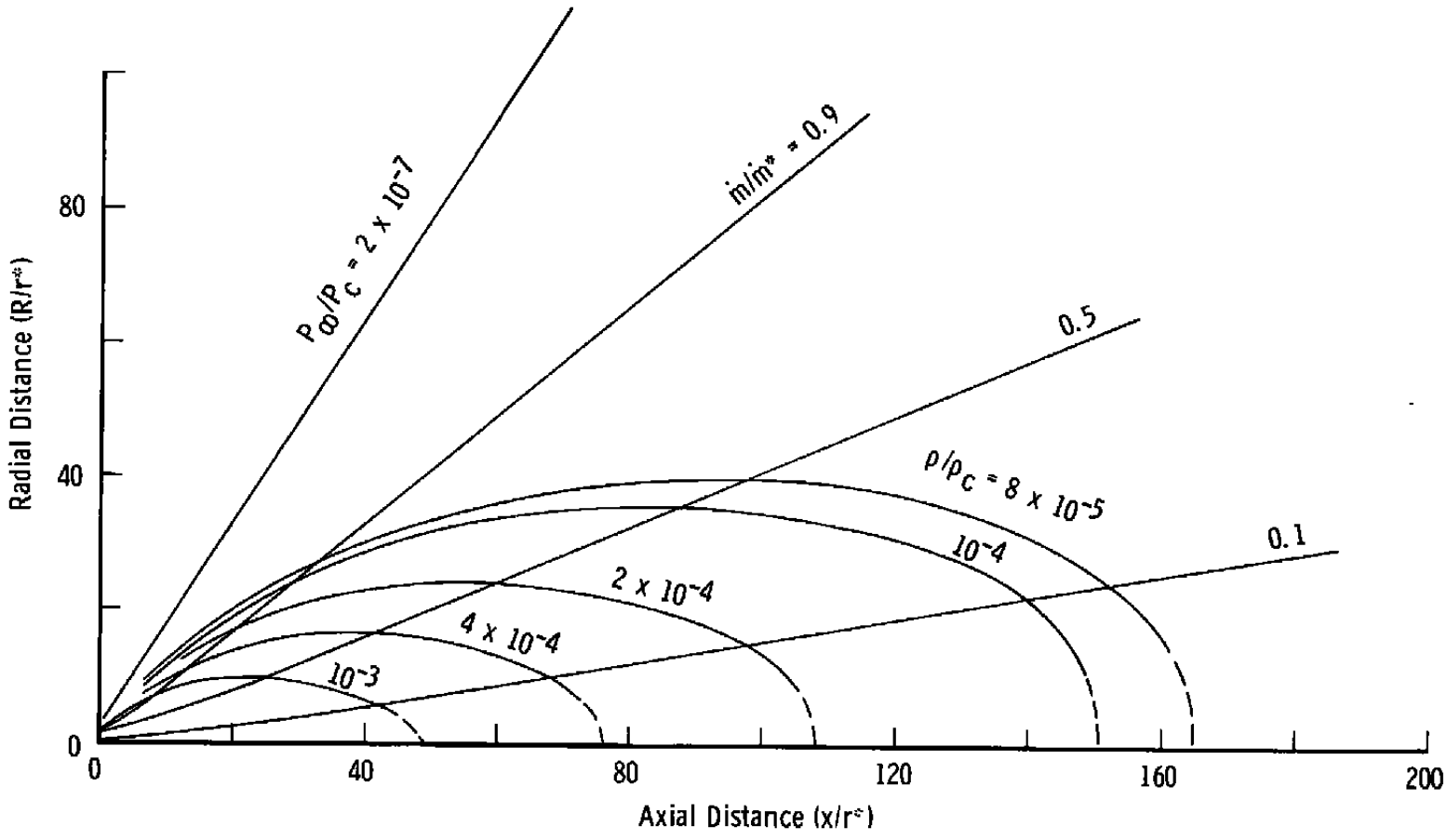

Fig. 7 Method of Characteristics Flow Field Solution: $A_e/A^* = 3.73$, $\gamma = 1.67$, $M_e = 3.34$

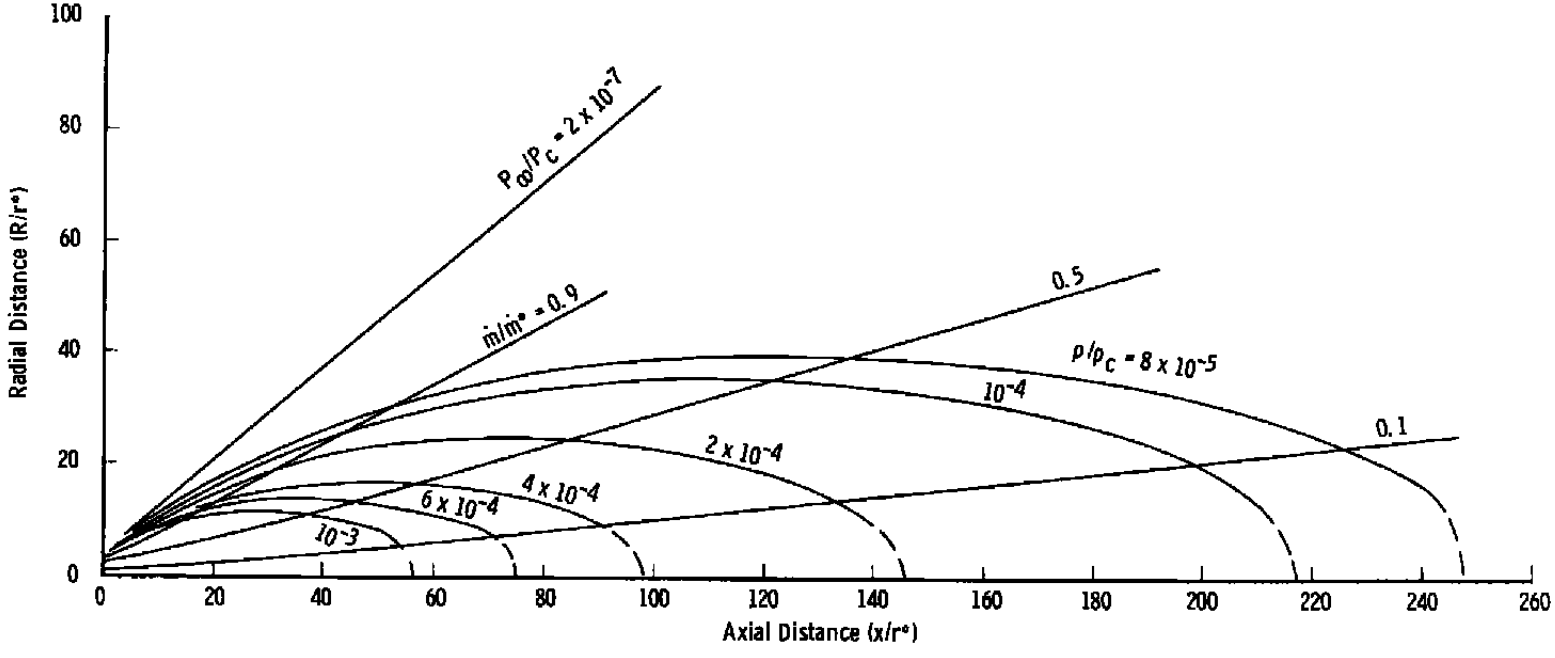

Fig. 8 Method of Characteristics Flow Field Solution; $A_e/A^* = 12.8$, $\gamma = 1.67$, $M_e = 5.56$

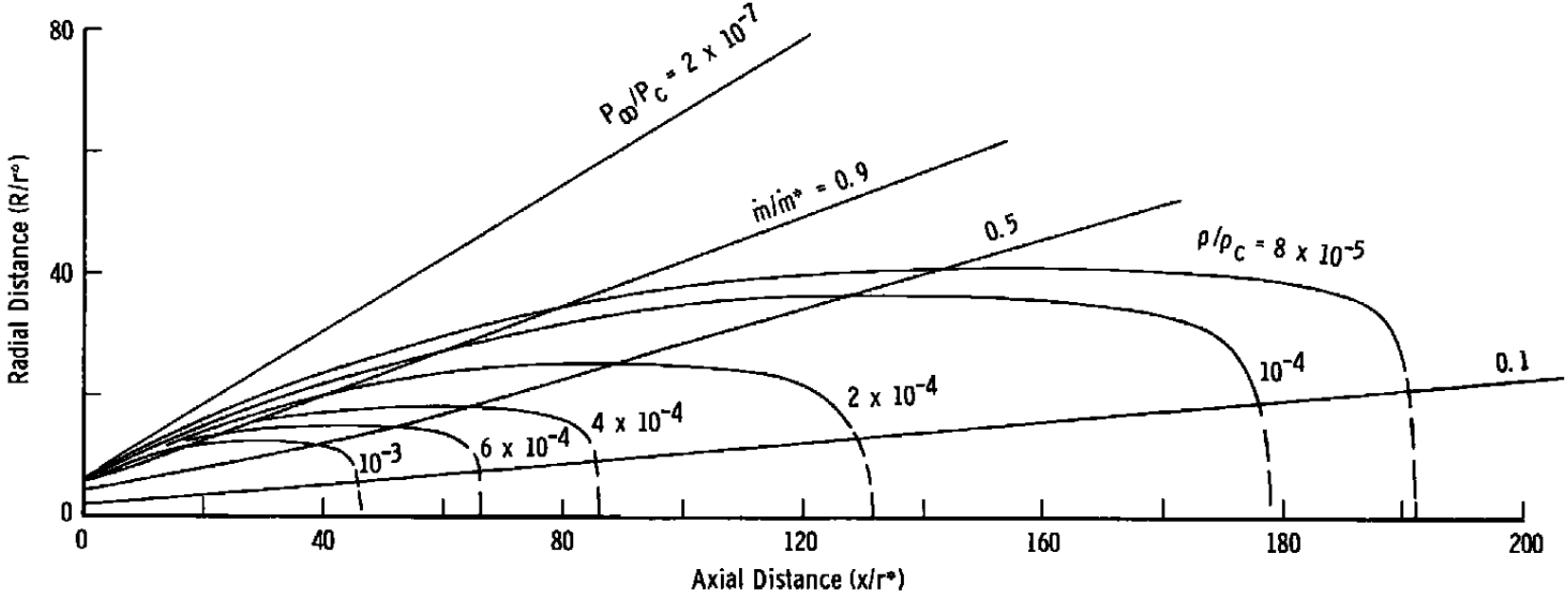

Fig. 9 Method of Characteristics Flow Field Solution; $A_e/A^* = 36.3$, $\gamma = 1.67$, $M_e = 8.14$

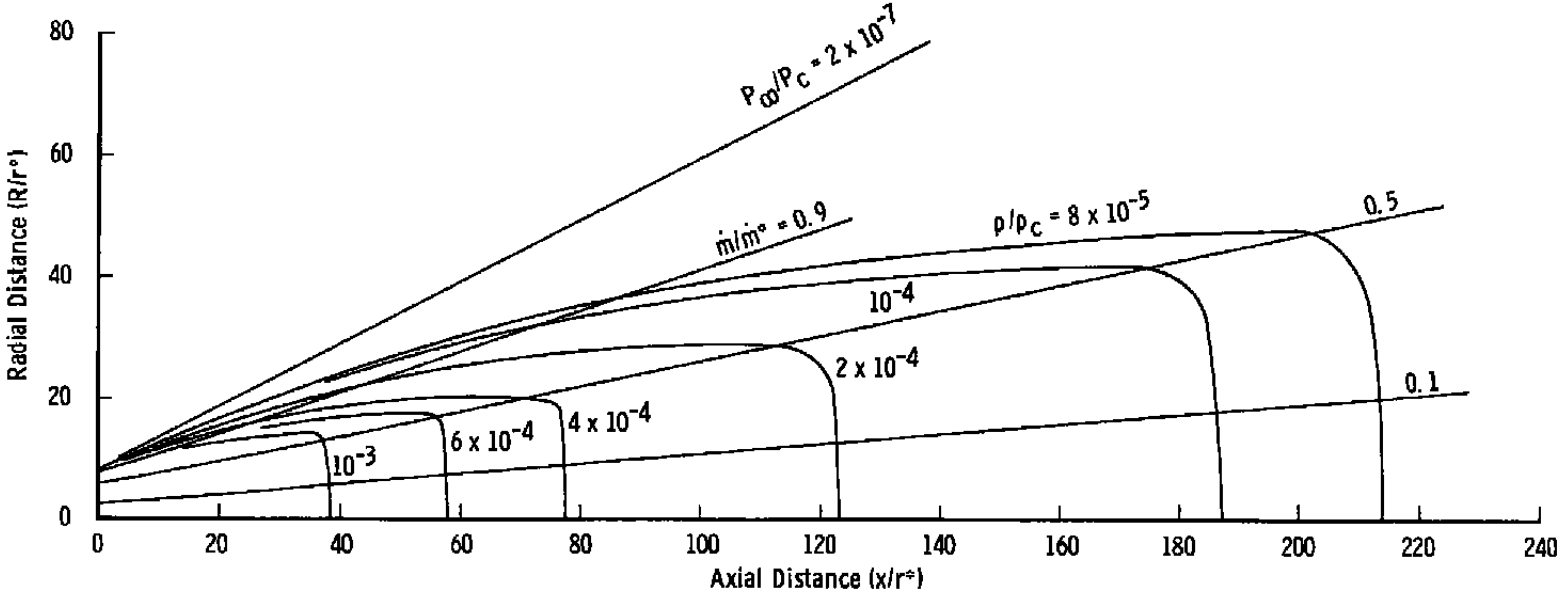

Fig. 10 Method of Characteristics Flow Field Solution; $A_e/A^* = 69.6$, $\gamma = 1.67$, $M_e = 10.24$

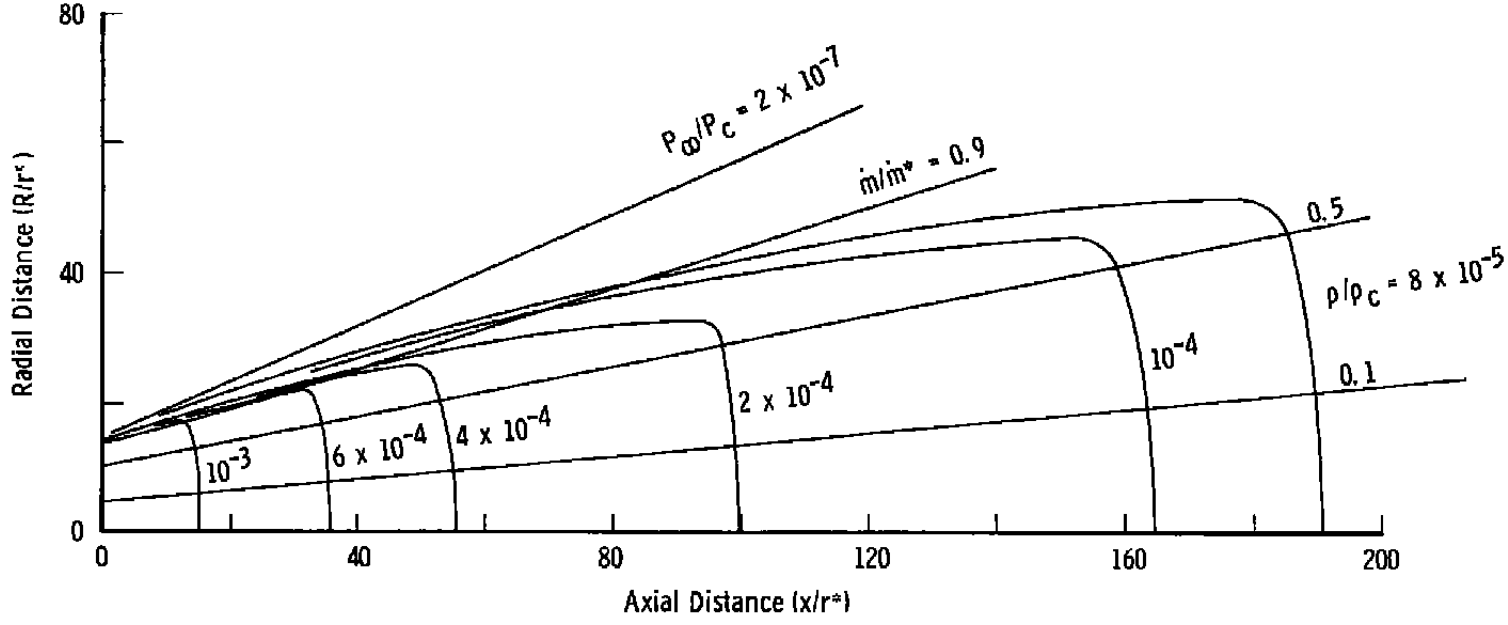

Fig. 11 Method of Characteristics Flow Field Solution; $A_e/A^* = 207$, $\gamma = 1.67$, M_e 14.9

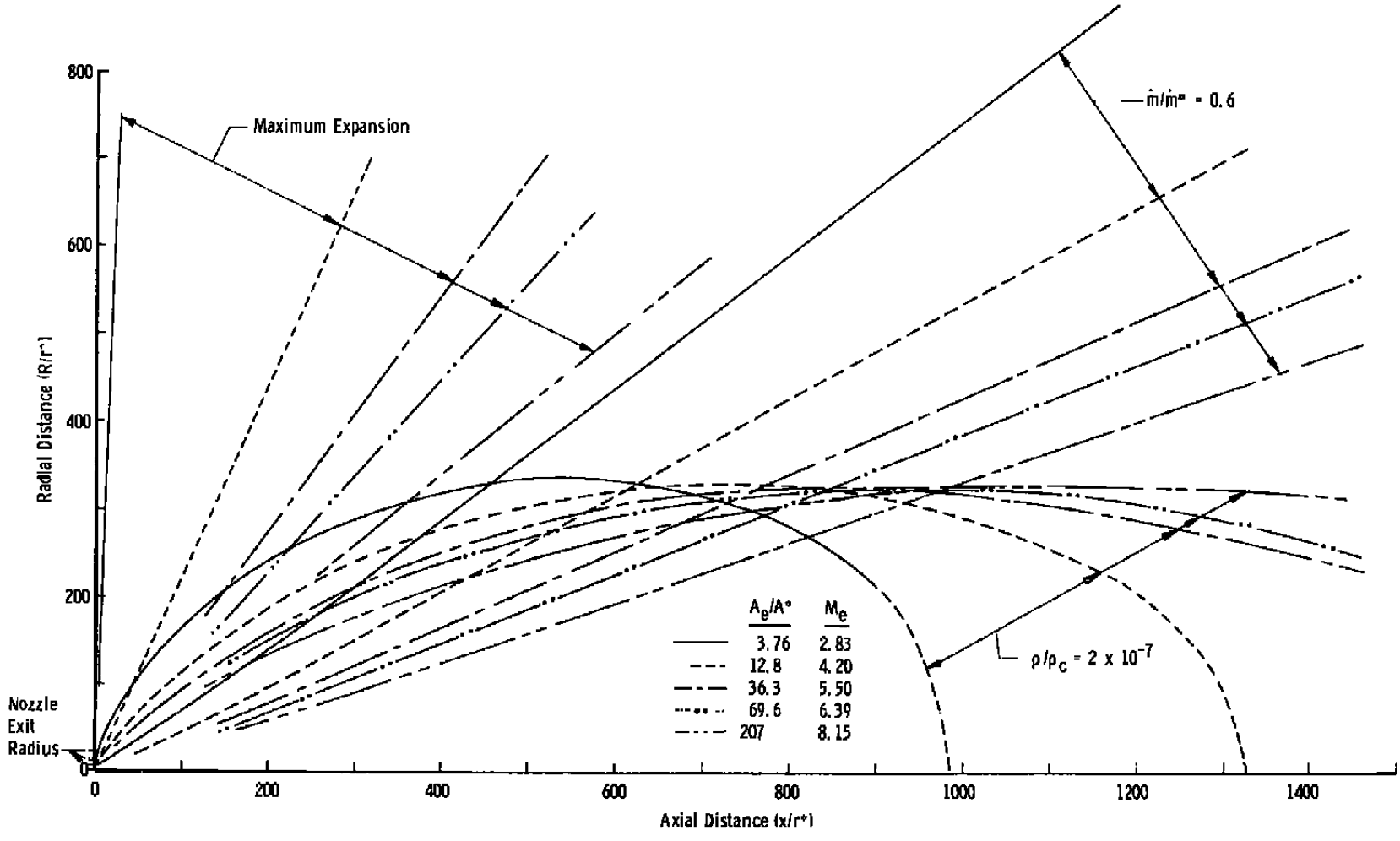

Fig. 12 Effect of Nozzle Exit Area Ratio; $P_\infty/P_c = 2 \times 10^{-8}$, $\gamma = 1.4$, $\theta_N = 15$ deg

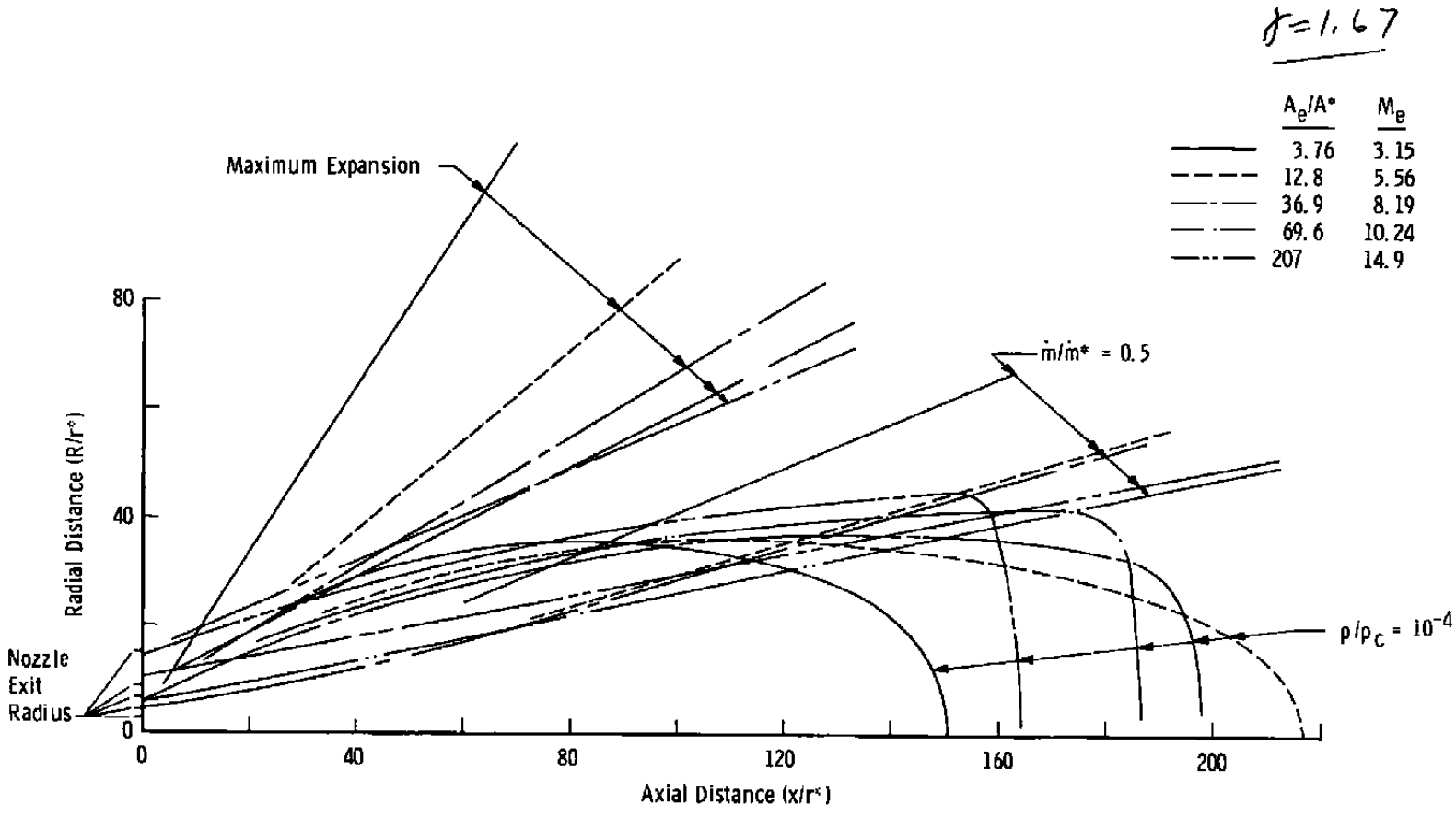

Fig. 13 Effect of Nozzle Exit Area Ratio; $P_\infty/P_c = 2 \times 10^{-7}$, $\theta_N = 15$ deg

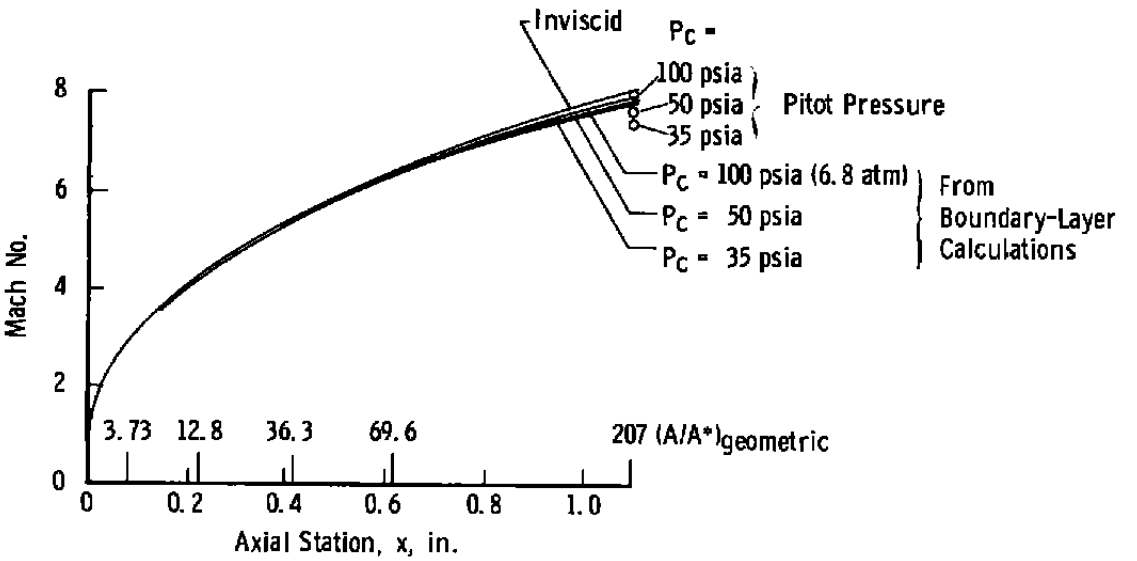

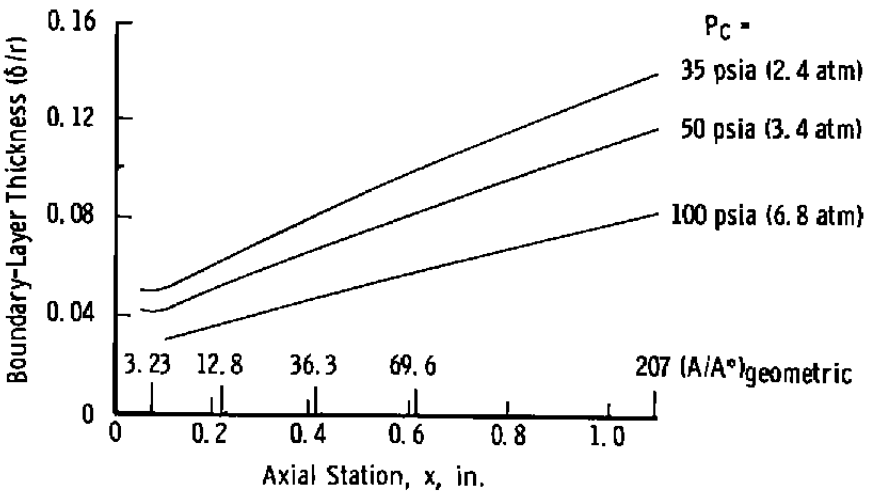

a. Nitrogen

Fig. 14 Nozzle Mach No. and Boundary Layer, γ = 1.4, 1.67

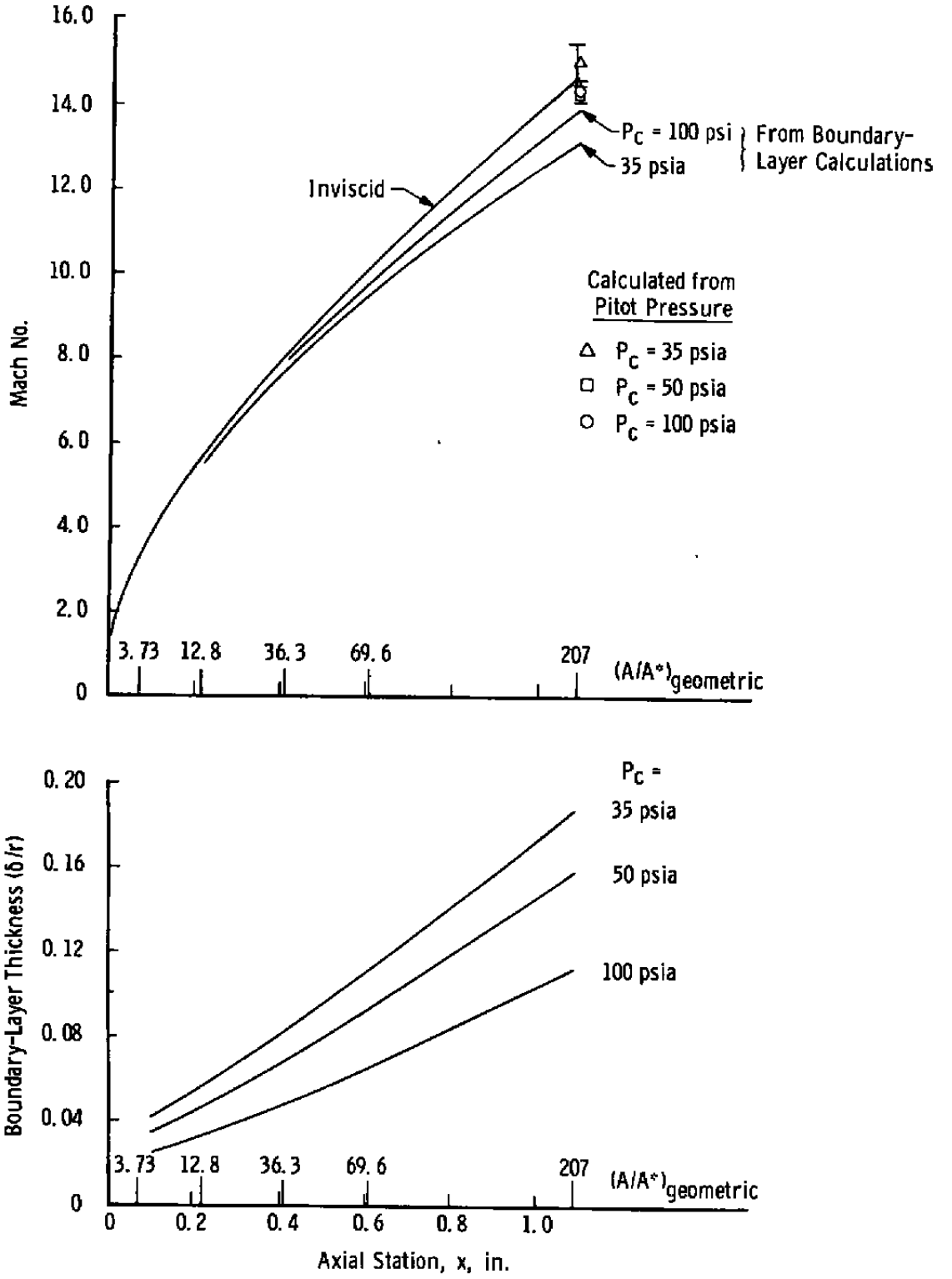

b. Argon

Fig. 14 Concluded

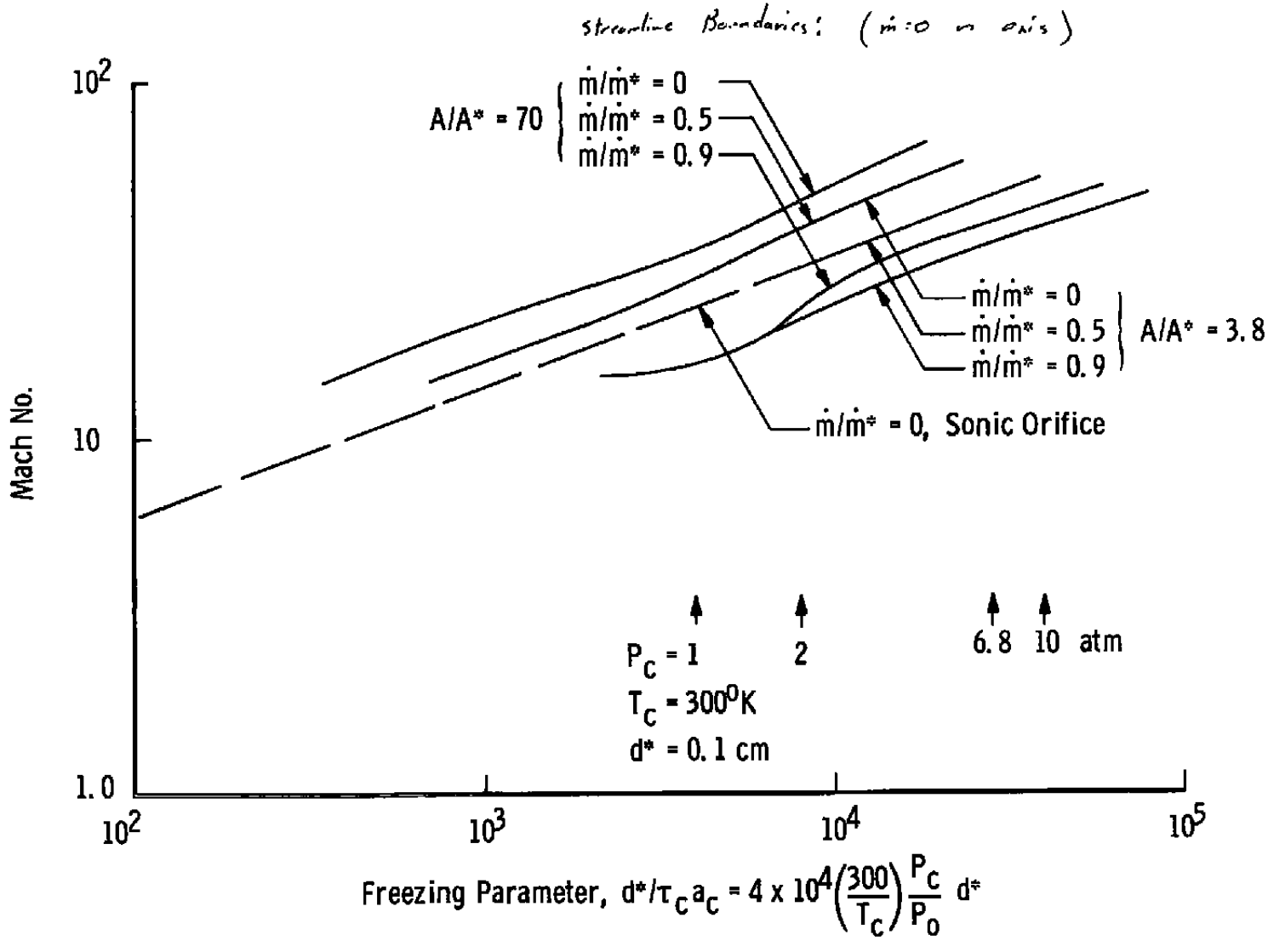

Fig. 15 Rotational Freezing, γ = 1.4

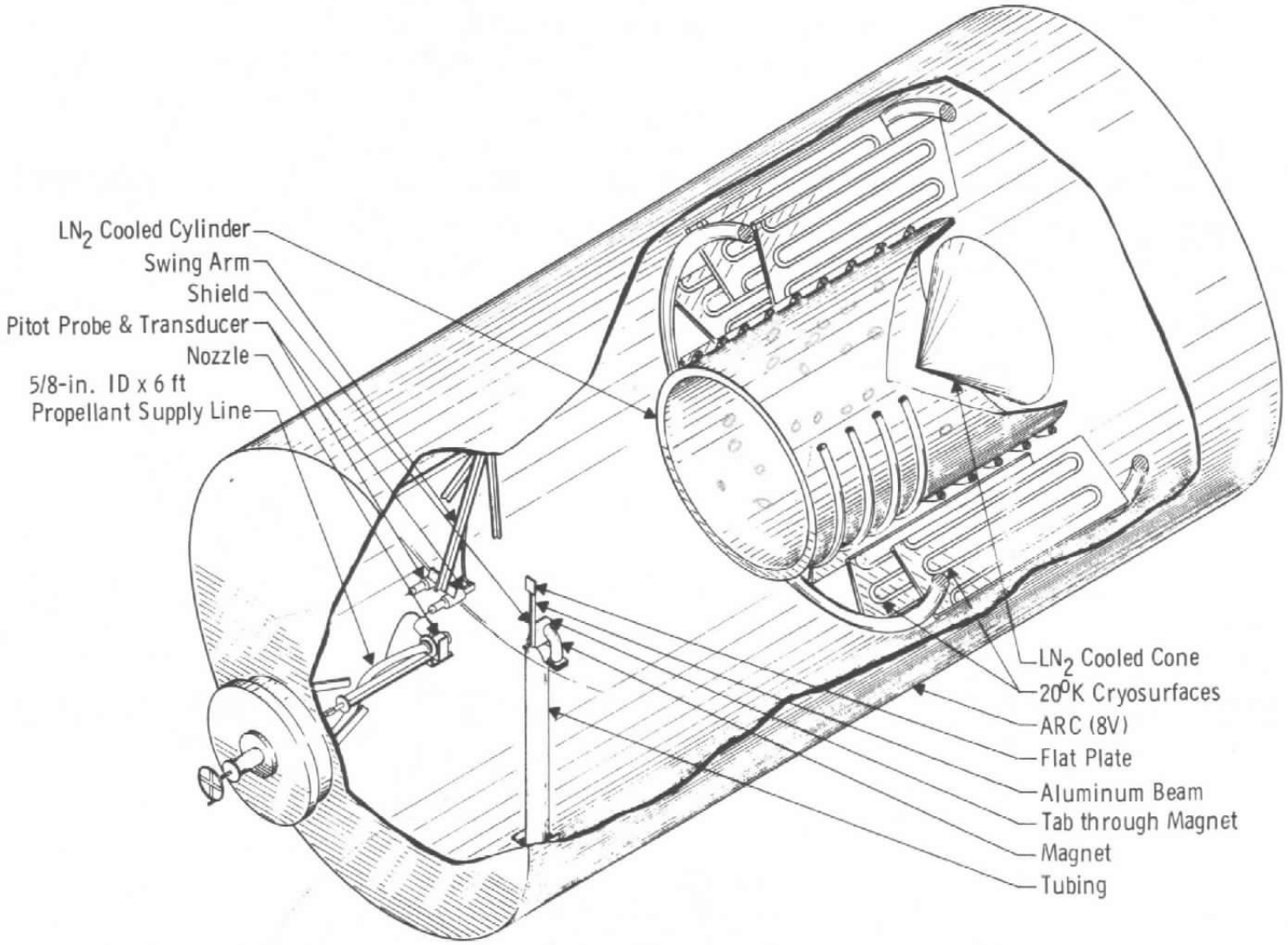

Fig. 16 Nozzle Installation – ARC (8V)

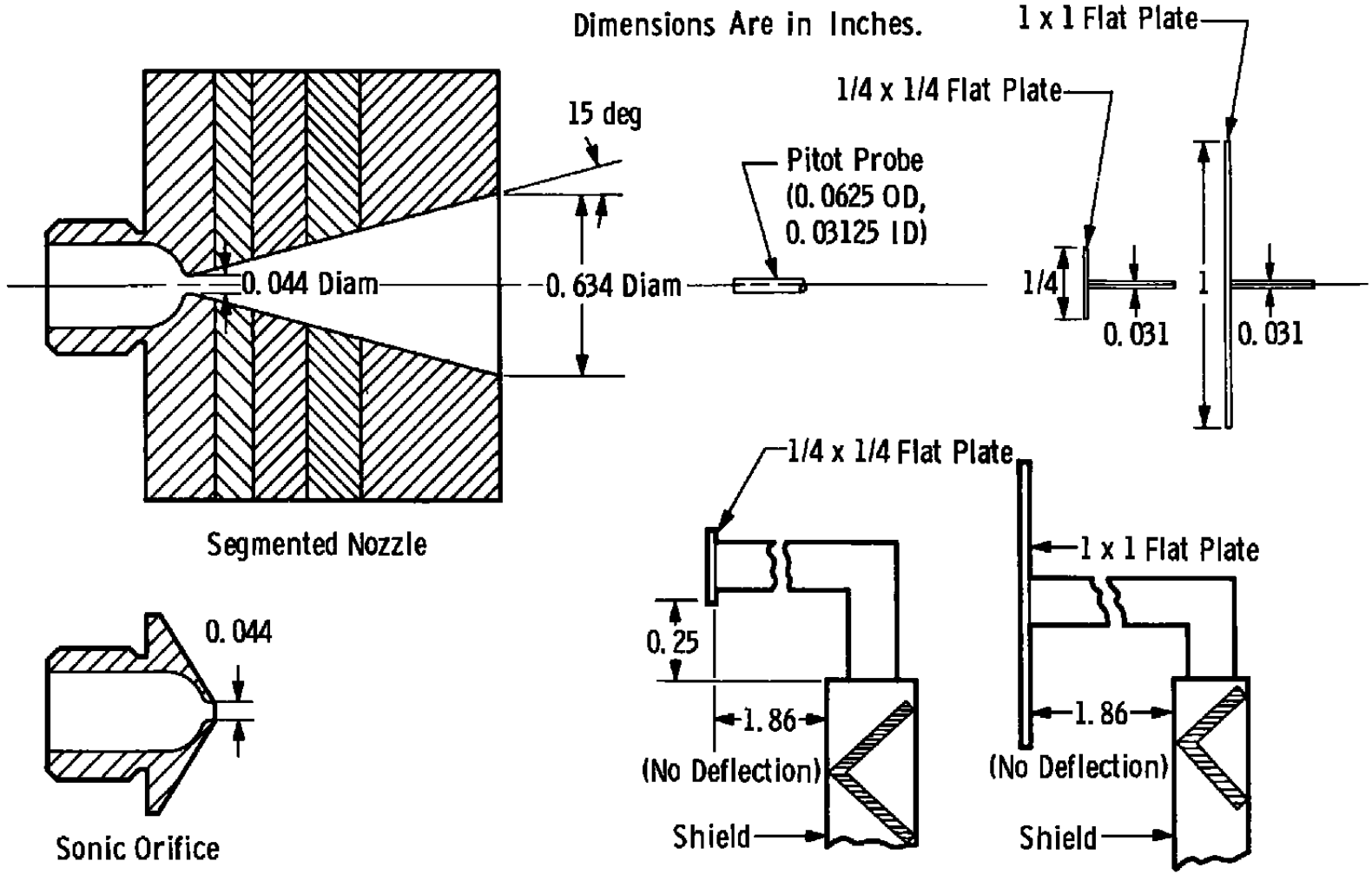

Fig. 17 Nozzle Assembly and Flat Plates

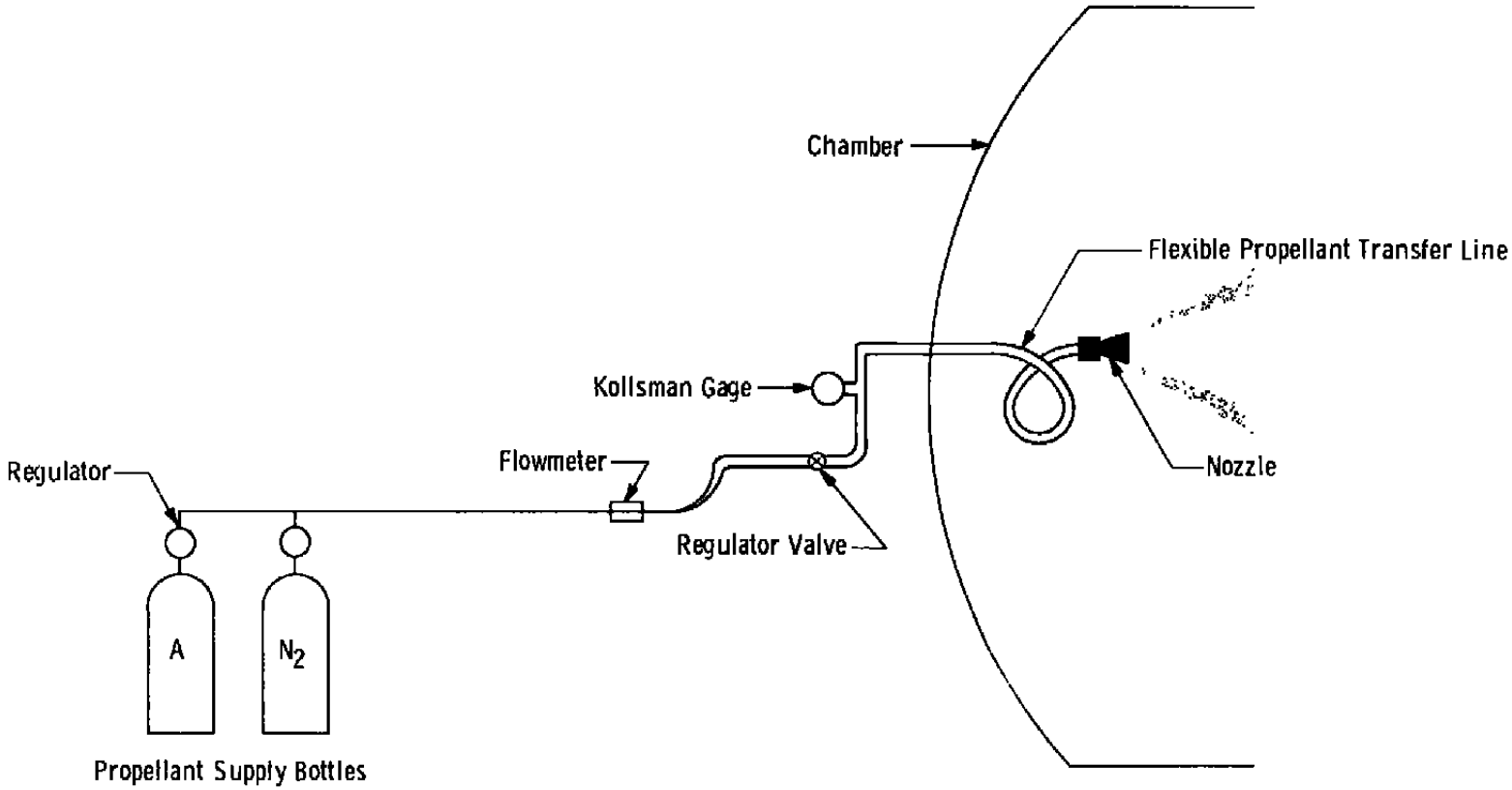

Fig. 18 Propellant Supply System

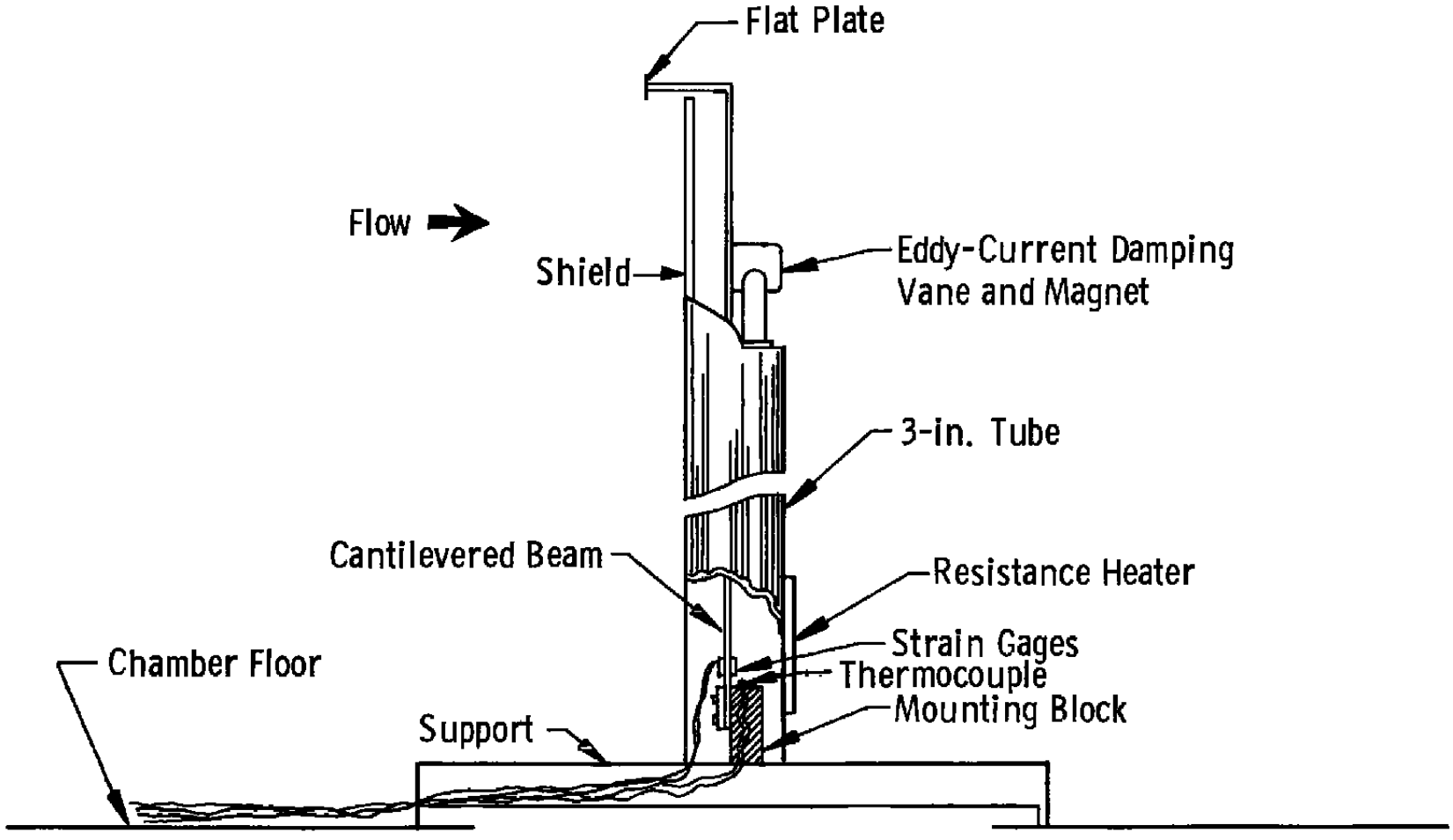

Fig. 19 Cantilevered Flat Plate

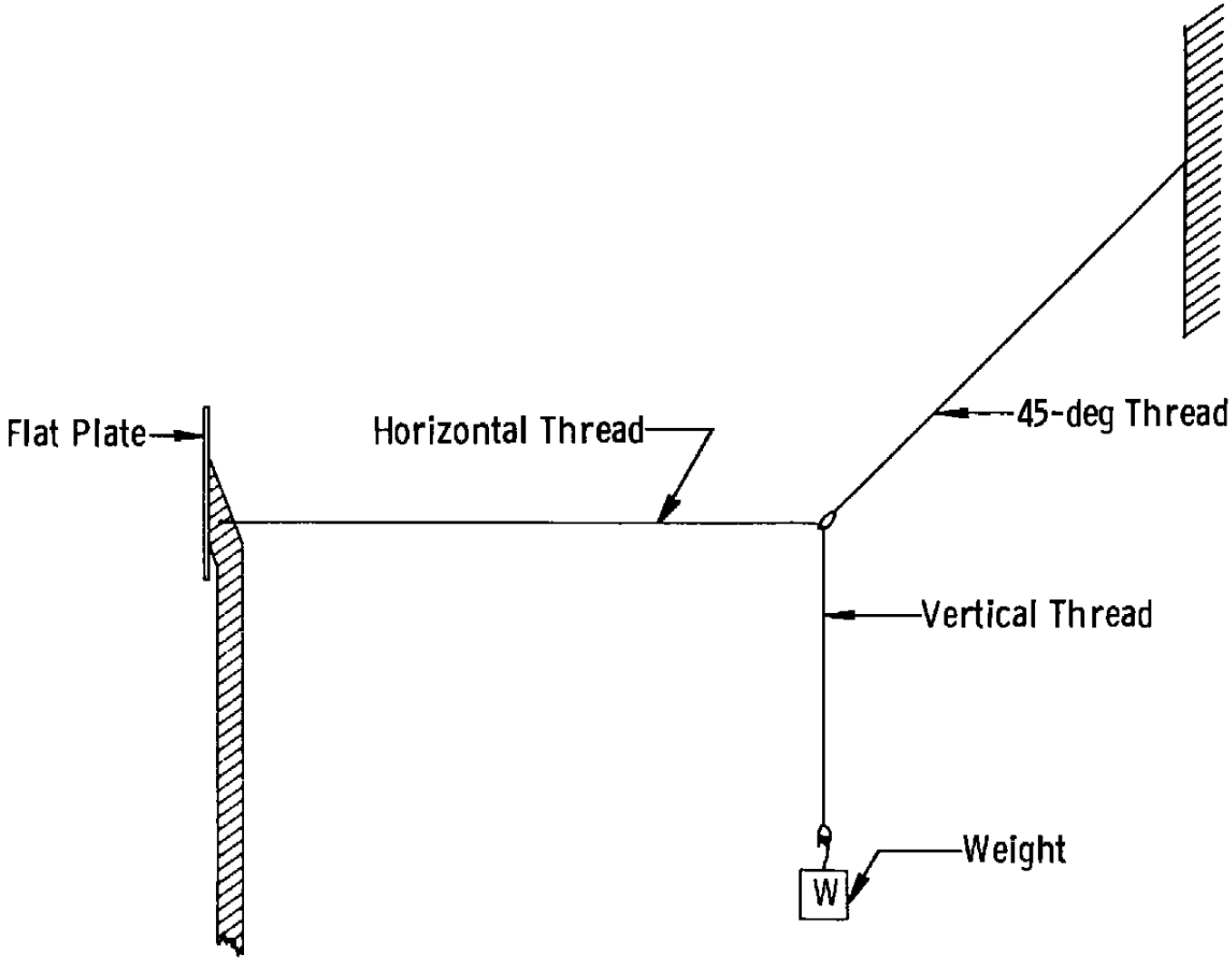

Fig. 20 Flat Plate Calibration

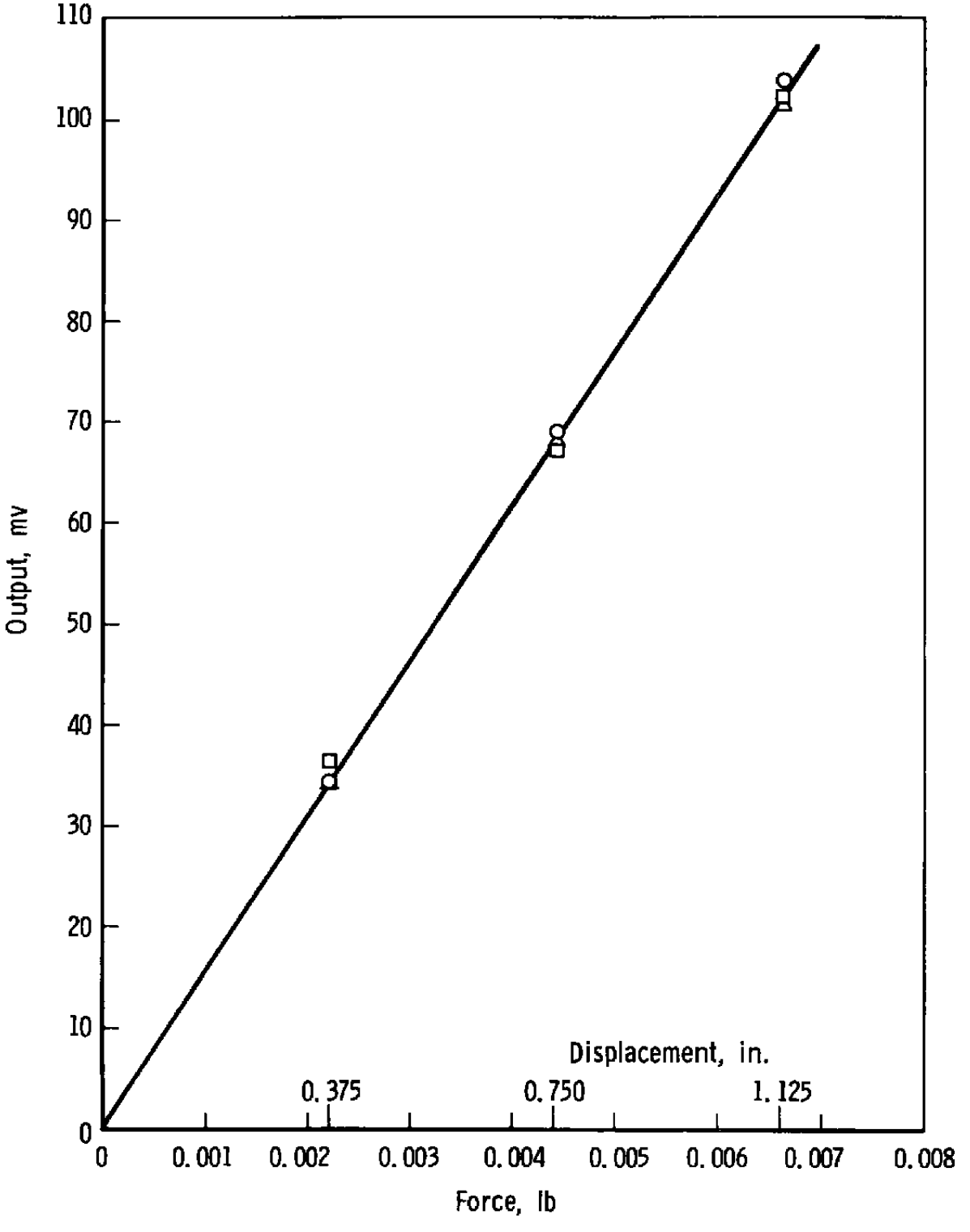

Fig. 21 Flat Plate Calibration Curve

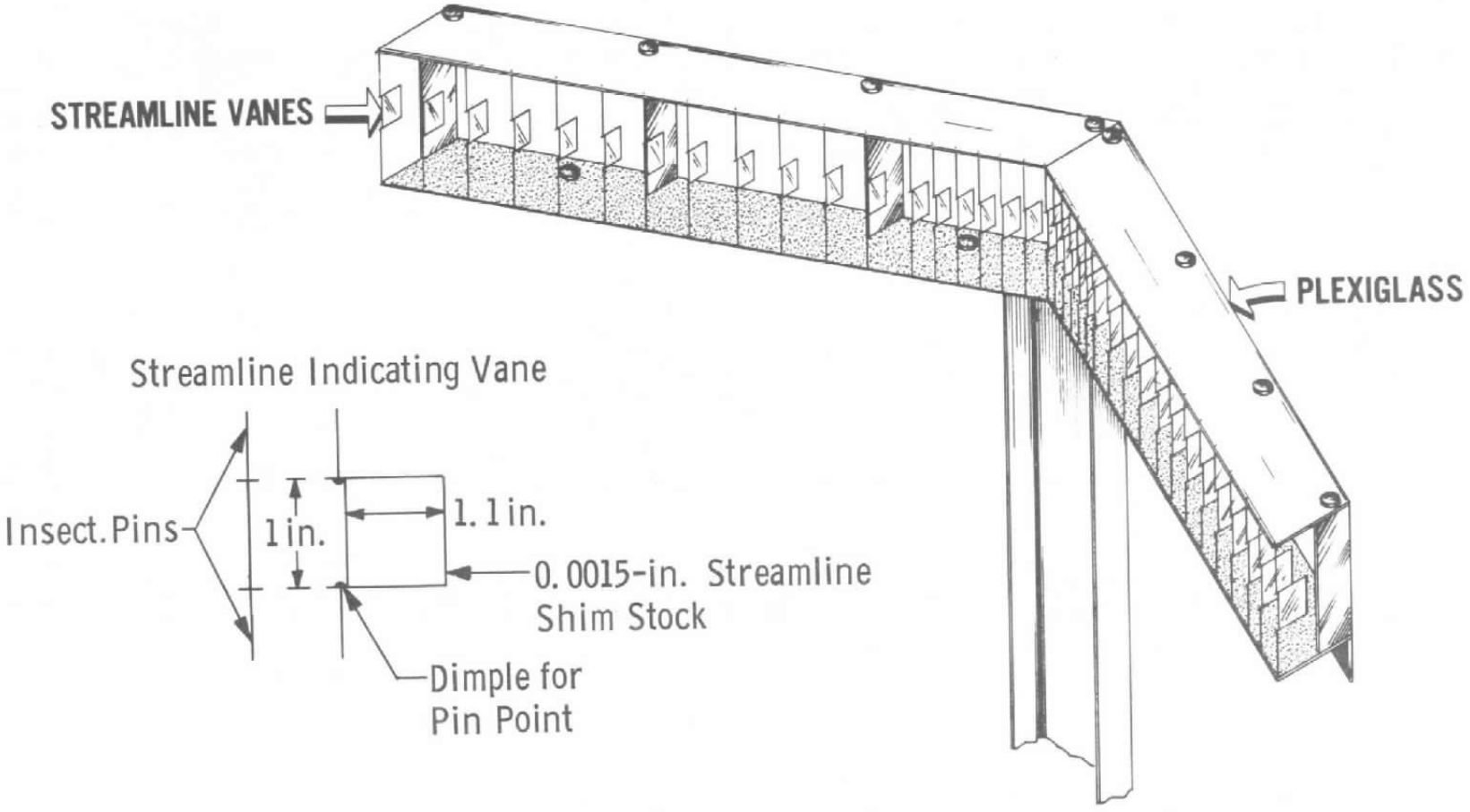

Fig. 22 Streamline Vane Assembly

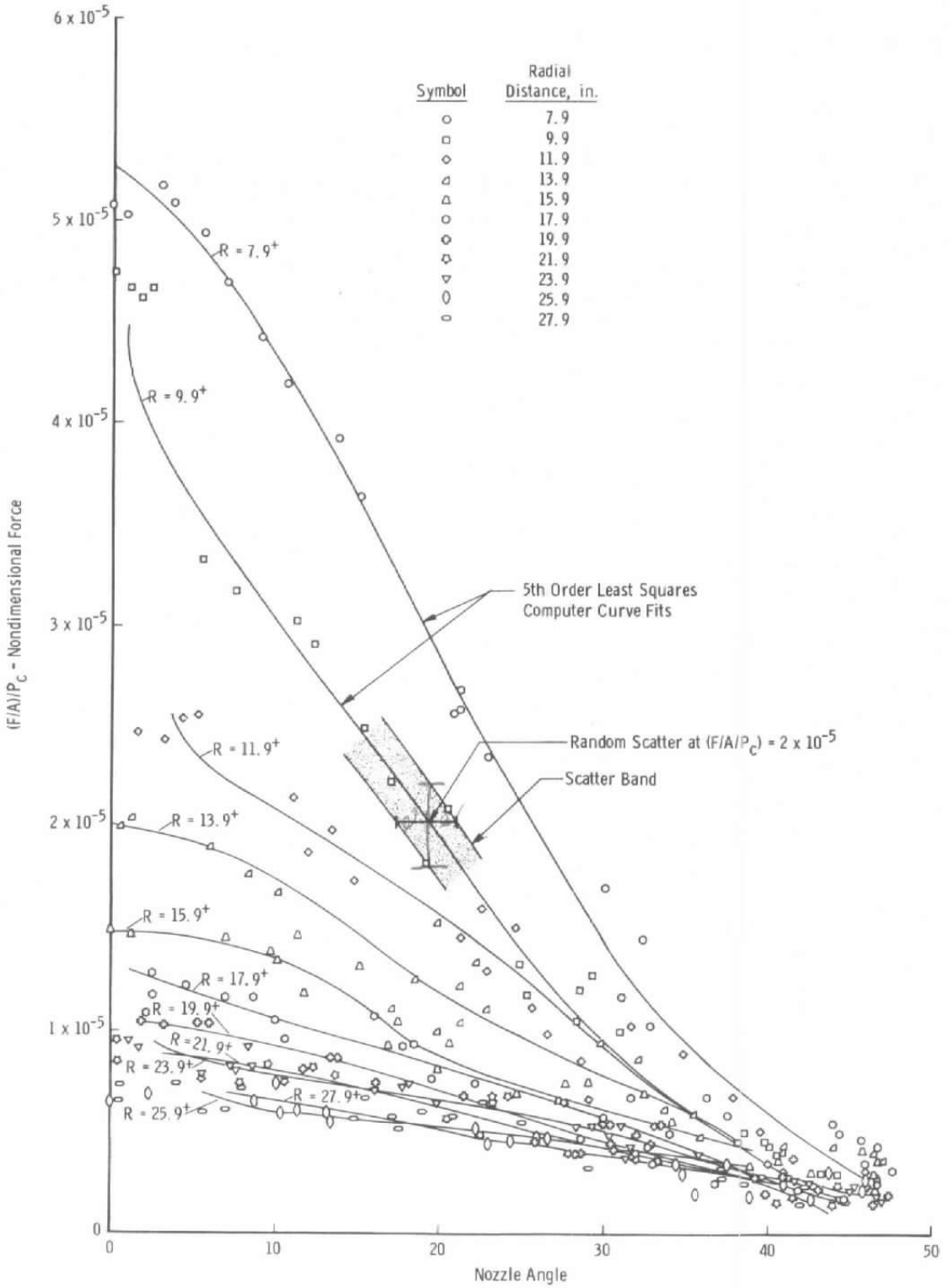

Fig. 23 Force Distribution (Typical); Nitrogen, P_c = 50 psia, A_e/A^* = 12.8, γ = 1.4, 1- x 1-in. Flat Plate

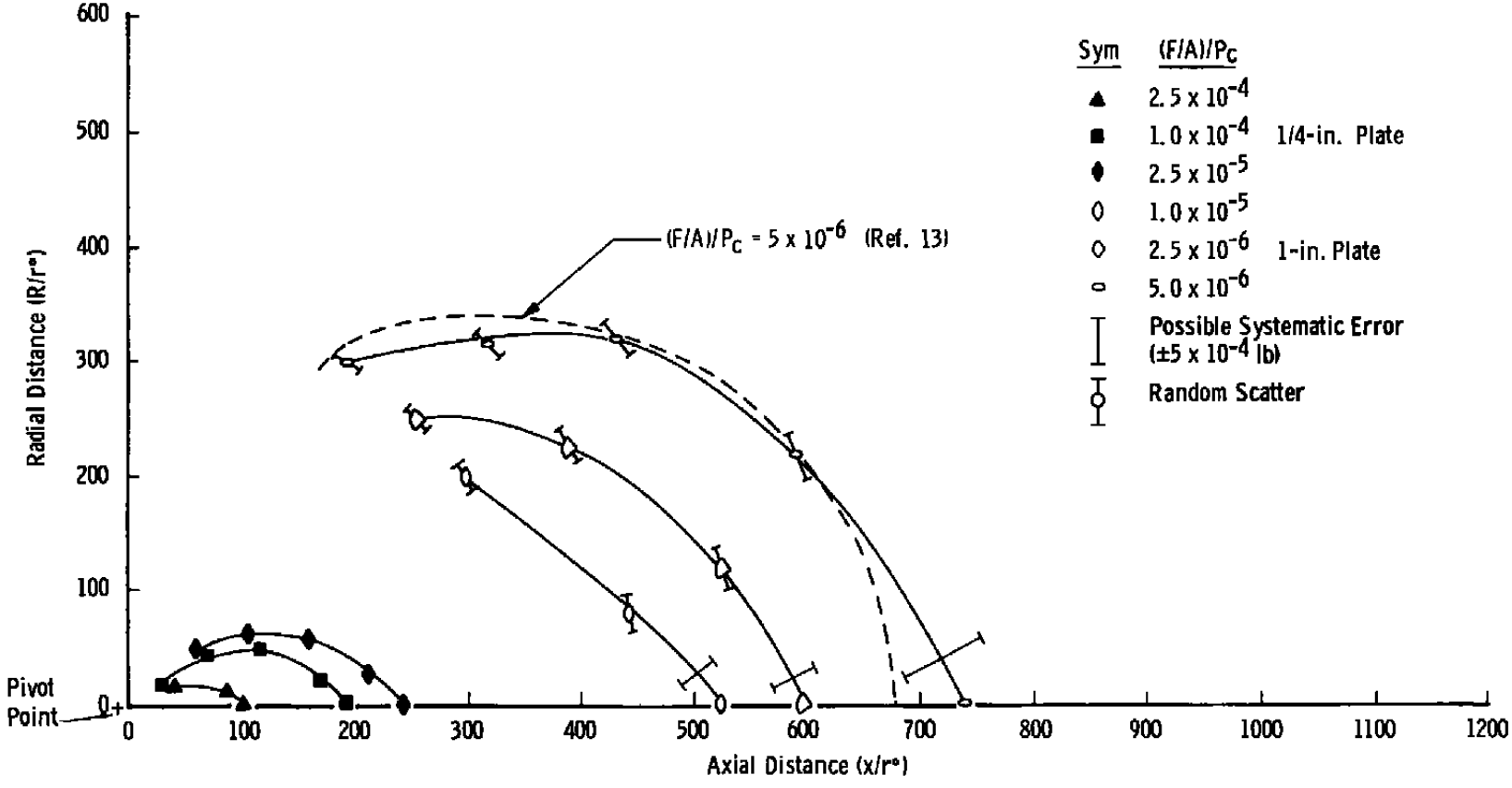

Fig. 24a Constant Force Map; $A_e/A^* = 1$, Nitrogen, $P_c = 100$ psia

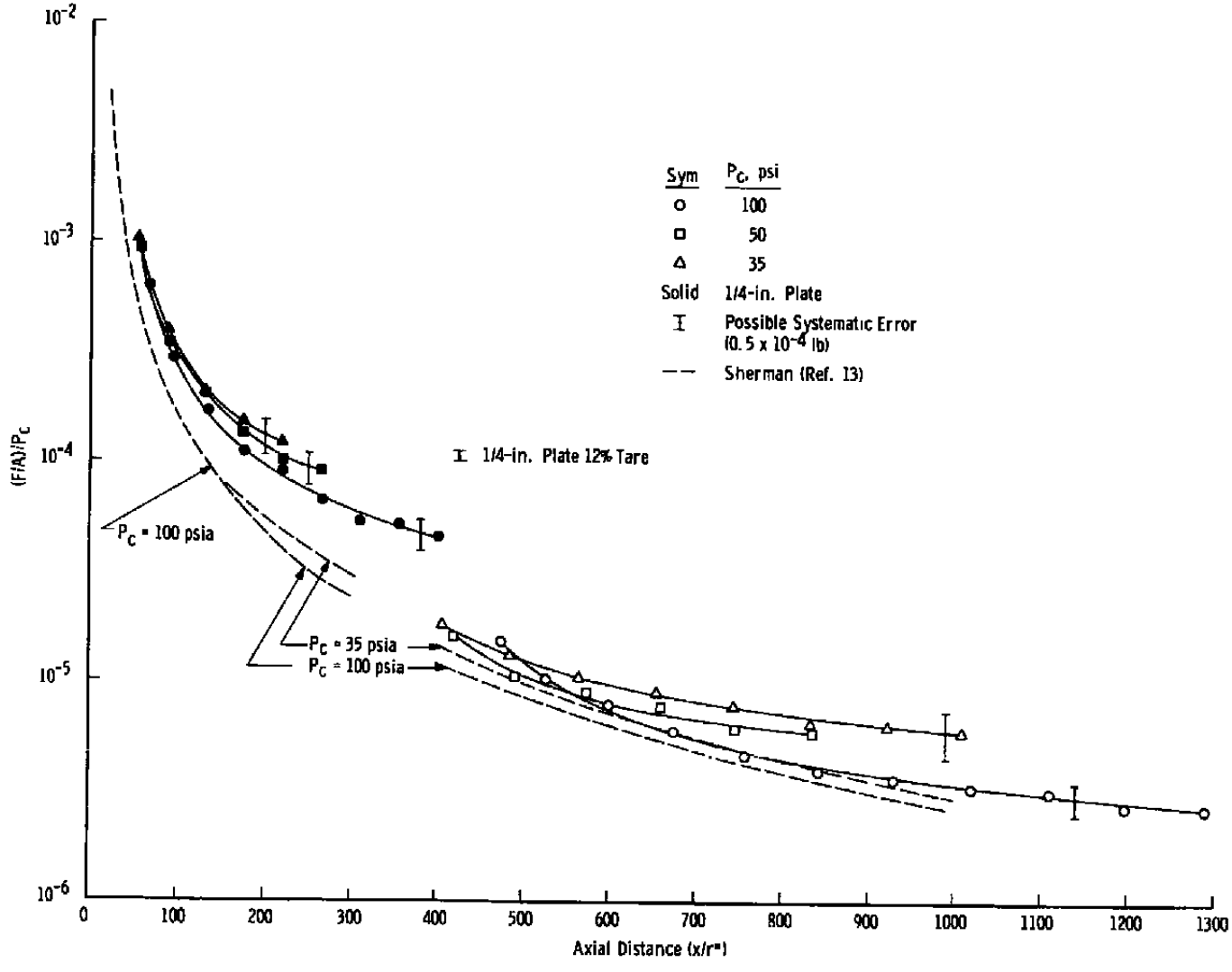

Fig. 24b Axial Distribution of Flat Plate Force; A_e/A^* = 1.0, Nitrogen

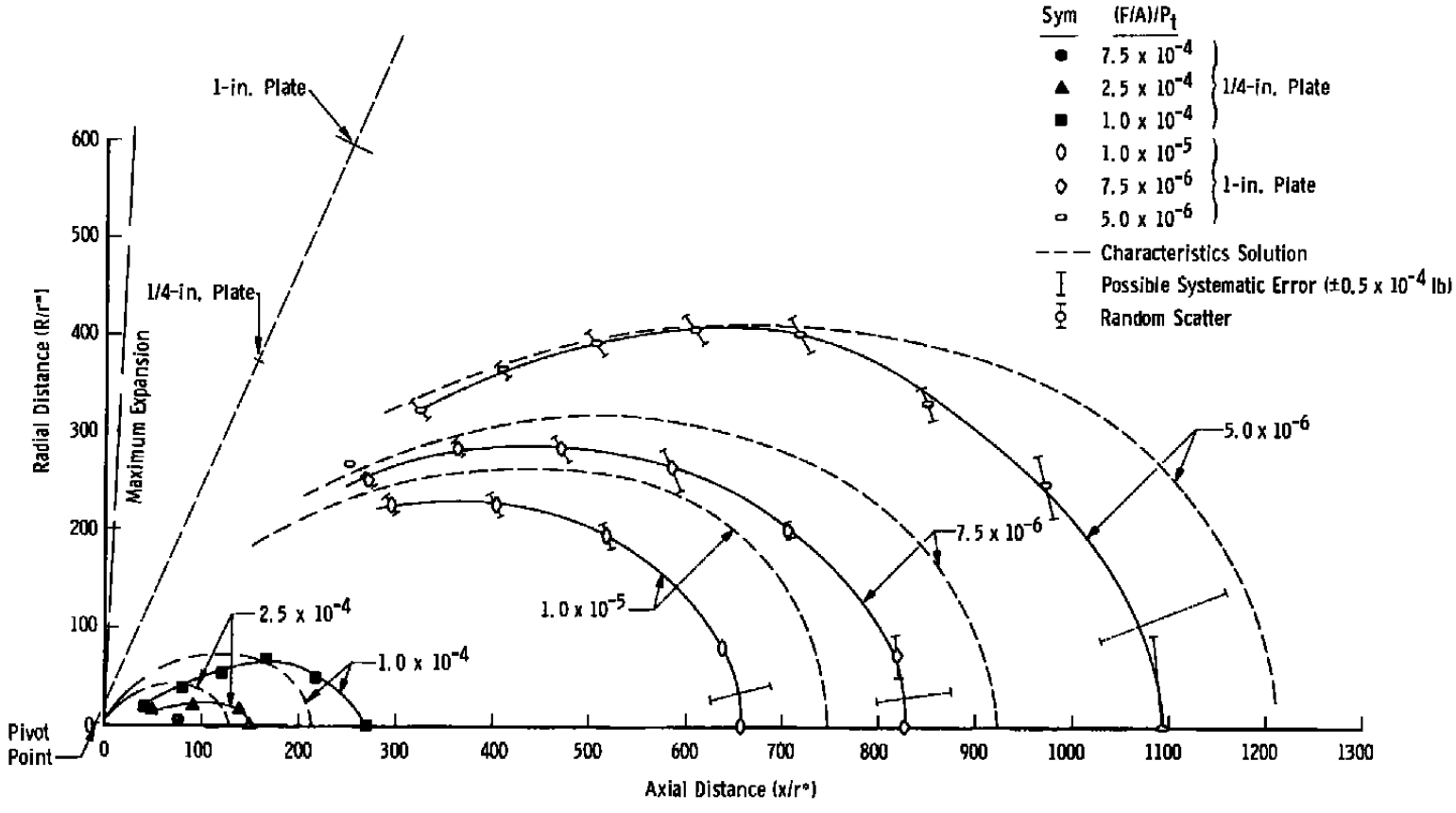

Fig. 25a Constant Force Map; A_e/A^* = 3.73, Nitrogen, P_c = 100 psia

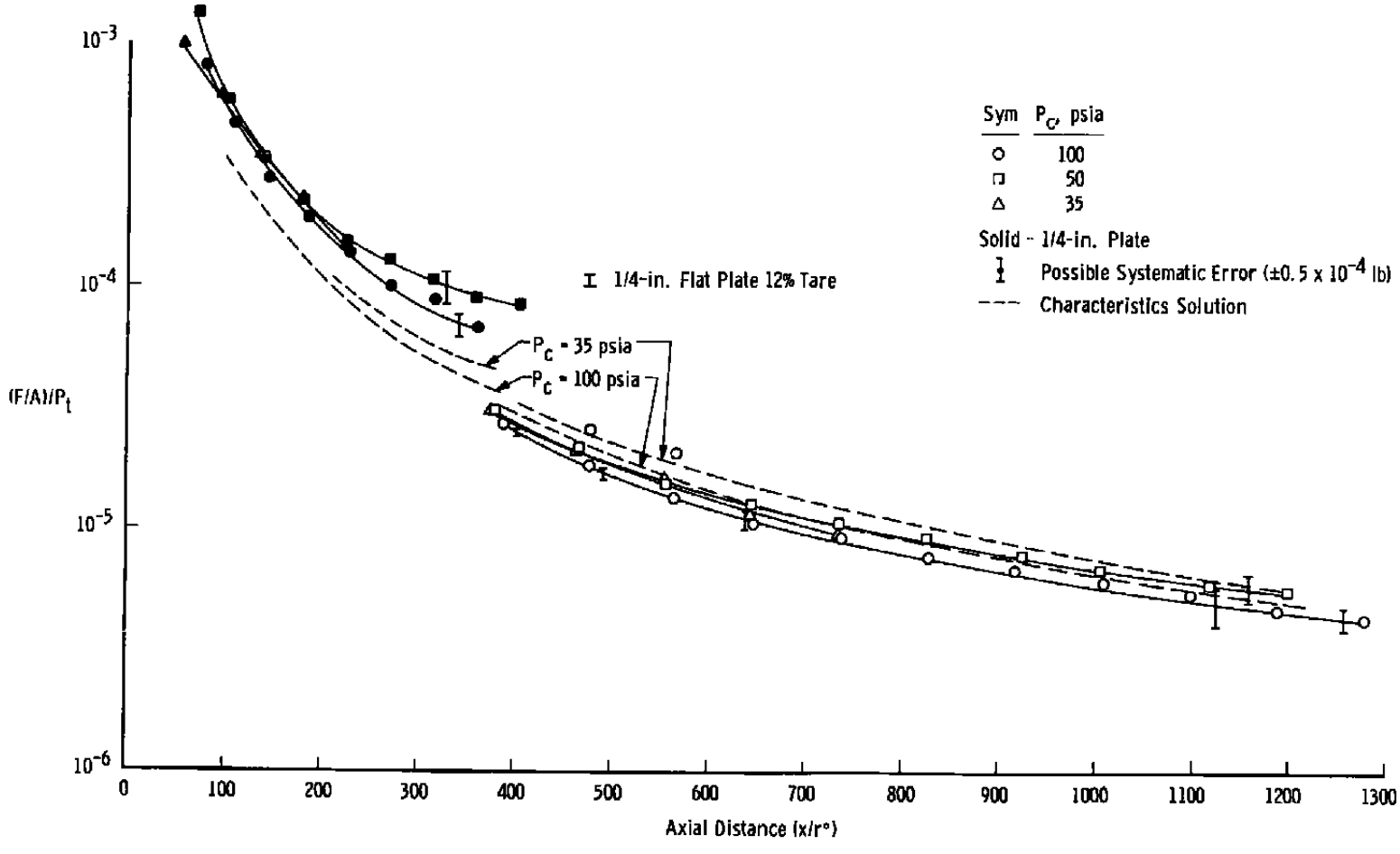

Fig. 25b Axial Distribution of Flat Plate Force; A_e/A^* = 3.73, Nitrogen

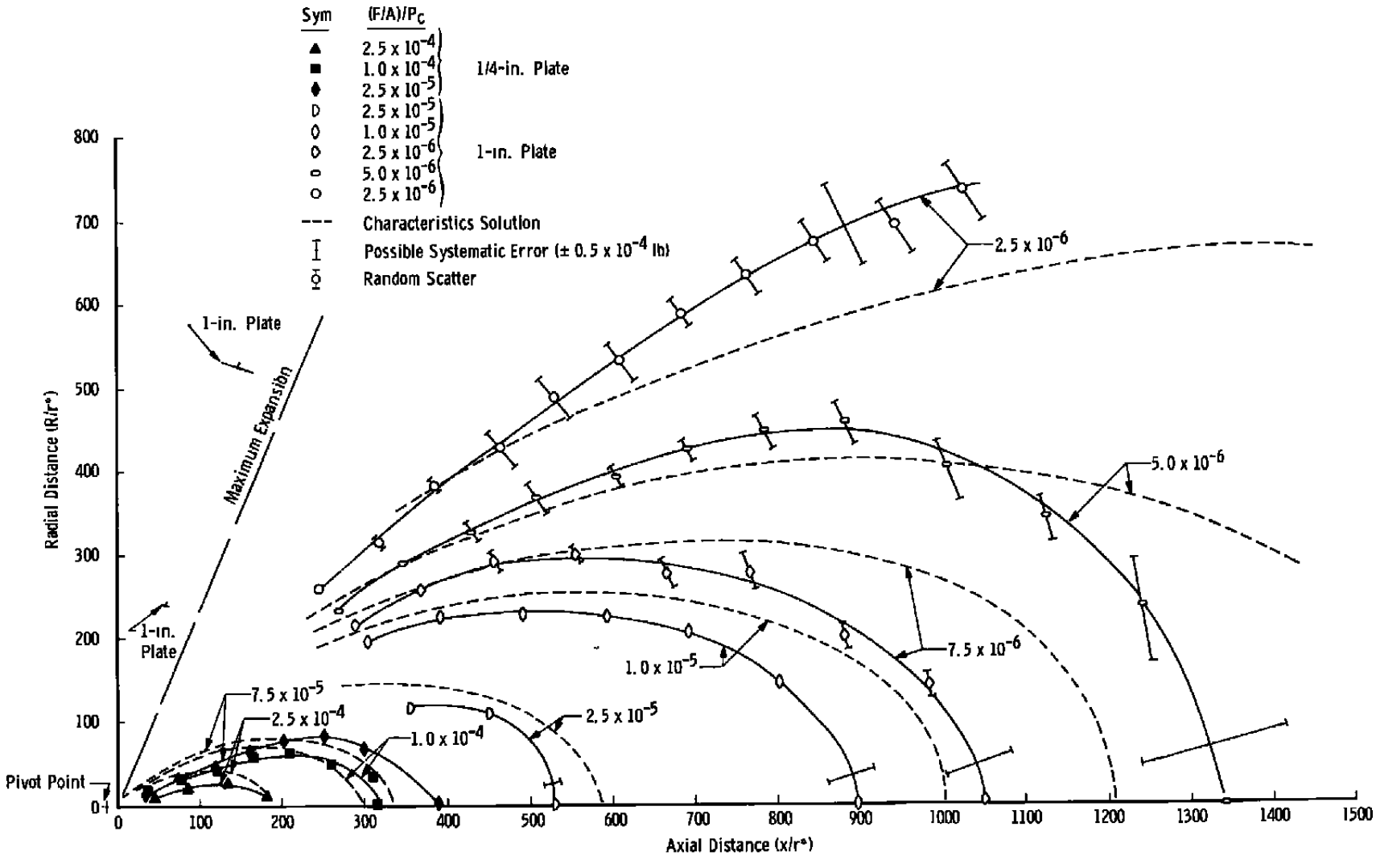

Fig. 26a Constant Force Map; A_e/A^* = 12.8, Nitrogen, P_c = 100 psia

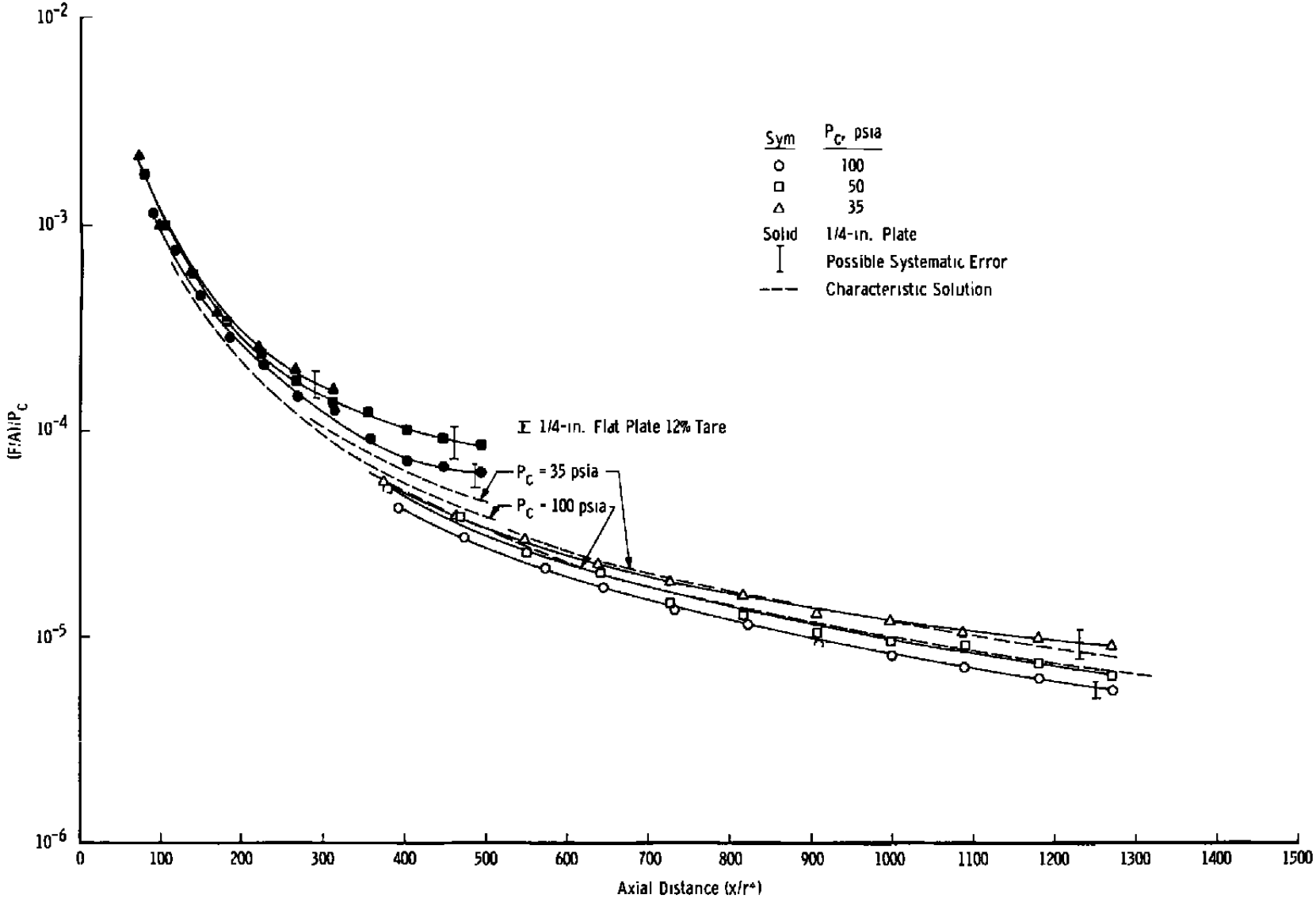

Fig. 26b Axial Distribution of Flat Plate Force; A_e/A^* = 12.8

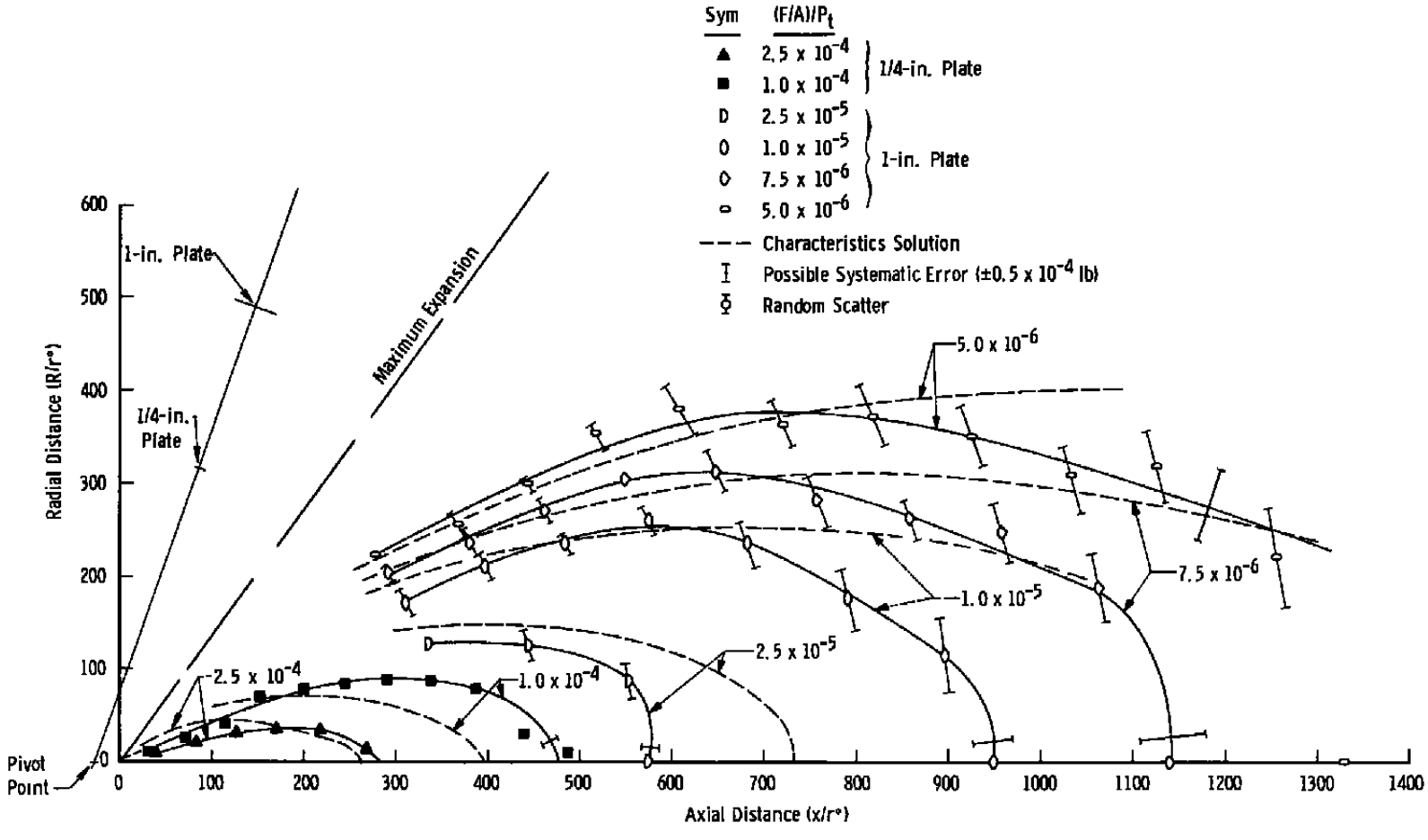

Fig. 27a Constant Force Map; $A_e/A^* = 36.3$, Nitrogen, $P_c = 100$ psia

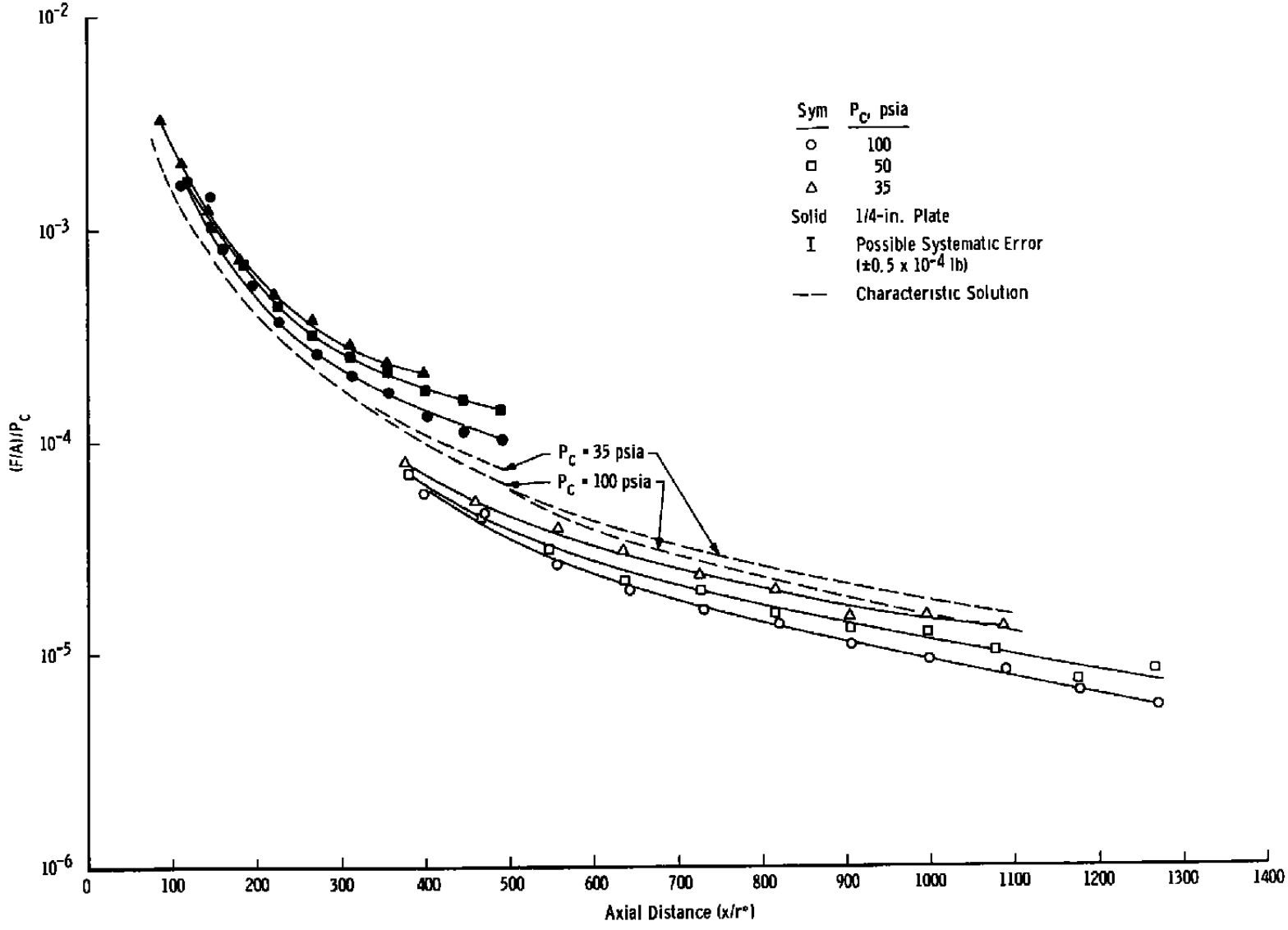

Fig. 27b Axial Distribution of Flat Plate Force; A_e/A^* = 36.3

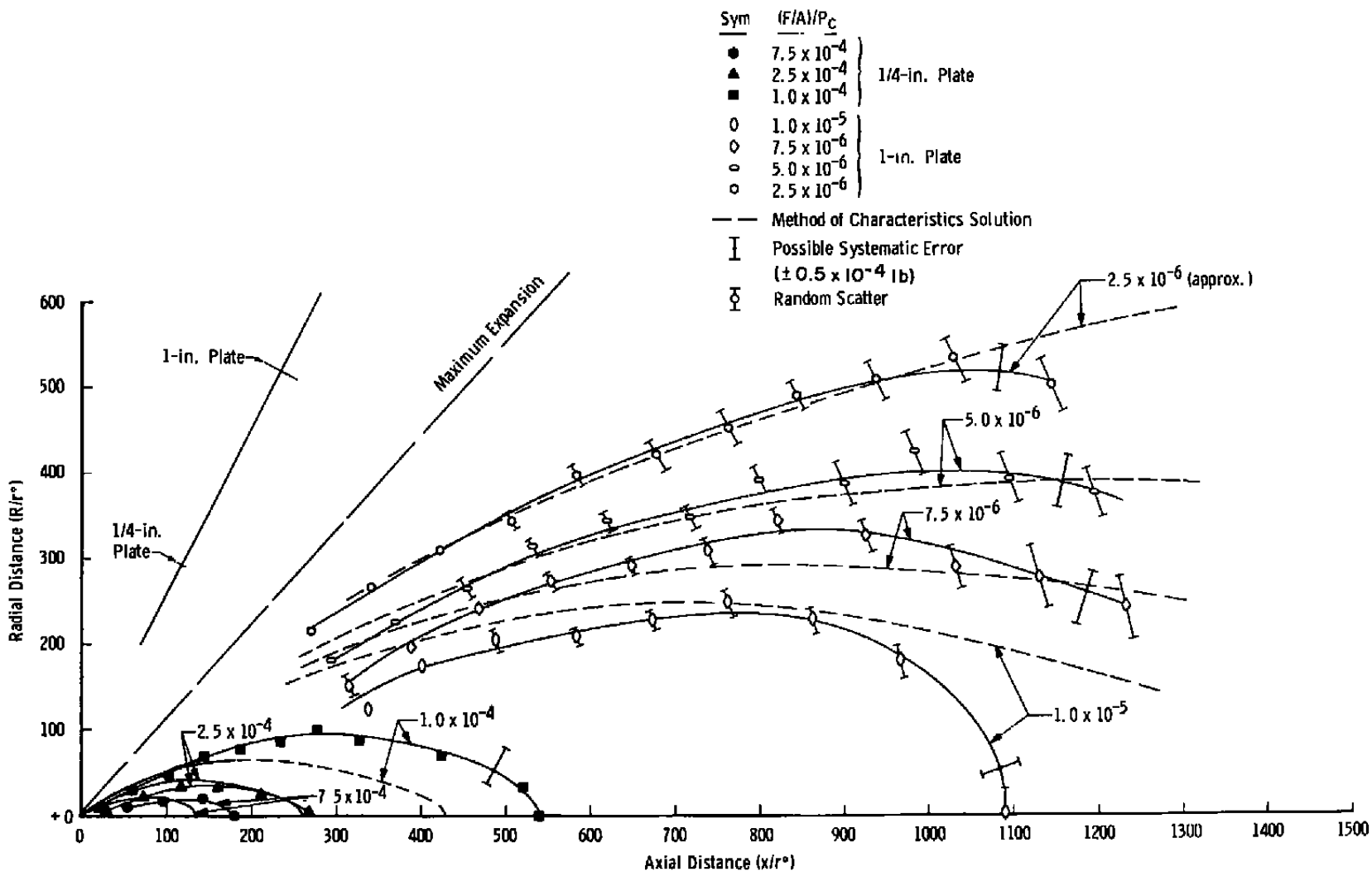

Fig. 28a Axial Distribution of Flat Plate Force; $A_e/A^* = 69.6$, Nitrogen, $P_c = 100$ psi

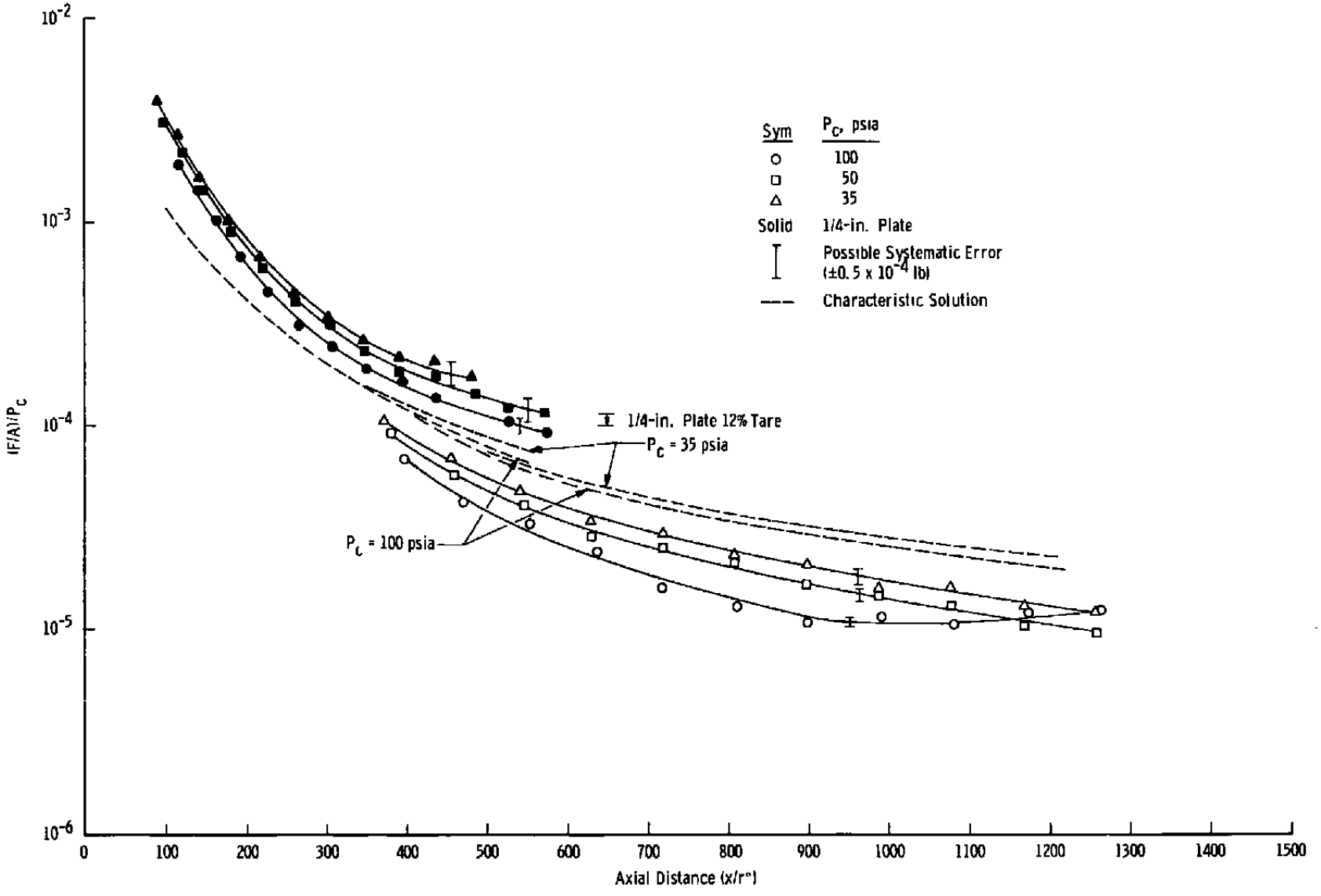

Fig. 28b Axial Distribution of Flat Plate Force; A_e/A^* = 69.6 , Nitrogen

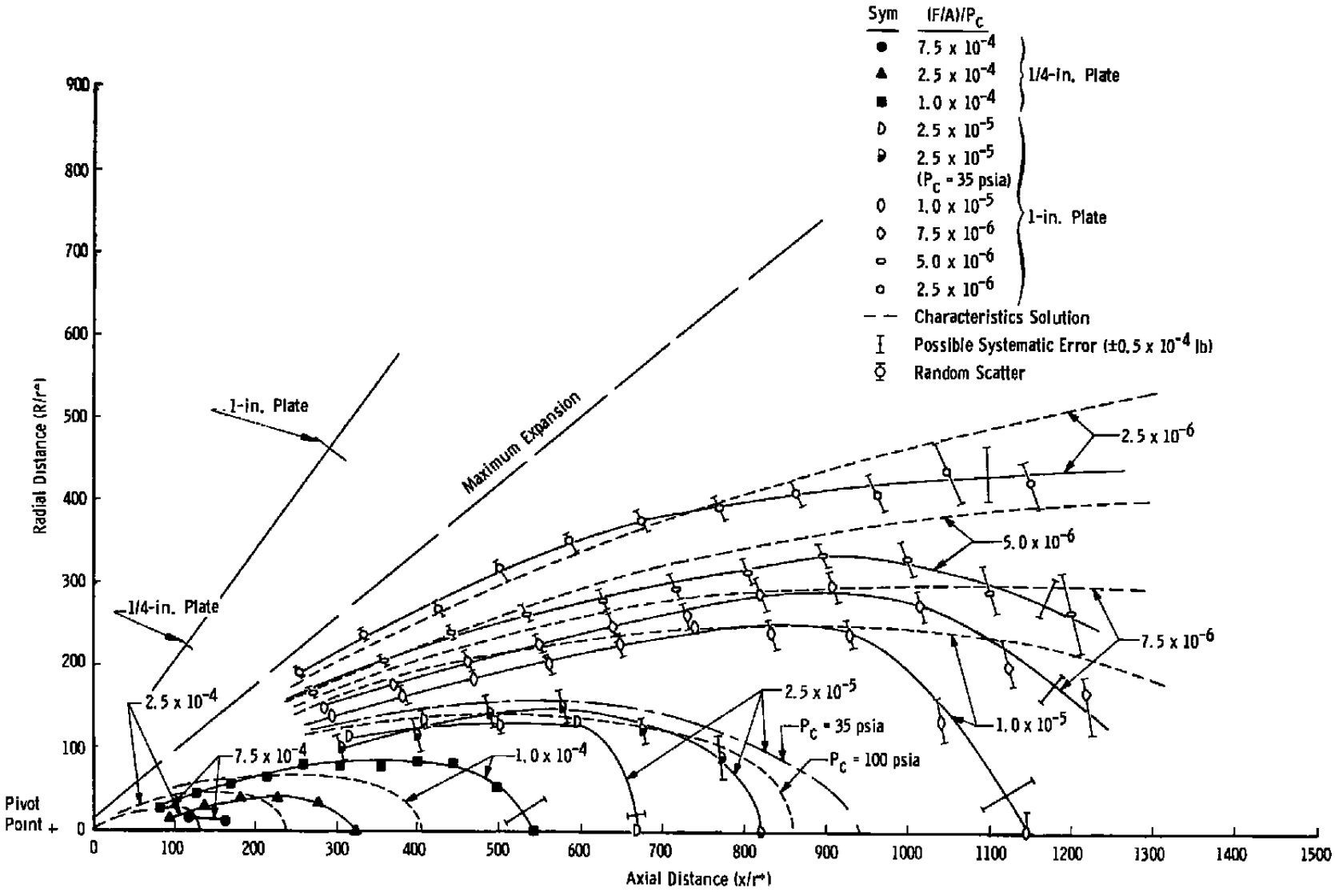

Fig. 29a Constant Force Map; $A_e/A^* = 207$, Nitrogen

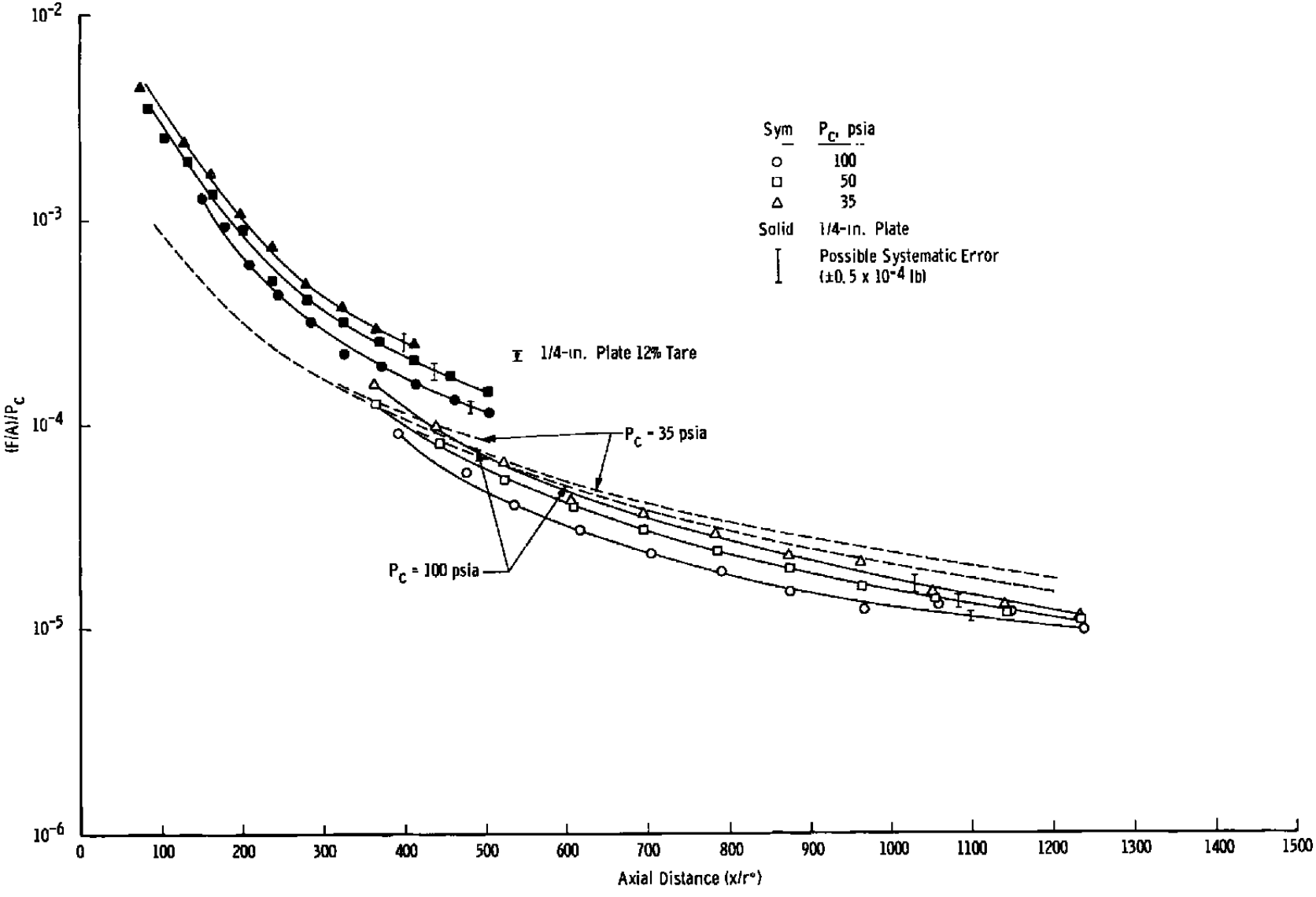

Fig. 29b Axial Distribution of Flat Plate Force; A_e/A^* = 207, Nitrogen

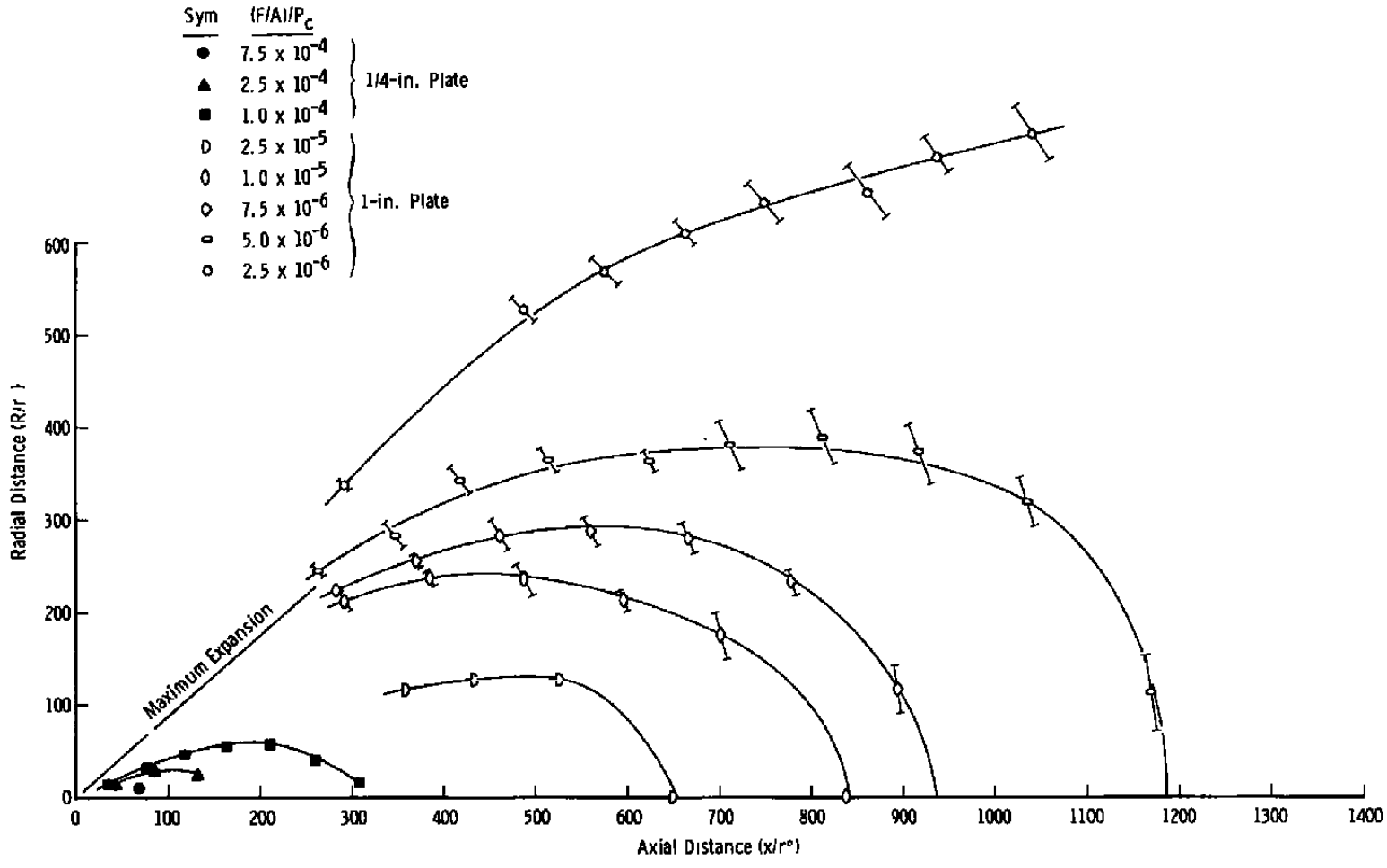

Fig. 30a Constant Force Map; A_e/A^* = 12.8, Argon, P_c = 100 psia

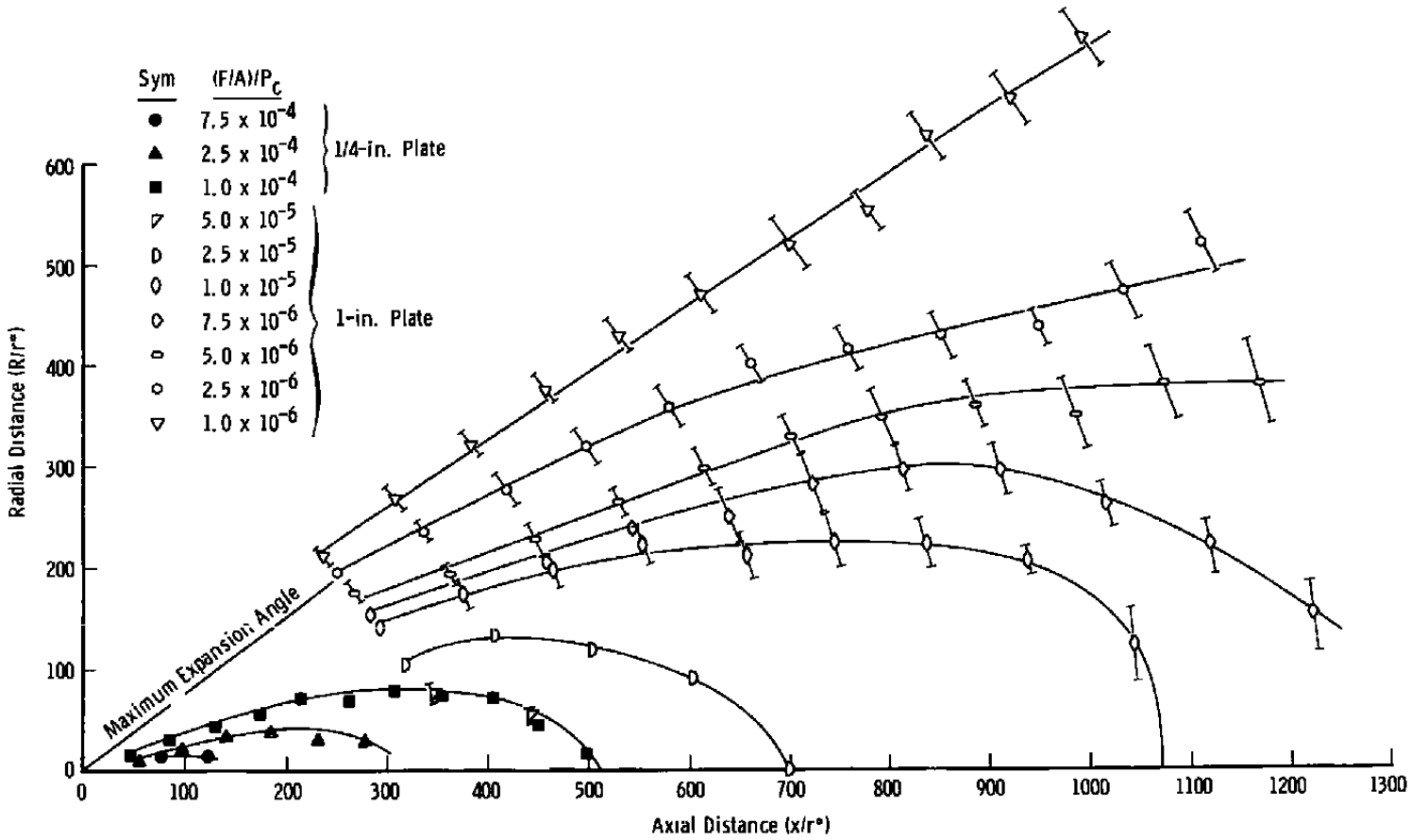

Fig. 30b Constant Force Map; $A_e/A^* = 207$, Argon, $P_c = 100$ psia

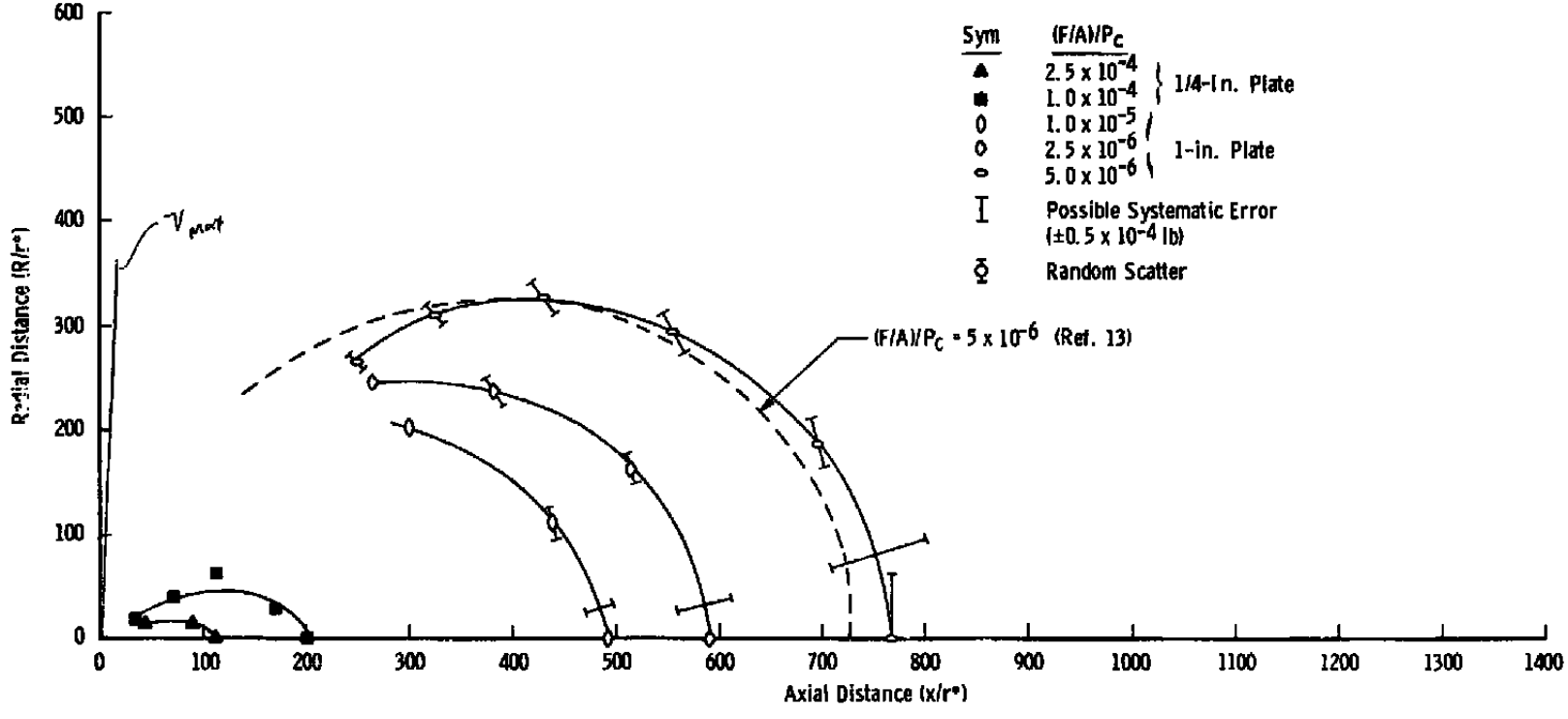

Fig. 31a Constant Force Map, Argon, $A_e/A^* \sim 1.0$, $P_c = 100$ psia

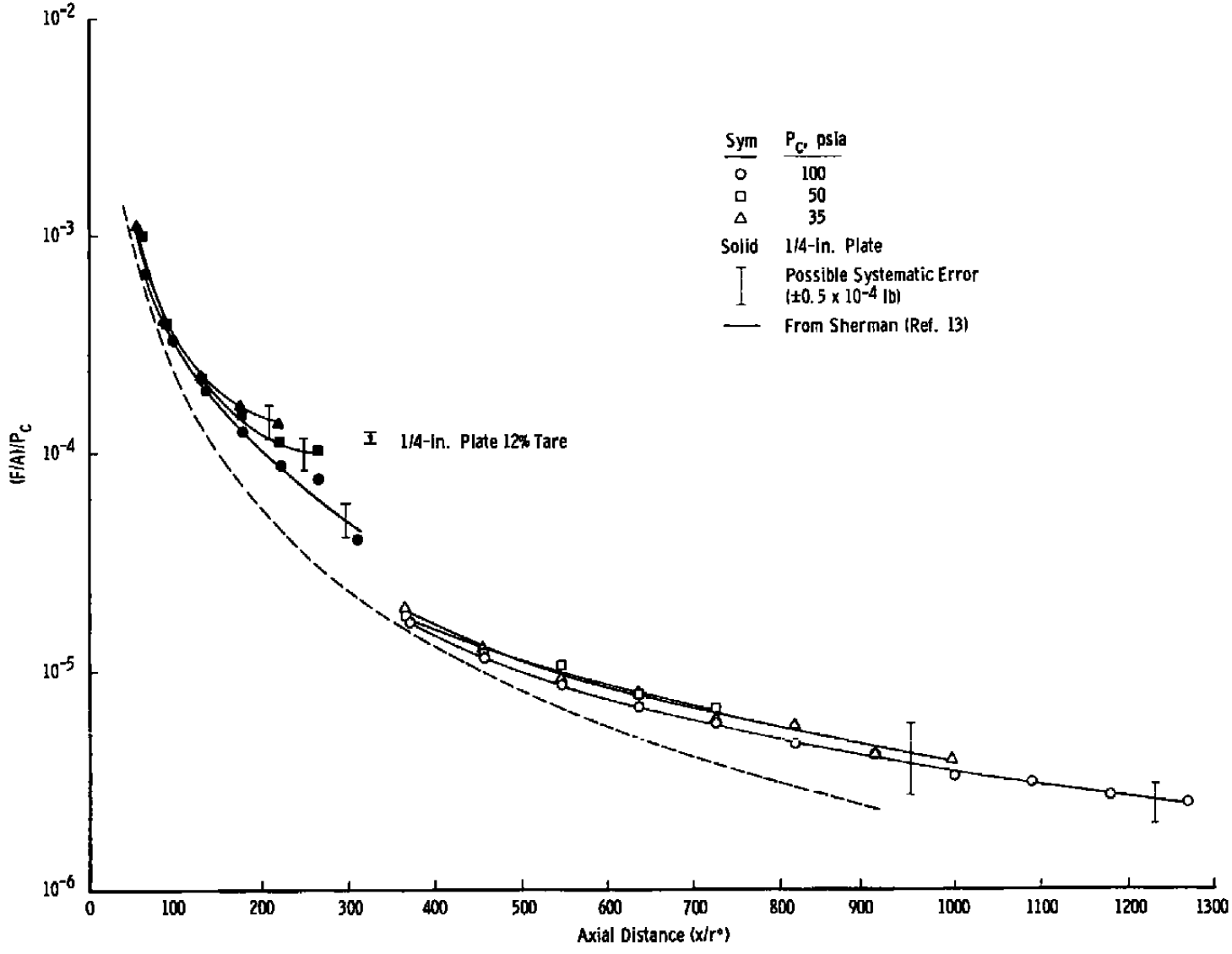

Fig. 31b Axial Distribution of Flat Plate Force; A_e/A^* = 1.0, Argon

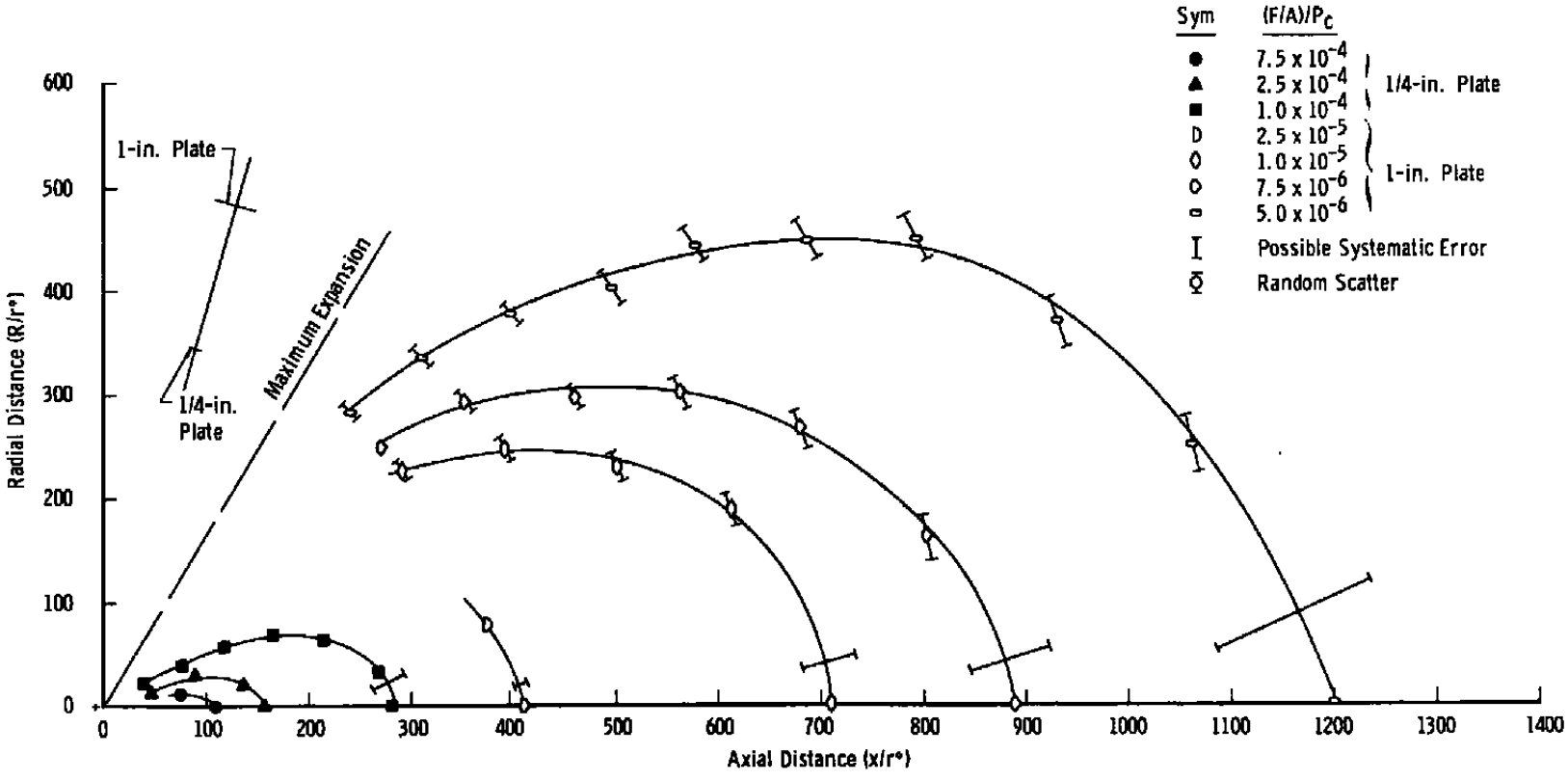

Fig. 32a Constant Force Map; $A_e/A^* = 3.73$, Argon, $P_c = 100$ psia

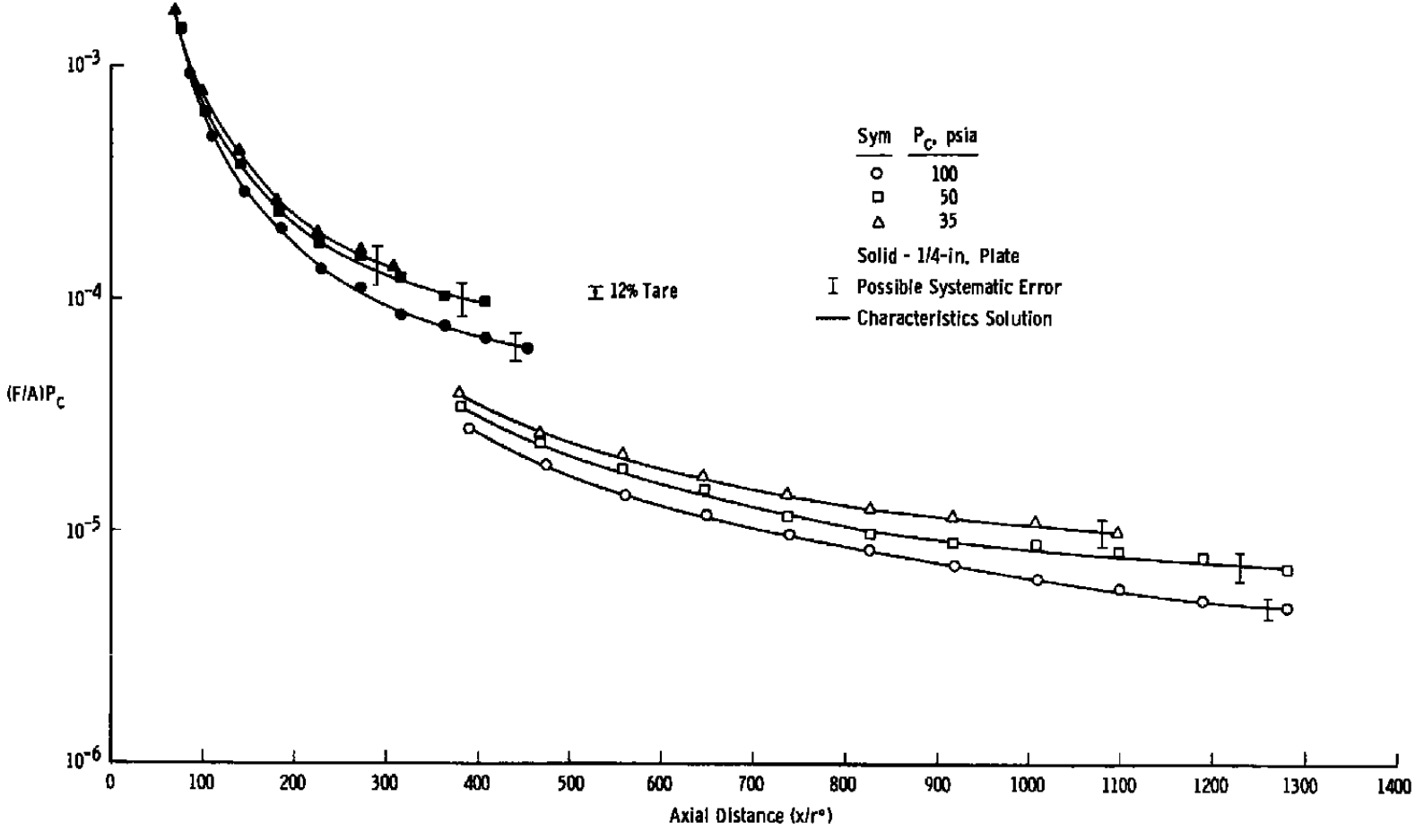

Fig. 32b Axial Distribution of Flat Plate Force; A_e/A^* = 3.73, Argon

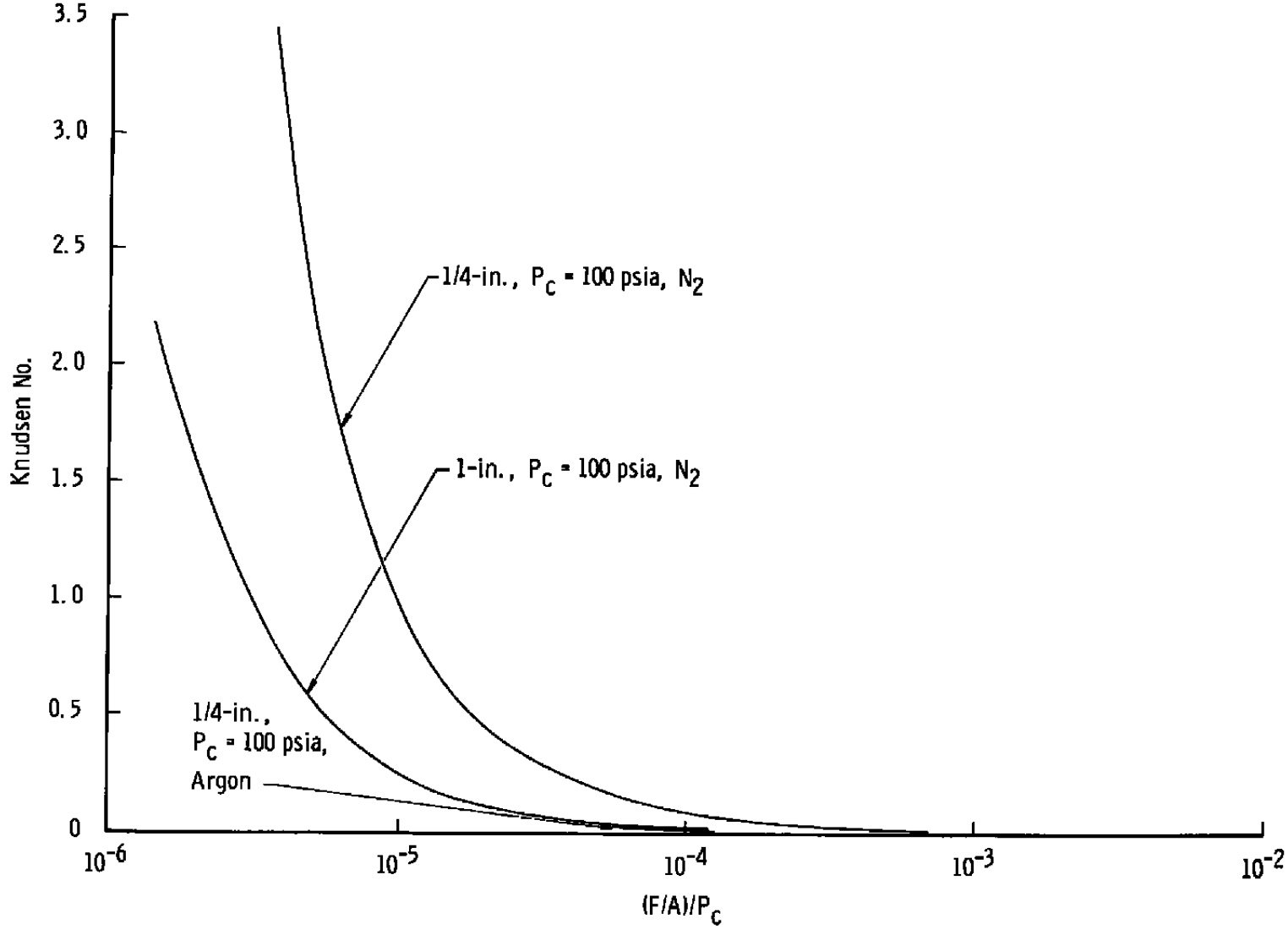

Fig. 33 Flat Plate Knudsen Number

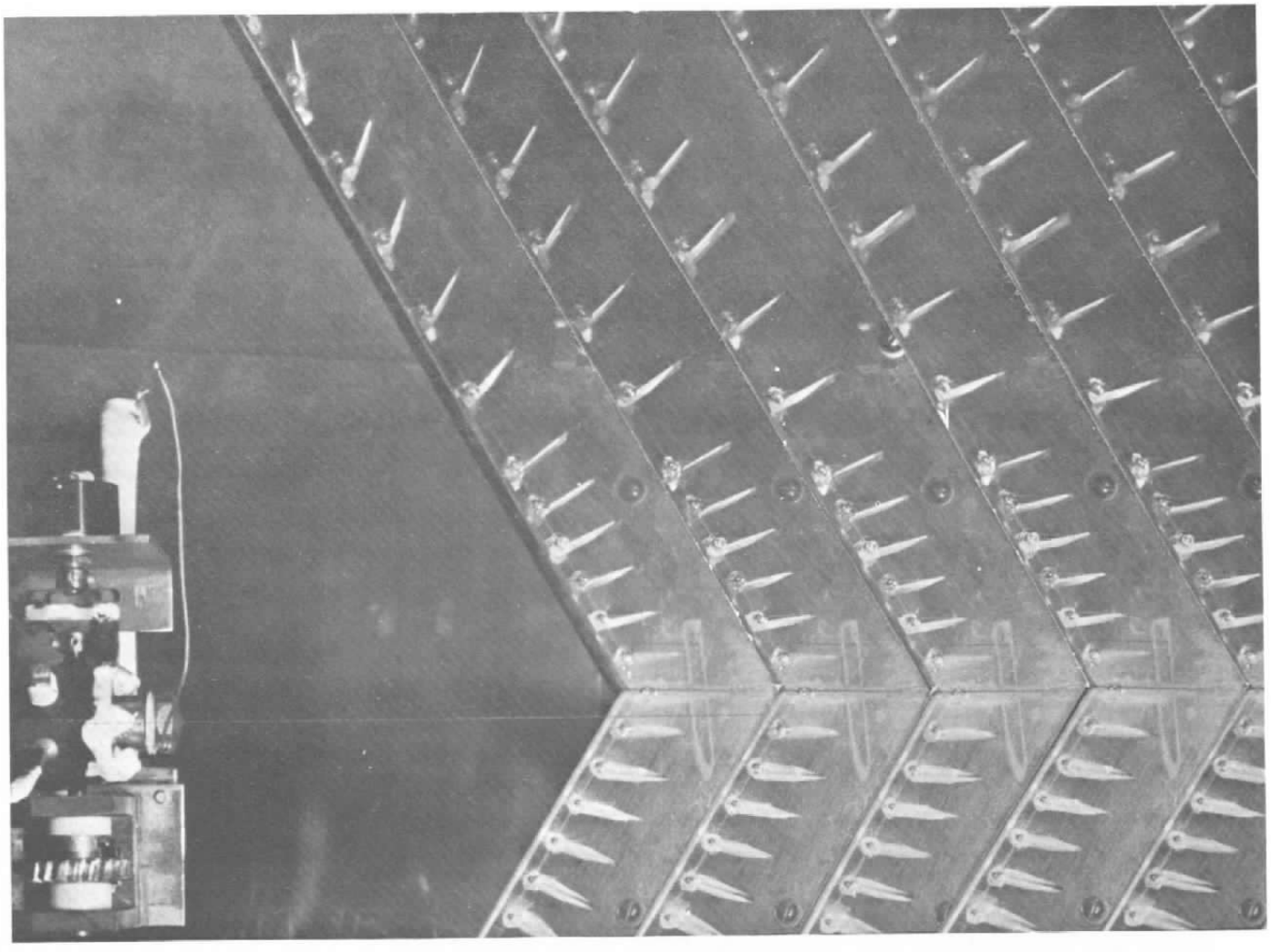

Fig. 34 Flow Direction by Streamline Vanes; A_e/A^* = 1.0, Nitrogen, P_c = 100 psia

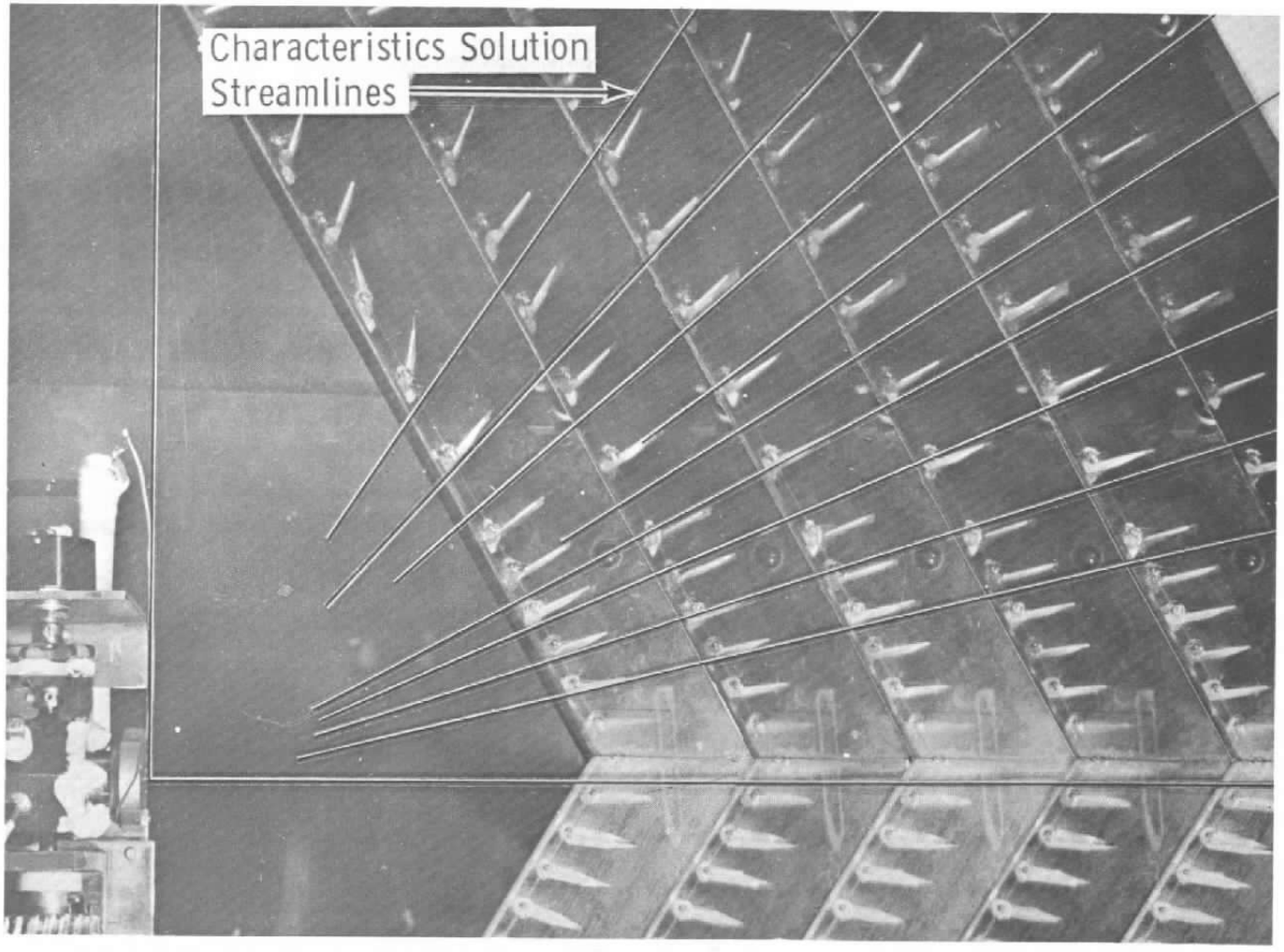

Fig. 35 Flow Direction by Streamline Vanes; A_e = 3.73, Nitrogen, P_c = 50 psia

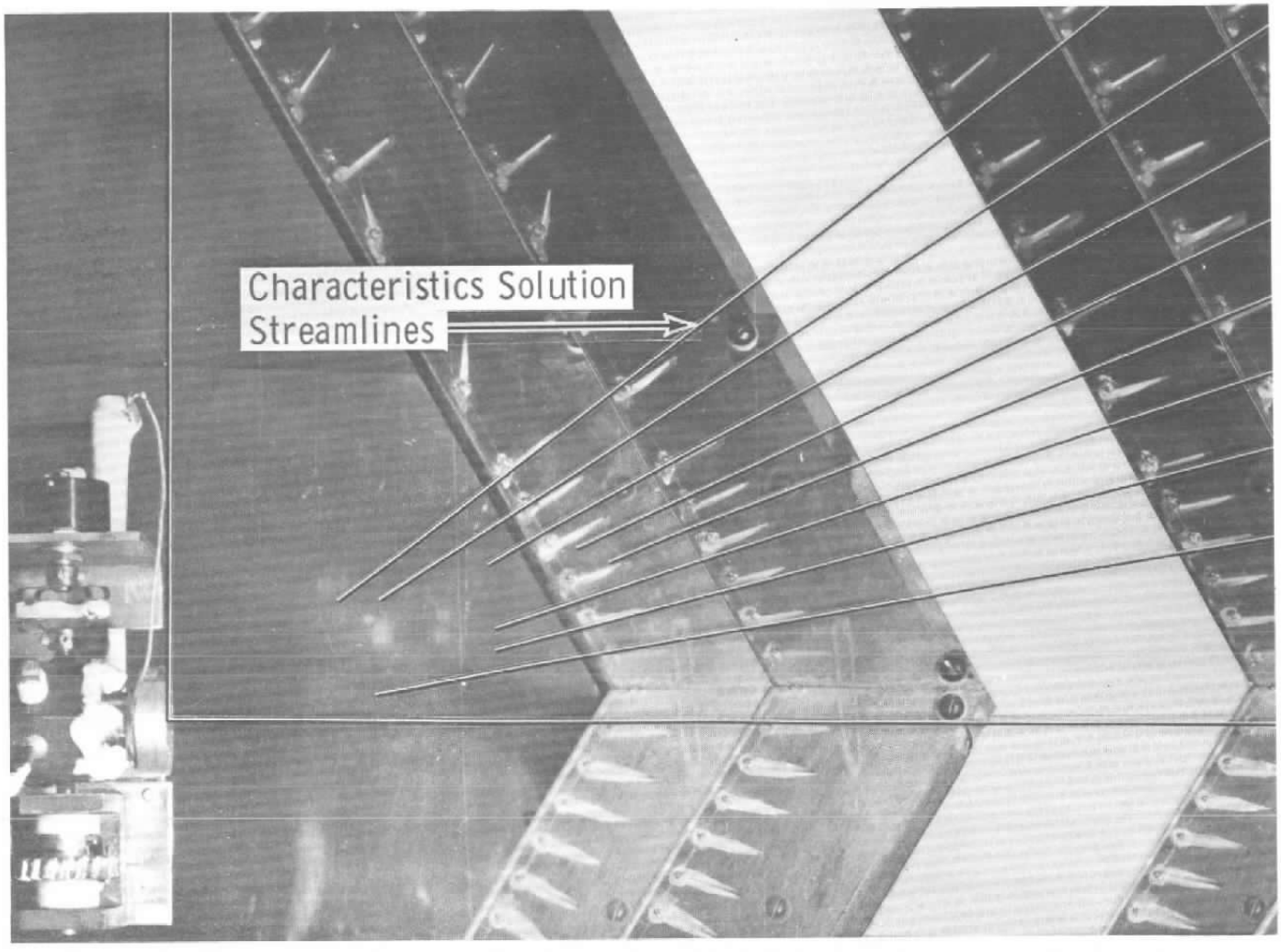

Fig. 36 Flow Direction by Streamline Vanes; A_e/A^* = 12.8, Nitrogen, P_c = 50 psia

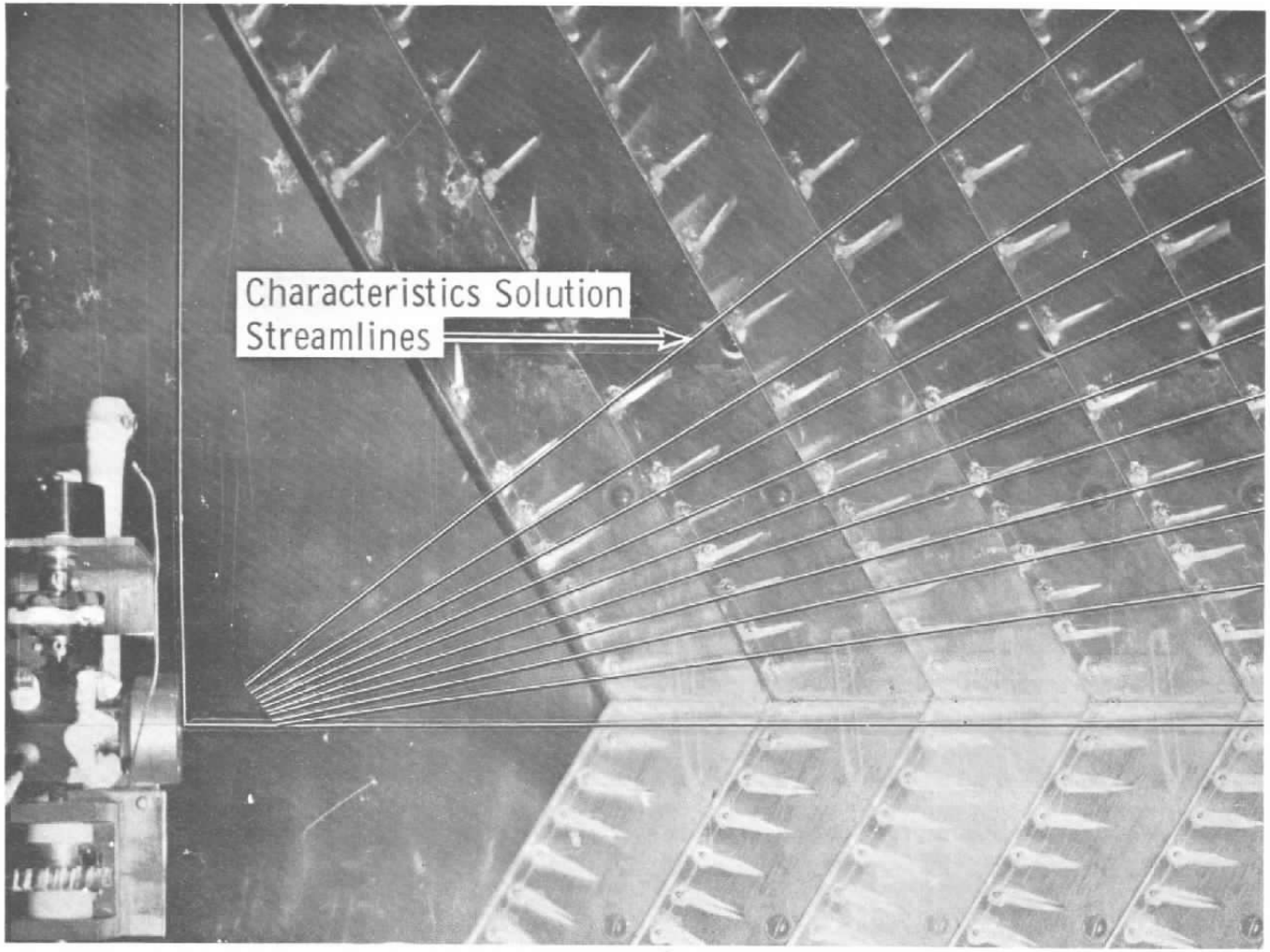

Fig. 37 Flow Direction by Streamline Vanes; A_e/A^* = 36.3, Nitrogen, P_c = 100 psia

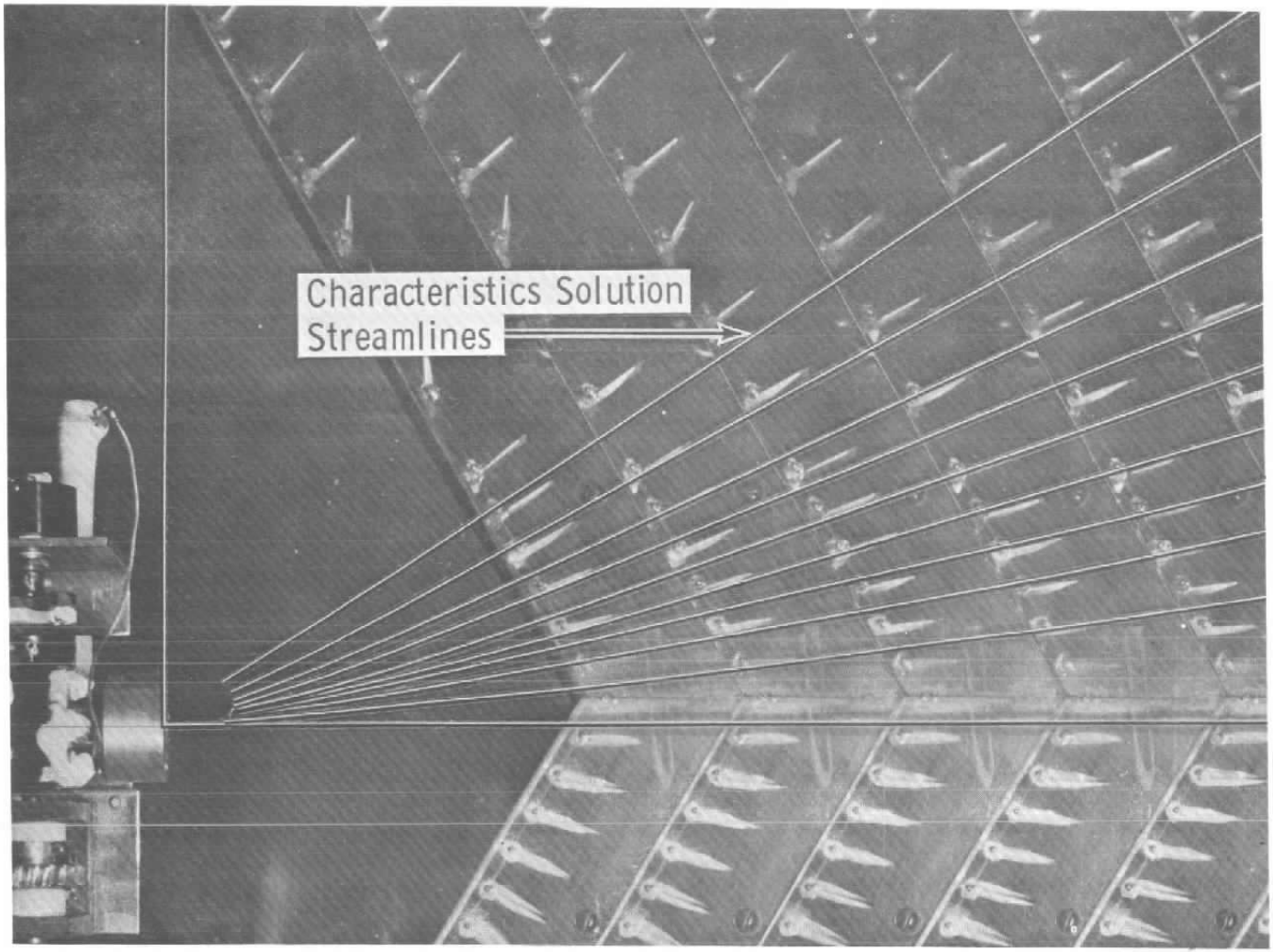

Fig. 38 Flow Direction by Streamline Vanes; A_e/A^* = 69.6, Nitrogen, P_c = 100 psia

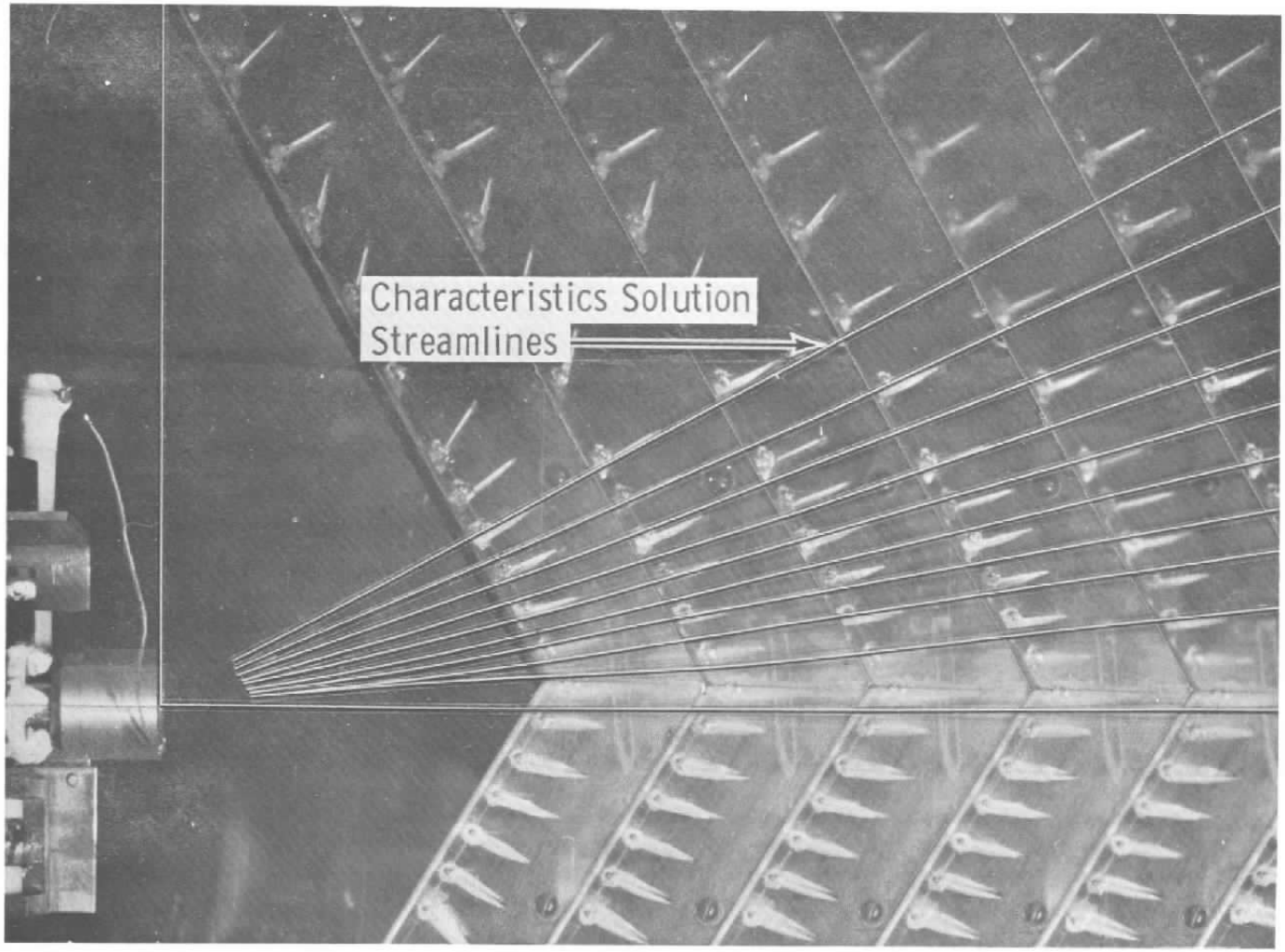

Fig. 39 Flow Direction by Streamline Vanes; A_e/A^* = 207, Nitrogen, P_c = 100 psia

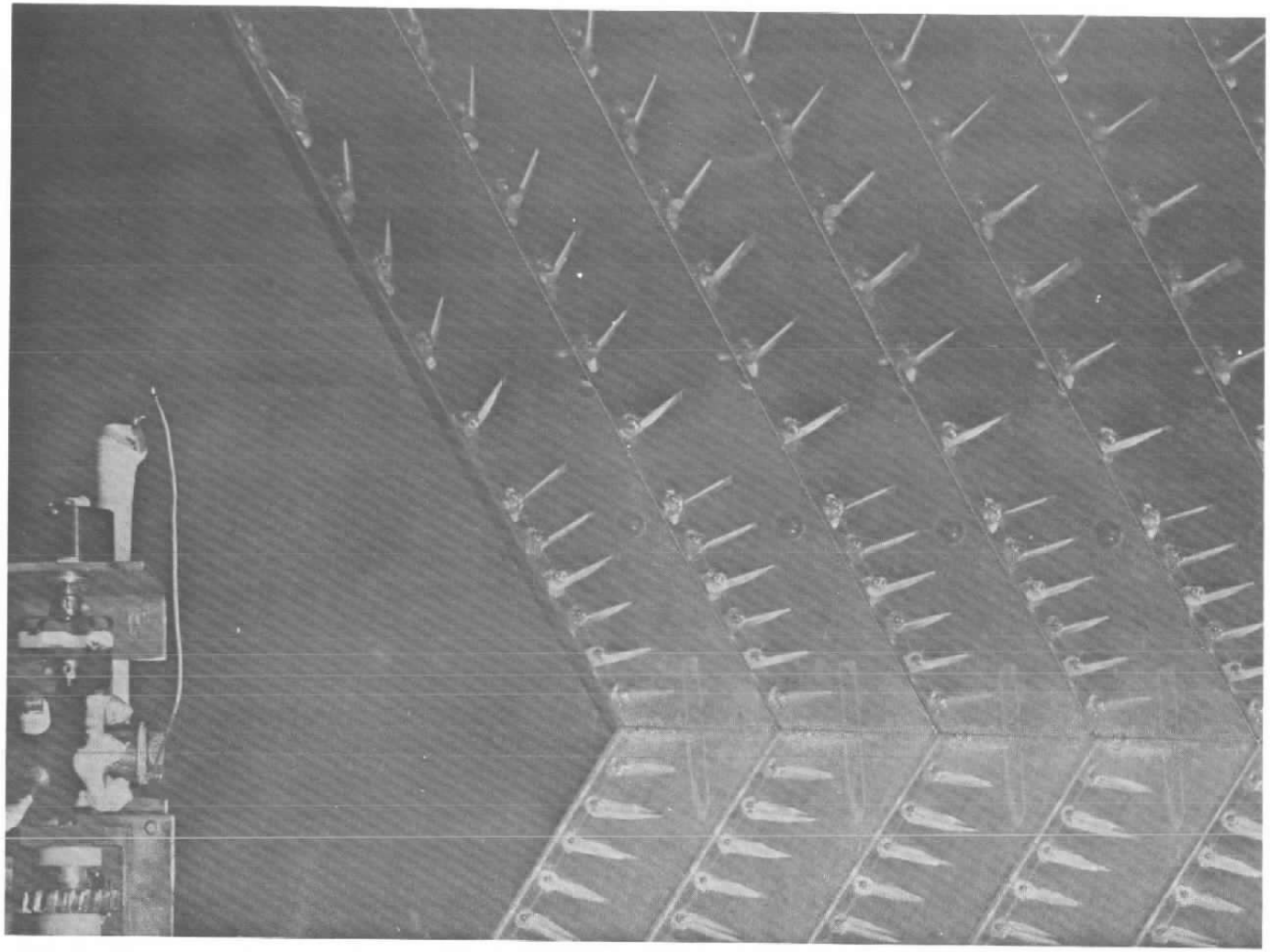

Fig. 40 Flow Direction by Streamline Vanes; A_e/A^* = 1.0, Argon, P_c = 100 psia

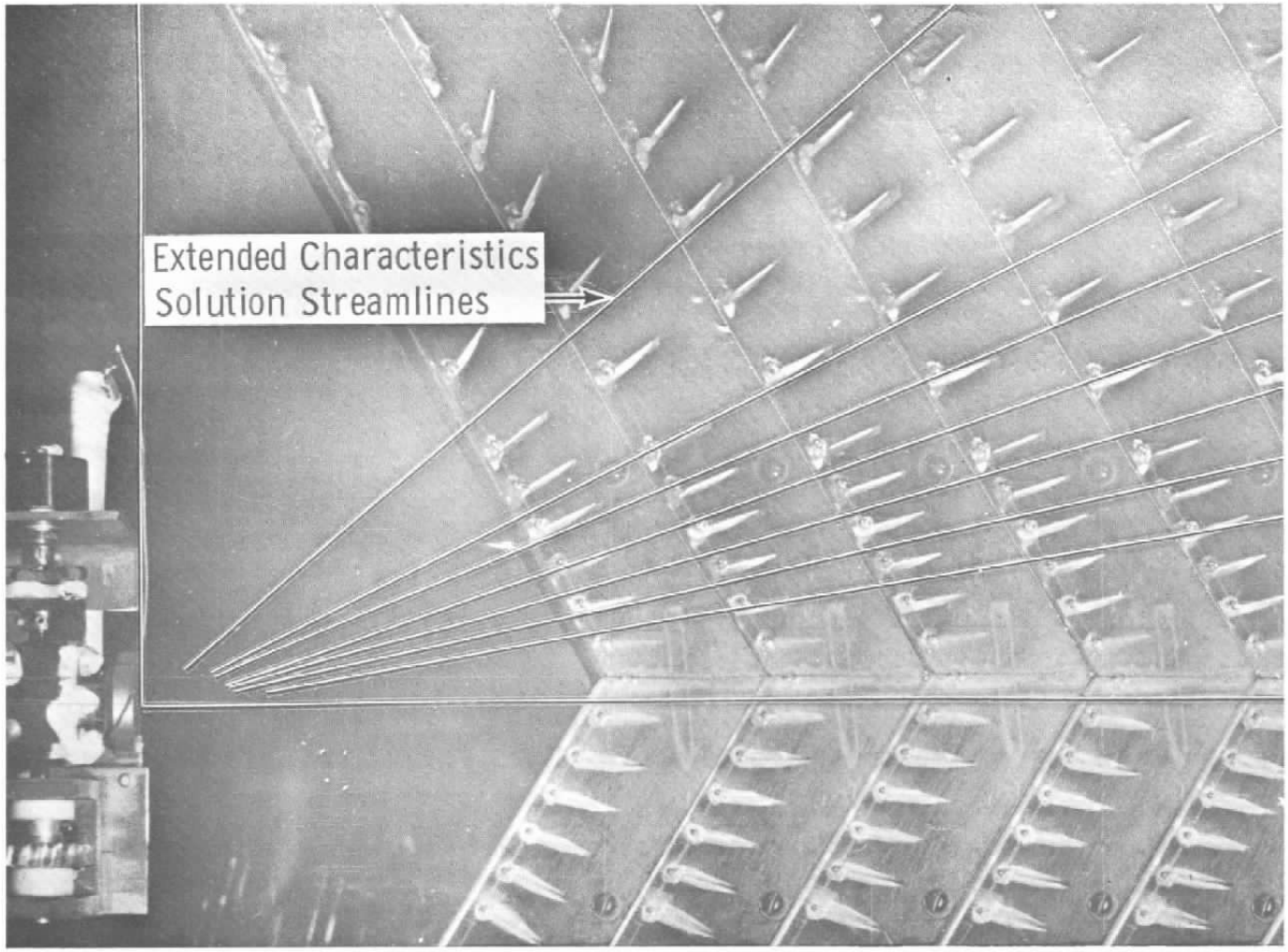

Fig. 41 Flow Direction Streamline Vanes; $A_e/A^* = 3.73$, Argon, $P_c = 100$ psia

APPENDIX I
CONDENSATION IN SUPERSONIC NOZZLE FLOW

When an ideal gas expands isentropically through a nozzle, the temperature and pressure decrease such that $P/(T)^{\gamma/\gamma-1} = \text{Const}$. This isentrope will cross the saturated vapor pressure, $P_v = f(T)$, on a $P - T$ plane and the gas will tend to condense in liquid or solid droplets. The amount of supersaturation that can be sustained before condensation is observed has been the subject of a great deal of theoretical and experimental work. The experimental data from various wind tunnels show the amount of supersaturation that can be tolerated in terms of the effects on certain measurable quantities for the specific nozzle. The operating limits for the facilities are satisfactorily defined. However, the generalization of these results to predict condensation for arbitrary conditions is not possible. The classical theory of condensation outlined below is a valid description of the phenomenon at higher pressures, but it appears to give ambiguous results in the usual wind tunnel operating range.

THE CLASSICAL CONDENSATION THEORY

References 1 and 2 discuss the theory of condensation in isentropic expansions developed by Oswatitsch, Volmer, Becker and Doring, Frenkel and others to account for observations in supersonic wind tunnels. When the gas is in a supersaturated state, droplets will form by the aggregation of molecules and the transfer of the heat condensation by the surrounding gas. The size and rate of formation of these droplets is predicted from the theory. The concept of the critical droplet size is essential to the theory since it is the formation rate and growth rate of these that determine condensation.

The critical droplet is of a size that it is unstable with respect to the surrounding saturated vapor; if a molecule evaporates, the critical droplet will continue to shrink, or if one is added it will grow. When droplets of critical size are formed, condensation proceeds rapidly. Both the critical radius and rate of formation of droplets of critical size depend upon the state of the gas and the surface tension which binds a molecule to the droplet:

$$r_{crit} = \frac{2\sigma V_g}{KT \ln p/p_\infty}$$

critical radius

$$\frac{1}{N}\frac{dN}{dt} = \frac{4}{3}\frac{P}{KT}(r_{crit})^3\sqrt{\frac{2\pi\sigma}{m}} - \frac{4\pi\sigma(r_{crit})^2}{3KT}$$

rate of condensation fraction

where: σ = Surface tension

V_ℓ = Volume of molecule in liquid

m = Mass of molecule in liquid

P_∞ = Equilibrium vapor pressure at T

T & P = Temperature and pressure of supersaturated vapor

The situation on a P - T plane is shown schematically in the figure below:

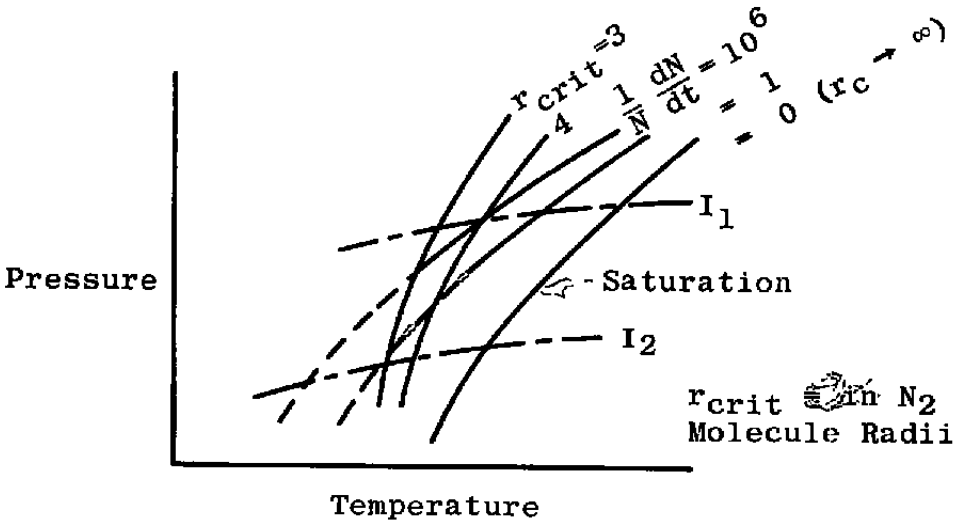

Along the isentropic expansion, I , the critical droplet size decreases, and the formation rate increases after the saturation line is crossed. This rate increases slowly at first and then rises rapidly as indicated by the lines $\frac{1}{N}\frac{dN}{dt} = 1$ and 10^6 per second. Knowing the flow velocity, one can calculate the fraction of the flow condensed by integrating along the isentrope. Lowering the supply pressure or increasing stagnation temperature shifts the isentrope from I_1 to I_2 and evidently increases the amount of supersaturation. It is also evident that the critical droplet radius is decreased at the point where appreciable formation rates are encountered.

The last observation and the absence of any evidence of condensation in the NOL wind tunnel lead Bogdonoff and Lees (Ref. 1) to postulate a breakdown of the theory when the droplet radius is small, i.e., of the order of the gas molecule radius. For small droplets the surface tension is reduced from that in an infinite body of liquid because fewer molecules are near a surface molecule on a surface of small radius. This leads to the conclusion that droplets predicted by the theory are smaller than

critical size and therefore they evaporate rapidly instead of growing. A cut-off in the nucleation rate will appear when the predicted droplet radius is small as indicated on the sketch above. Therefore, when an isentrope intersects the saturation curve below a fixed temperature, condensation will not occur at all.

A modification of the classical theory is given by Stever and Rathbun (Ref. 2) in which the effect of droplet radius on surface tension is computed. The result of this refinement is to shift both the lines of constant critical droplet radius and condensation rate toward the saturation line. Therefore, the amount of supersaturation estimated is considerably less than the original theory for constant surface tension would estimate. Experimental results were presented which tended to substantiate the modified theory, and it was suggested that the observations of Ref. 1 were insensitive to the existence of condensation. However, the breakdown of the theory for small droplets is not precluded, and two of the data points appear to substantiate it.

EXPERIMENTAL CONDENSATION RESULTS

The most recent compilation of wind tunnel data concerning condensation are from Daum (Ref. 3). Figure I-1 shows the data of this report and some additional points from AEDC wind tunnel experience. Isentropic lines, the condensation rate, and critical droplet contours from the theory of Ref. 2 are also included. These data support the nucleation theory of Ref. 2 as well as the hypothesis of Bogdonoff and Lees, at least to the extent of indicating much higher supersaturations when the isentrope crosses the saturation curve lower than 10 mm Hg pressure. This occurs when the droplet radius is less than about 3 nitrogen molecule radii at high nucleation rates. It is interesting to observe that the limit of the data falls along a single isentrope which is a little below the point where the theory appears to be invalid. The lack of data below this limiting isentrope is the result of (1) limitation of wind tunnel operating characteristics or (2) densities too low to make reliable measurements.

The quantitative correlation of wind tunnel data is rendered difficult by the variety of methods used to detect the onset of condensation. In Ref. 1 a condensation shock (or absence of it) was anticipated to be observable by the schlieren system. In Ref. 2 condensation effects were observed (1) in the nozzle wall static pressure, (2) in the shock wave angle on a 5.5° wedge, and (3) in the dispersion of light by droplets in the flow. The deviation of static and pitot pressures as the total temperature

was lowered was used in Ref. 3 to indicate the onset of condensation. Reference 4 used the nozzle wall static pressure and observed no measurable effect on pitot pressure. In Ref. 5 the deviation of the surface pressure on an ogive-cylinder was observed. Reference 6 employs the test section static pressure derived from an extrapolation of flat plate induced pressures to an infinite distance downstream. All the methods are indirect measurements and are therefore more or less related to condensation itself. Further, the regime of interest in the present experiment (T_c = 300°K, P_c = 1 - 7 atm) lies in the area of condensation where the orthodox nucleation theory becomes doubtful.

A KINETIC MODEL METHOD OF CORRELATING CONDENSATION DATA

Since there is no reliable guide in the conventional nucleation theory, a simple kinetic model appears to be justified; this is to count the number of molecular collisions in an isentropic expansion from the point of saturation to condensation in order to correlate the experimental data. The collision frequency can be calculated using a rigid sphere model:

$$\frac{dN}{dt} = \frac{\bar{V}}{\lambda} = \frac{\bar{V}_o}{\lambda_o}\frac{\rho_c}{\rho_o}\sqrt{\frac{T_c}{T_o}}\left(\frac{\rho}{\rho_c}\right)\sqrt{\frac{T}{T_c}} \qquad (1)$$

$\bar{V}$ = Mean molecular velocity

λ = Mean free path

ρ = Density

T = Temperature

Sub o = Standard T and P

Sub c = Nozzle reservoir

The collisions per unit distance traveled:

$$\frac{dN}{dx} = \frac{1}{U}\frac{dN}{dt}\frac{\sqrt{\frac{\gamma-1}{2}}\frac{dN}{dt}}{a_t\frac{U}{U_{max}}} \qquad (2)$$

U = Stream speed

a_c = Reservoir acoustic speed

$U_{max} = \sqrt{\frac{2}{\gamma-1}}\,a_c$ = Limit speed

$\sqrt{\frac{2}{\gamma-1}}\sqrt{\frac{RT_c}{M}}$ $\quad M$ - Mol. Wt.

Then,

$$\Delta N = k \frac{\rho_c}{\rho_o} \ell \int_{\left(\frac{x}{\ell}\right)_1}^{\left(\frac{x}{\ell}\right)_2} \frac{U_{max}}{U} \frac{\rho}{\rho_{T_1}} \sqrt{\frac{T}{T_c}}\, d\left(\frac{x}{\ell}\right) \qquad (3)$$

is the number of collisions between x_1 and x_2. $K = \sqrt{\frac{\gamma - 1}{2}} \frac{\bar{V}_o}{\lambda_o a_o}$ is a constant for the gas. Since the quantity inside the integral is a function of the nozzle area ratio, it is convenient to transform the equation by taking an area ratio-distance relation of the following form:

$$\frac{A}{A^*} = 1 + \text{const} \left(\frac{x}{\ell}\right)^n$$

and defining the constant such that ℓ_{10} corresponds to an area ratio of 10. Then the number of collisions between an area ratio of 10 and $\frac{A}{A^*}$ is

$$\frac{\Delta N}{k \frac{\rho_c}{\rho_o} \ell_{10}} = \frac{1}{n(9)^{1/n}} \int_{10}^{A/A^*} f\left(\frac{A}{A^*}\right) \frac{d(A/A^*)}{\left(\frac{A}{A^*} - 1\right)^{n-1/n}}$$

where $$f\left(\frac{A}{A^*}\right) = \frac{U_{max}}{U} \frac{\rho}{\rho_c} \frac{T}{T_c}$$

The exponent, n is nearly unity for two-dimensional nozzles, two for conical, and generally larger for the free expansion of a jet into a vacuum. Figure I-2 shows the effects of γ and n on the collision number for several examples.

The theory above is at least qualitatively in agreement with observation. Equation (4) shows that a reduction of the reservoir density $\frac{\rho_c}{\rho_o}$ results in greater supersaturation. The linear effect of nozzle size (ℓ_{10}) is evident in comparing the greater degree of supersaturation (~ 25°K) observed in a small nozzle (~ 13 cm long) in Ref. 4 compared to Ref. 5 (~ 6 m long nozzle) where it was only a degree or two. It is interesting to observe that the integral has a finite limit; therefore, expansions from a low density reservoir or a small nozzle could be expected to continue to infinity without the occurrence of condensation. As might be anticipated, the more rapid the expansion, ($n > 1$), the fewer are the collisions and therefore greater supersaturation should occur. The reason for a smaller number of collisions with larger ratio of specific heats, γ, is that for a fixed expansion $\left(\frac{A}{A^*}\right)$ the temperature drops further.

To correlate condensation results, it is necessary to compute the area ratios at saturation and at condensation and take the difference in ΔN.

ESTIMATE OF THE PROBABILITY OF CONDENSATION IN THE PRESENT EXPERIMENTS

In the present experiments, conical nozzles with area ratios up to 200 were used. Argon and nitrogen were the test gases at a reservoir temperature about 300°K and pressures from 0.7 to 7 atm. It was observed in a previous test (Ref. AEDC-TDR-64-124) that the exhaust plume of nitrogen was approximately the shape calculated by the method of characteristics whereas argon had a much wider expansion. It was suggested that a condensation shock reduced the exit Mach number in argon, but it was absent in nitrogen. The classical nucleation theory gives the following results for $A/A^* = 70$:

	Argon	Nitrogen	
r_{crit}	1.09×10^{-8} cm	2.34×10^{-8} cm	Critical Radius
$\frac{1}{N}\frac{dN}{dt}$	2.26×10^{4}/sec	8.95×10^{4}/sec	Rate of Condensation
Δx	0.13 cm	0.67 cm	Distance from Saturation to Exit
$\sqrt{T_c/M}$	2.74	3.27	Proportional to ~~Transit Time~~ Vel. thru Nozzle.
$\frac{1}{N}\left(\frac{dN}{dt}\right)\frac{\Delta x}{\sqrt{T_c/M}}$	1.44×10^{4}	3.28×10^{4}	Proportional to Condensation

M — Mol. wt.

These figures indicate practically the same degree of condensation for both gases and give no clue to the divergent results observed. However, the critical radius is on the same order as that of the molecule and this indicates the nucleation theory is not applicable in the regime of these experiments.

Recourse was then made to the collision theory of the previous section by correlating the data of Daum (Ref. 3) for nitrogen. Figure I-3 shows the number of collisions for nitrogen and argon in nozzles with area ratios up to 200. The data points of Daum and Ref. 6 are tabulated below in terms of number of collisions between saturation and condensation:

	P_c (atm)	T_c (°K)	$\frac{\Delta N_{sat}}{N}$	ΔT (°K)	Measurement
Ref. 3	15.5	622	1.97×10^{-2}	14.5	Pitot Pressure Deviation
(Air)	27.2	708	1.86×10^{-2}	8.3	
	47.7	838	$1.4^{+} \times 10^{-2}$	23	
	68.0	933	1.0×10^{-2}	30	
Ref. 6	$\frac{P_c}{P_0} =$	184 (Amagat)	1.98×10^{-1}	7	Tunnel F Wall Static
(N_2)	"	184	4.8×10^{-1}	~35	Tunnel F Flat Plate Static
	"	184	2.4×10^{-1}	~30	Hot Shot II Flat Plate Static

If to be conservative one disregards the last two points, the supersaturation temperature increment ΔT_{s-c} can be plotted as a function of the number of collisions ΔN_{s-c}, which gives the following estimates for the test nozzles with nitrogen:

		A/A* = 70			A/A* = 200		
P_c (atm)	T_c (°K)	$\frac{\Delta N}{K}$	ΔT (Calc)	ΔT (Expansion)	$\frac{\Delta N}{K}$	ΔT (Calc)	ΔT (Expansion)
1	300	1.47×10^{-3}	>30°K	15°K	2.18×10^{-3}	>30°K	27°K
6.8	300	1.52×10^{-2}	22	22	2.0×10^{-2}	16	34
10.0	300	2.65×10^{-2}	15	24	3.36×10^{-2}	12	36

For the test conditions from 2 to 7 atm supply pressure, condensation is not expected for the 70:1 area ratio nozzle but may occur at the higher pressure in the 200:1 nozzle

The case for argon is inconclusive because of a lack of experimental data of the type for air and nitrogen. A comparison between nitrogen and argon is made below.

		$\Delta N/K\ell_{10}$	
	P_c	A/A* = 70	A/A* = 200
N_2	1	0.25×10^{-2}	0.44×10^{-2}
	10	4.4×10^{-2}	6.4×10^{-2}
A	1	1.73×10^{-2}	1.88×10^{-2}
	10	20.9×10^{-2}	22.4×10^{-2}

Although argon undergoes 4 to 6 times as many collisions at the same density, the decrease in density of argon by a factor of 10 did not alter the shape of the jet expansion. The number of collisions for condensation in a monatomic gas is evidently different from that for a diatomic one. Systematic experimentation is required to provide consistent results for correlation by this method.

REFERENCES

1. Bogdonoff, S. M. and Lees, L. "Study of the Condensation of the Components of Air in Supersonic Wind Tunnels." Symposium on Aerothermodynamics, NOLR-1134, Paper No. 4, June 1949.

2. Stever, H. G. and Rathbun, K. C. "Theoretical and Experimental Investigation of Condensation of Air in Hypersonic Wind Tunnels." NACA Tech. Note 2559, November 1951.

3. Daum, F. L. "The Condensation of Air in a Hypersonic Wind Tunnel." ARL-63-42, 1963 (Also IAS Paper No. 63-53 presented at IAS 31st Annual Meeting, January 21-23, 1963).

4. Arthur, P. D. and Nagamatsu, H. T. "Experimental Supersaturation of Gases in Hypersonic Wind Tunnels." GALCIT Memo No. 10, July 1952. ATI 168735

5. Fitch, C. R., Coats, J. D., and Trimmer, L. L. "Air Liquefication Effects on the Aerodynamic Characteristics of the AGARD Calibration Model B at Mach Nos. 5 and 8." AEDC-TN-61-24, February 1961.

6. Griffith, B. J., Deskins, H. E. and Little, H. R. "Condensation in Hotshot Tunnels." AEDC-TDR-64-35 (AD 431046), February 1964.

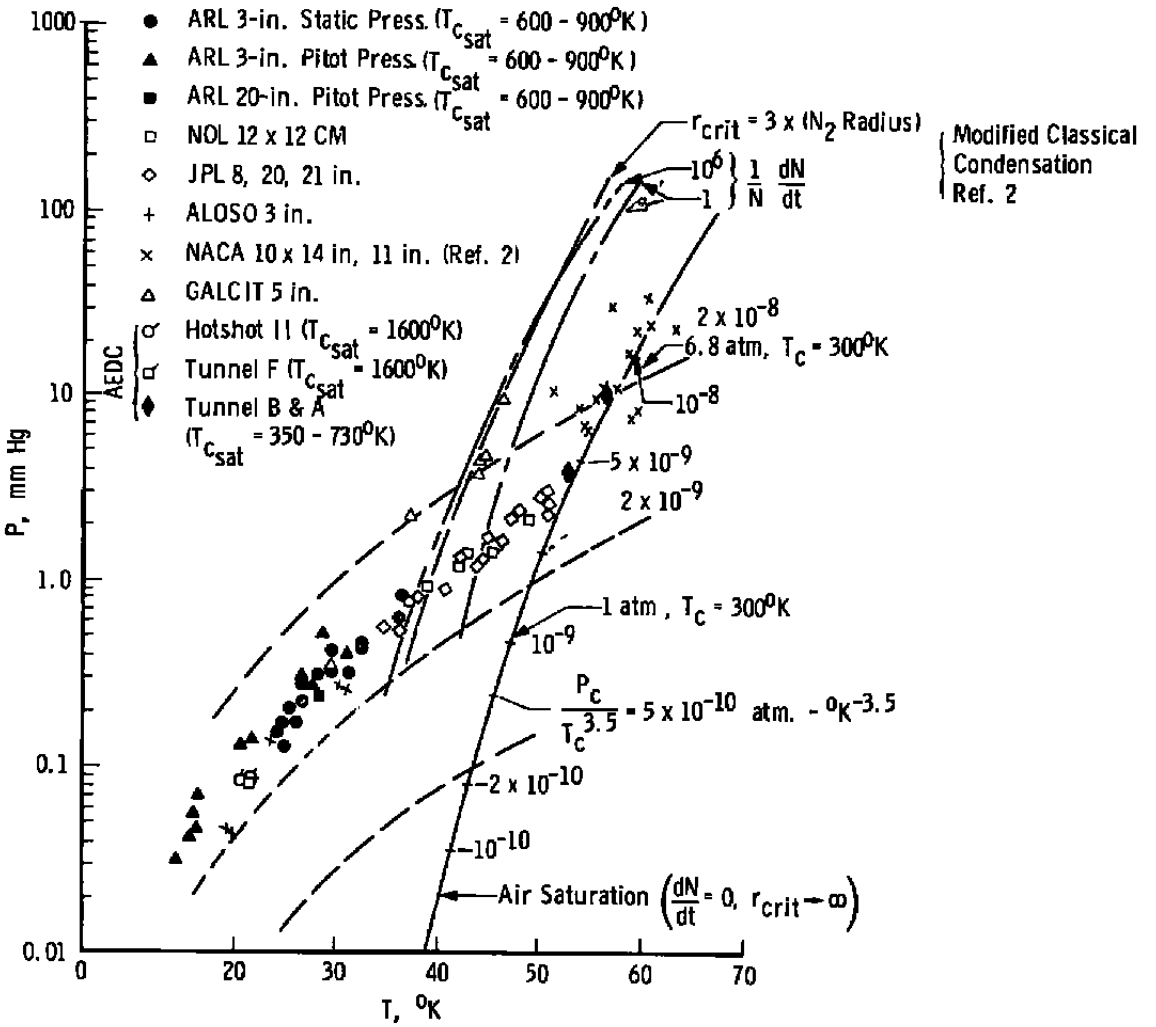

Fig. I-1 Summary of Condensation Data

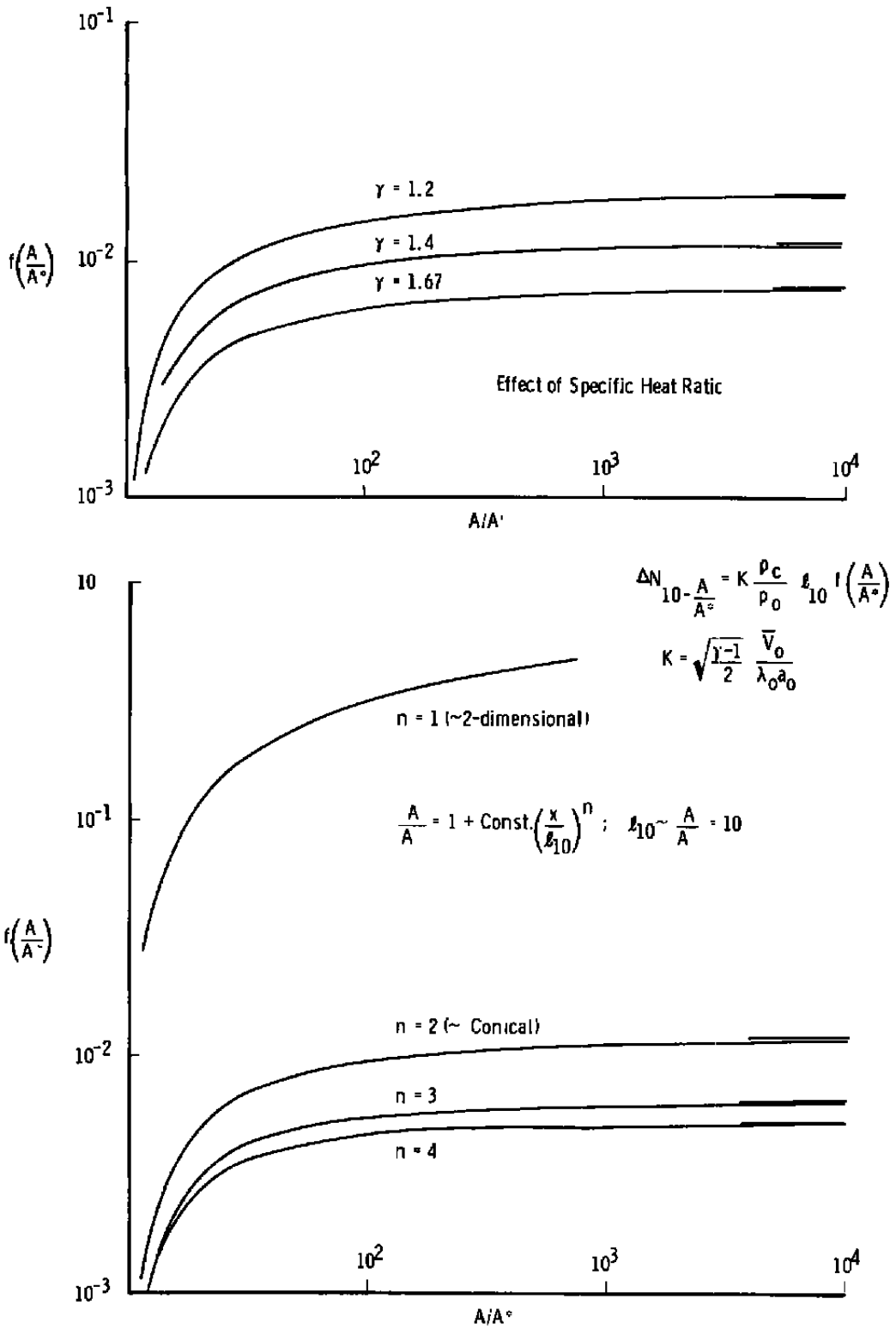

Fig. I-2 Number Collisions in Isentropic Expansion

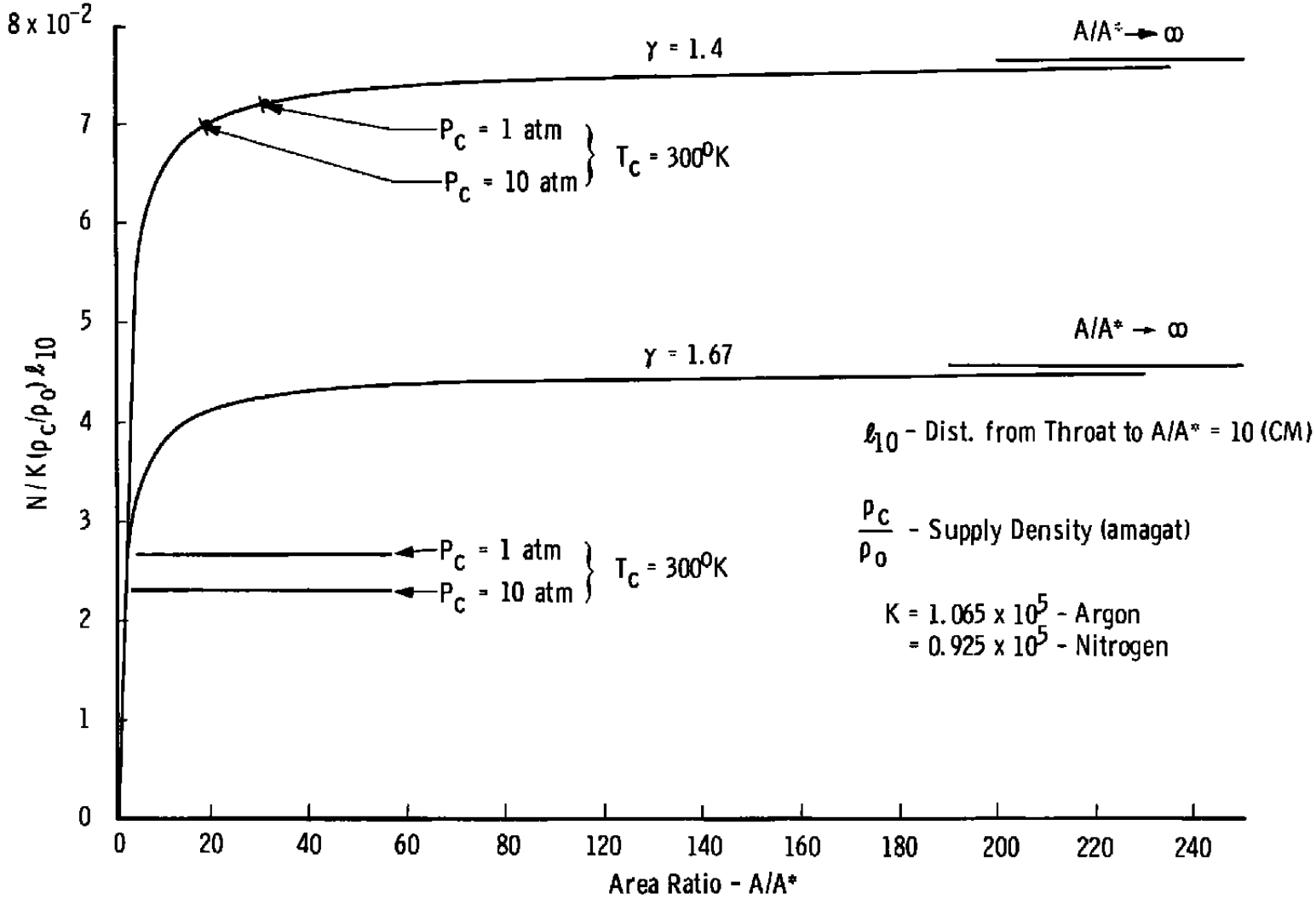

Fig. I-3 Number Molecular Collisions in Isentropic Expansion

APPENDIX II
DRAG OF NORMAL FLAT PLATE FROM CONTINUUM TO FREE-MOLECULE FLOW CONDITIONS

Correlation of flow characteristics in the jet exhaust through measurement of the force on a plate normal to the flow requires an estimate of the drag-coefficient over a wide range of flow regimes. Actual experimental data in the transition between the continuum model and the free-molecule regime are very limited, and consistent theoretical methods are lacking. The method of estimating the drag coefficient is to assemble experimental data giving the trends with departure from well established limits of the continuum or free molecule flow regimes.

CONTINUUM LIMIT

Hoerner (Ref. 1) summarizes the high Reynolds number regime drag data obtained from wind tunnels and ballistic ranges. Although these data were obtained from discs and short cylinders, they should be applicable in the hypersonic regime of interest because both skin friction and base drag components are negligible. In Fig. II-1 the base drag ($M < 4$) is subtracted out and plotted separately.

FREE MOLECULE LIMIT

The free-molecule formulas of Ref. 2 can be written for the flat plate with diffuse reflection at the wall temperature, T_w as:

$$C_D = \left[\frac{1}{\sqrt{\pi}\, s} + \frac{1}{2}\sqrt{\frac{\gamma - 1}{\gamma}}\,\frac{\sqrt{T_w/T_T}}{s\left(\frac{T}{U_{max}}\right)}\right] e^{-s^2}$$

$$+ \left[1 + \frac{1}{s^2} + \frac{\sqrt{\pi}}{2}\sqrt{\frac{\gamma - 1}{\gamma}}\,\frac{\sqrt{T_w/T_T}}{(U/U_{max})}\right](1 - \mathrm{erf}\, s)$$

where $s = \dfrac{U}{\sqrt{2RT_\infty}} = \sqrt{\dfrac{\gamma}{2}}\, M =$ Speed ratio

T_T = Total temperature

γ = Ratio of specific heats

The substitution,

$$\frac{T_w}{T_\infty} = \frac{\gamma - 1}{\gamma} \frac{s^2}{(U/U_{max})} \frac{T_w}{T_T}$$

has been made for convenience in computation. The adiabatic wall condition, $T_{AW} = r T_T$, is shown in Fig. II-I for the recovery factor,

$$r = \frac{\gamma}{\gamma + 1} f(s)$$

$\gamma = 1.4$ and $f(s)$ is given in Ref. 2.

TRANSITION REGIME (LOW REYNOLDS NO. VISCOUS EFFECTS)

In the supersonic low density regime, the effects of viscosity (low Reynolds number) dominate the flow field about a blunt body; and it is assumed that pitot pressure gives a good measure of the variation away from the continuum drag value. Therefore, it is assumed that the ratio of drag coefficient to the high Reynolds number C_D is the same as the ratio of pitot pressure to the Rayleigh stagnation pressure. The data of Refs. 3, 4, and 5 are cross plotted to provide the Mach number variation at constant Reynolds numbers from 1.0 to 10. The Knudsen number $\left(Kn = \frac{\lambda}{d}\right)$ is uniquely related to Mach and Reynolds numbers by $Kn = \sqrt{\frac{\pi\gamma}{2}} \frac{M}{R_e}$ for a rigid sphere molecule model. Constant Knudsen number contours are included in Fig. II-1 to provide continuity into the hypersonic regime.

TRANSITION REGIME (HYPERSONIC NEAR-FREE MOLECULE FLOW)

Reference 6 provides experimental two-dimensional flat plate drag data at Mach numbers from 6 to 10 and Knudsen numbers from about unity to 20 or 30, where a close approach to the free molecule value is demonstrated. Over the Mach number range of the experiments, the drag coefficient depended only on Knudsen number. All the experimental data are summarized for the insulated wall case in Fig. II-1 as solid lines. This conforms to the conditions of the experimental procedure in which the supply temperature and surrounding chamber wall were room temperature.

DRAG AT EQUILIBRIUM WALL TEMPERATURE

The flat plate in the Aerospace Research Chamber (8V) is exposed, in addition to the convective heat transfer from the gas stream, to

radiation from the liquid-nitrogen-cooled shroud and cryopump downstream and to the room temperature chamber end upstream. The radiative heat transfer is

$$\dot{q}_{rad} = \epsilon k \ (T_w^4 - T_R^4) + \epsilon k \ (T_w^4 - T_F^4)$$

The convective rate is

$$\dot{q}_{conv} = s_t \ \rho V C_p \ (T_{AW} - T_w)$$

Equating the two yields a fourth-order equation:

$$T_w^4 + \left(\frac{s_t \ \rho V C_p}{2 \epsilon k}\right) T_w = \frac{T_F^4 + T_R^4}{2} + \left(\frac{s_t \ \rho V C_p}{2 \epsilon k}\right) r T_T$$

If the speed ratio is large, the accommodation coefficients and emissivity (ϵ) are unity, and $\gamma = 1.4$:

$s_t = 1/2 \ \frac{\gamma + 1}{\gamma} = 0.86$ - Stanton Number

$k = 5.67 \times 10^{-12}$ w/cm^2/(°K)^4 - Boltzman Constant

$C_p = .24 \times 4.186 = 1.005$ joule/gm/°K - specific heat

$V = 7.40 \times 10^4 \sqrt{T_T / 300} \ \frac{cm}{sec}$ - flow velocity

$\rho = 1.14 \times 10^{-3} \ P_{T_t} \left(\frac{300}{T_c}\right) (\rho/\rho_c)$ gm/cc - density

$r = 1.166$ - recovery factor

$T_F = 300$°K - front wall temperature

$T_R \equiv 80$°K - rear wall temperature

$$\frac{S_t \ \rho V C_p}{2k} = 6.60 \times 10^{12} \ P_c \sqrt{\frac{300}{T_c}} \ (\rho/\rho_c) \ (°K)^3$$

P_c – Supply pressure (atm)

The two limits, (a) negligible convective heat transfer - low density and (b) negligible radiative heat transfer - high density, give wall temperatures of 250°K and 350°K, respectively. The limits of hypersonic drag coefficient are 2.85 and 3.0 for these cases. It is evident that the equilibrium wall remperature depends upon the product $P_c \ (\rho/\rho_c)$, and Fig. II-2 gives the variation of drag coefficient for a supply temperature

of 300°K. This figure can be used to correct the insulated wall flat plate drag for the conditions of the test at large speed ratios. It is probable that the same trend will be exhibited also at lower speed ratios (or Mach numbers). In Fig. II-3 the insulated flat plate drag of Fig. II-1 are faired into smooth curves.

REFERENCES

1. Hoerner, S. F. Fluid Dynamic Drag; Practical Information on Aerodynamic Drag and Hydrodynamic Resistance. Midland Park, N. J., 1958. (Second Edition)

2. Schaff, S. A. and Talbot, L. "Handbook of Supersonic Aerodynamics-Mechanics of Rarefied Gases." NAVORD Report No. 1488, Vol. 5, Section 16, February 1959.

3. Enkenhus, K. R. "Pressure Probes at Very Low Density." UTIA Report No. R-43 (AD 126534), January 1957.

4. Kosterin, S. I., et al. "An Investigation into the Effect of the Rarefaction of a Supersonic Stream on the Readings of a Total-Head Probe." Translation, International Chem. Engr., Vol. 3, No. 2, April 1963, pp. 251-255.

5. Potter, J. L. and Bailey, A. B. "Pressures in the Stagnation Regions of Blunt Bodies in the Viscous-Layer to Merged-Layer Regimes of Rarefied Flow." AEDC-TDR-63-168, 1963.

6. Ko, D. R. "Drag of a Two-Dimensional Strip Normal to Hypersonic Near Free Molecule Flow." University of California Report No. AS-64-4, January 1964.

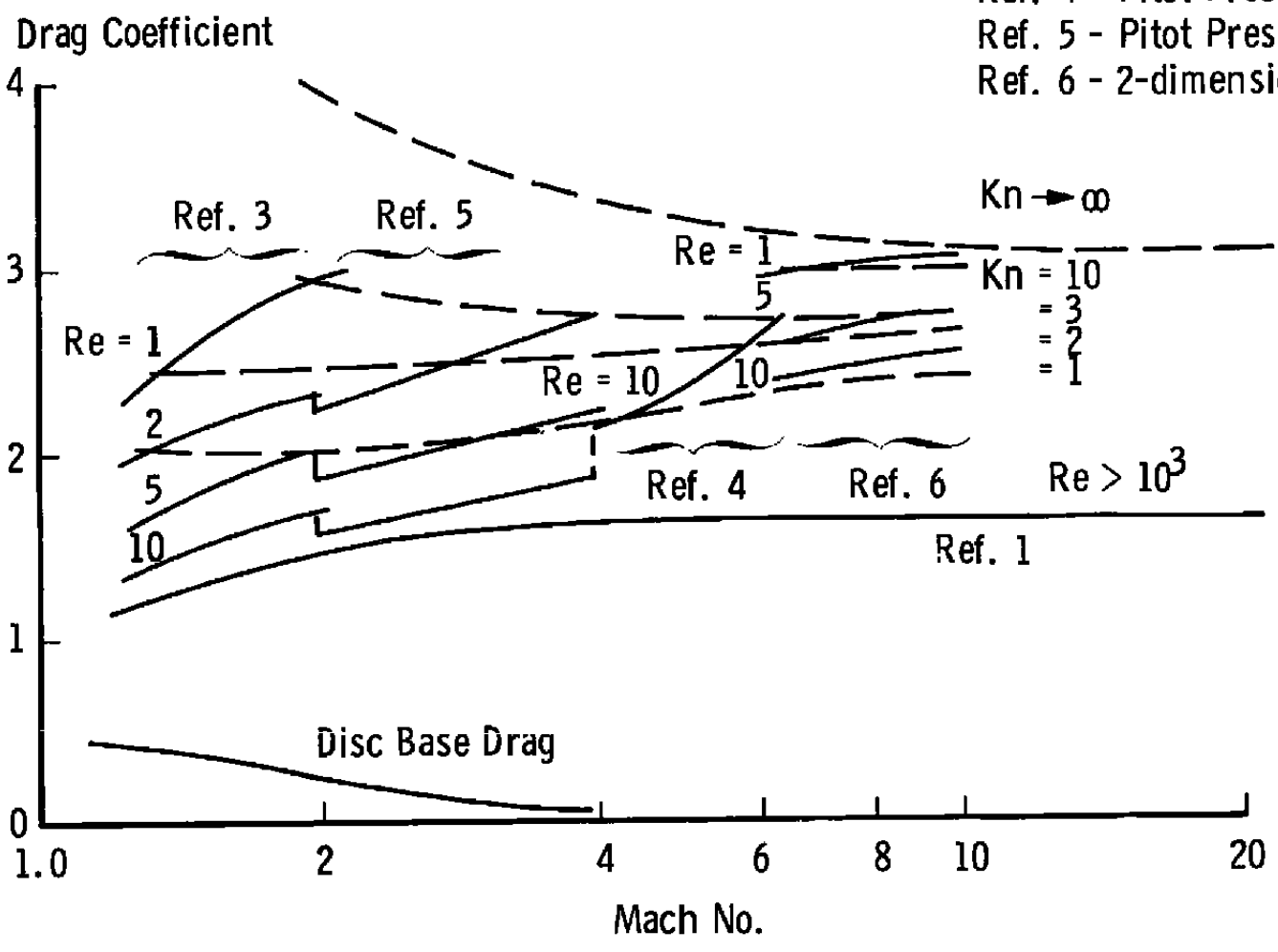

Fig. II-1 Flat Plate Drag Coefficient Experimental Data

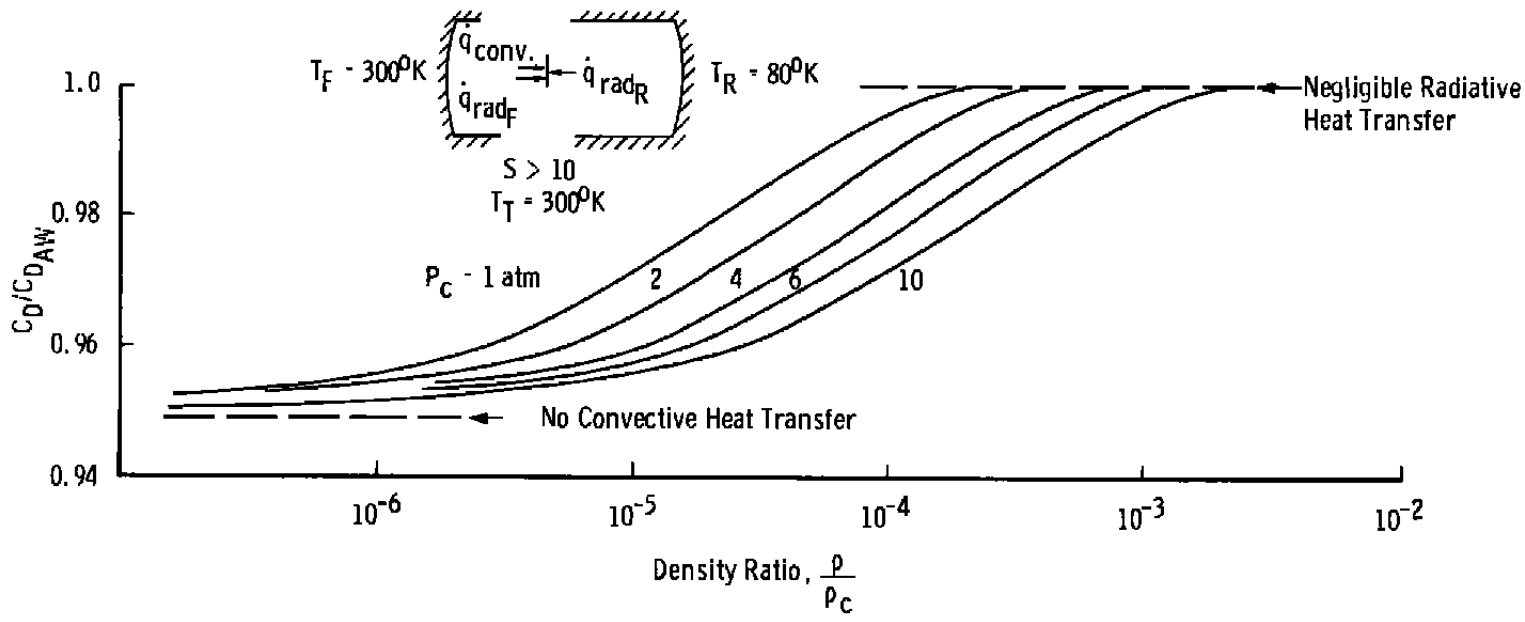

Fig. II-2 Ratio of Drag on Plate at Equilibrium Temperature to Drag of Insulated Plate in Free Molecule Flow

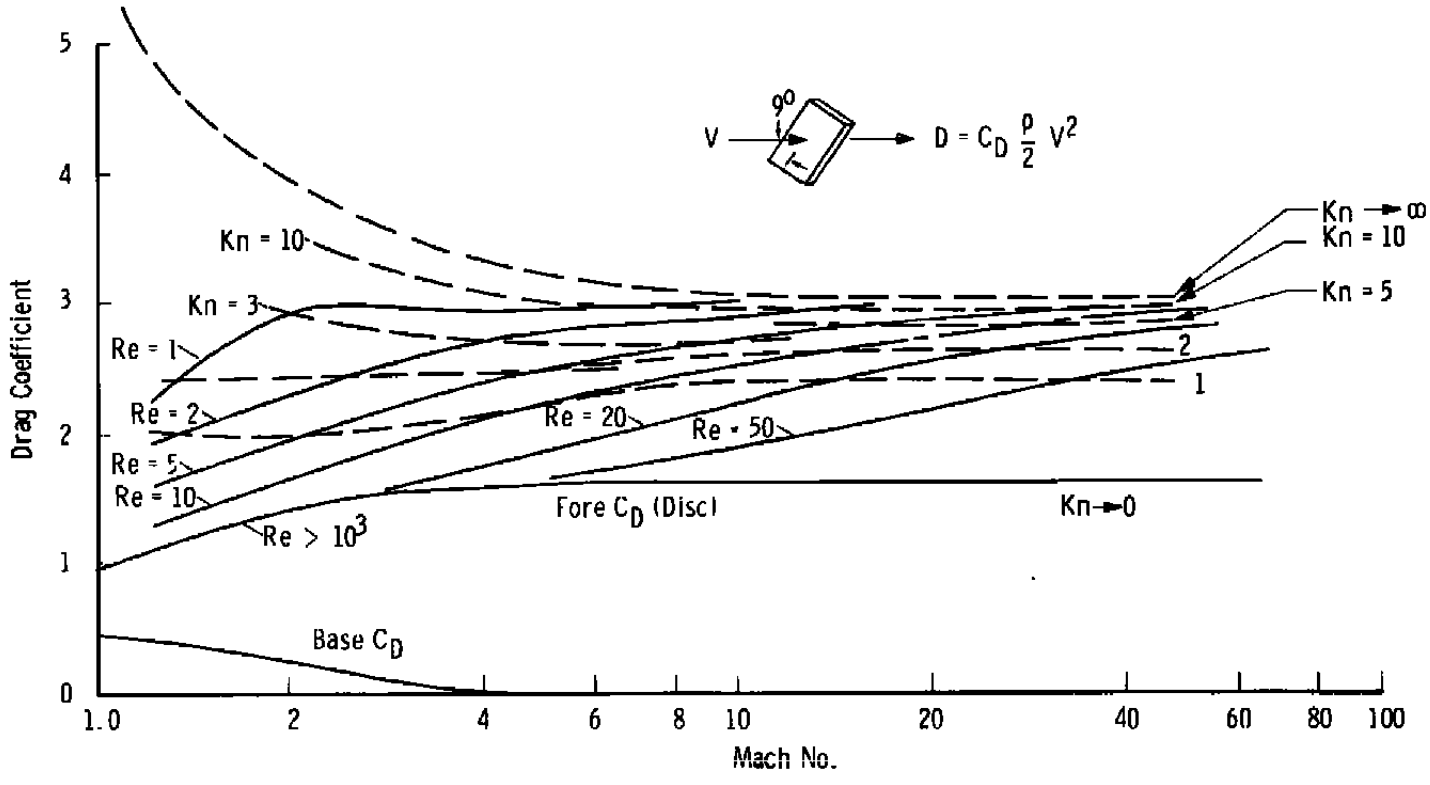

Fig. II-3 Insulated Flat Plate Drag Coefficient

DOCUMENT CONTROL DATA - R&D

(Security classification of title, body of abstract and indexing annotation must be entered when the overall report is classified)

1 ORIGINATING ACTIVITY (Corporate author)
Arnold Engineering Development Center
ARO, Inc., Operating Contractor
Arnold AF Station, Tennessee

2a REPORT SECURITY CLASSIFICATION
UNCLASSIFIED

2b GROUP
N/A

3 REPORT TITLE
EXPANSION OF A JET INTO NEAR VACUUM

4 DESCRIPTIVE NOTES (Type of report and inclusive dates)
N/A

5 AUTHOR(S) (Last name, first name, initial)
R. A. Cassanova and W. B. Stephenson, ARO, Inc.

6 REPORT DATE	7a TOTAL NO. OF PAGES	7b. NO. OF REFS
August 1965	96	13

8a CONTRACT OR GRANT NO.	9a. ORIGINATOR'S REPORT NUMBER(S)
AF 40(600)-1200 b. Program Element 65402234 c. d.	AEDC-TR-65-151 9b. OTHER REPORT NO(S) (Any other numbers that may be assigned this report) N/A

10. AVAILABILITY/LIMITATION NOTICES
Qualified requesters may obtain copies of this report from DDC.

11. SUPPLEMENTARY NOTES	12. SPONSORING MILITARY ACTIVITY
N/A	Arnold Engineering Development Center, Air Force Systems Command, Arnold AF Station, Tennessee

13 ABSTRACT

The flow field of nozzles exhausting into a vacuum was investigated both analytically and experimentally. The applicability of the method of characteristics for jet expansions into a free molecular environment is discussed. Fifteen-degree, half-angle, conical nozzles with area ratios of 1.0 to 207 were tested with argon and nitrogen at total pressures of 100, 50, and 35 psia. Ambient pressures of 10^{-4} to 10^{-6} torr yielded total pressure to ambient pressure ratios of 10^{7} to 10^{9}. Properties of the flow field were determined by the use of flat plates and flow direction vanes.

DD FORM 1 JAN 64 1473

14 KEY WORDS	LINK A		LINK B		LINK C	
	ROLE	WT	ROLE	WT	ROLE	WT
conical nozzles						
flow fields						
jet plumes						
velocity						
density						
method of characteristics						
nozzle exhausts						

INSTRUCTIONS

1. ORIGINATING ACTIVITY: Enter the name and address of the contractor, subcontractor, grantee, Department of Defense activity or other organization *(corporate author)* issuing the report.

2a. REPORT SECURITY CLASSIFICATION: Enter the overall security classification of the report. Indicate whether "Restricted Data" is included. Marking is to be in accordance with appropriate security regulations.

2b. GROUP: Automatic downgrading is specified in DoD Directive 5200.10 and Armed Forces Industrial Manual. Enter the group number. Also, when applicable, show that optional markings have been used for Group 3 and Group 4 as authorized.

3. REPORT TITLE: Enter the complete report title in all capital letters. Titles in all cases should be unclassified. If a meaningful title cannot be selected without classification, show title classification in all capitals in parenthesis immediately following the title.

4. DESCRIPTIVE NOTES: If appropriate, enter the type of report, e.g., interim, progress, summary, annual, or final. Give the inclusive dates when a specific reporting period is covered.

5. AUTHOR(S): Enter the name(s) of author(s) as shown on or in the report. Enter last name, first name, middle initial. If military, show rank and branch of service. The name of the principal author is an absolute minimum requirement.

6. REPORT DATE: Enter the date of the report as day, month, year; or month, year. If more than one date appears on the report, use date of publication.

7a. TOTAL NUMBER OF PAGES: The total page count should follow normal pagination procedures, i.e., enter the number of pages containing information.

7b. NUMBER OF REFERENCES: Enter the total number of references cited in the report.

8a. CONTRACT OR GRANT NUMBER: If appropriate, enter the applicable number of the contract or grant under which the report was written.

8b, 8c, & 8d. PROJECT NUMBER: Enter the appropriate military department identification, such as project number, subproject number, system numbers, task number, etc.

9a. ORIGINATOR'S REPORT NUMBER(S): Enter the official report number by which the document will be identified and controlled by the originating activity. This number must be unique to this report.

9b. OTHER REPORT NUMBER(S): If the report has been assigned any other report numbers *(either by the originator or by the sponsor)*, also enter this number(s).

10. AVAILABILITY/LIMITATION NOTICES: Enter any limitations on further dissemination of the report, other than those imposed by security classification, using standard statements such as:

(1) "Qualified requesters may obtain copies of this report from DDC."

(2) "Foreign announcement and dissemination of this report by DDC is not authorized."

(3) "U. S. Government agencies may obtain copies of this report directly from DDC. Other qualified DDC users shall request through _____."

(4) "U. S. military agencies may obtain copies of this report directly from DDC. Other qualified users shall request through _____."

(5) "All distribution of this report is controlled. Qualified DDC users shall request through _____."

If the report has been furnished to the Office of Technical Services, Department of Commerce, for sale to the public, indicate this fact and enter the price, if known.

11. SUPPLEMENTARY NOTES: Use for additional explanatory notes.

12. SPONSORING MILITARY ACTIVITY: Enter the name of the departmental project office or laboratory sponsoring *(paying for)* the research and development. Include address.

13. ABSTRACT: Enter an abstract giving a brief and factual summary of the document indicative of the report, even though it may also appear elsewhere in the body of the technical report. If additional space is required, a continuation sheet shall be attached.

It is highly desirable that the abstract of classified reports be unclassified. Each paragraph of the abstract shall end with an indication of the military security classification of the information in the paragraph, represented as *(TS), (S), (C), or (U)*.

There is no limitation on the length of the abstract. However, the suggested length is from 150 to 225 words.

14. KEY WORDS: Key words are technically meaningful terms or short phrases that characterize a report and may be used as index entries for cataloging the report. Key words must be selected so that no security classification is required. Identifiers, such as equipment model designation, trade name, military project code name, geographic location, may be used as key words but will be followed by an indication of technical context. The assignment of links, rules, and weights is optional.